

AD-A053 516

TEXAS UNIV AT AUSTIN

F/G 13/13

AN EXPLORATORY PHOTOELASTIC INVESTIGATION OF POST-TENSIONED CON--ETC(U)

AUG 77 S D VAUGHN

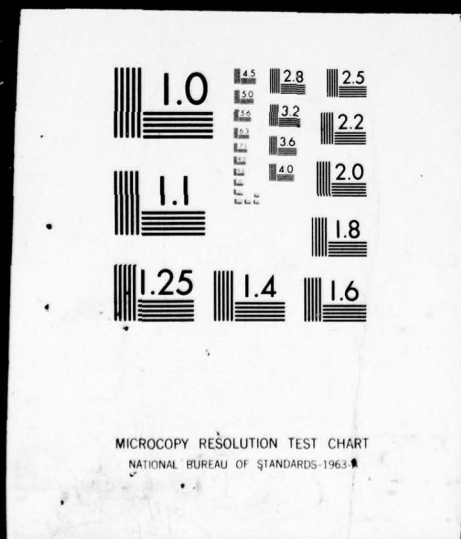
UNCLASSIFIED

. NL

1 OF 3
AD
A053516



1 OF 3
AD
A053516



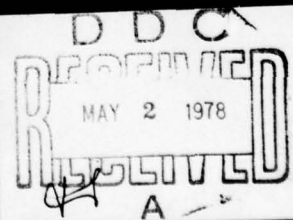
AD NO. _____

DDC FILE COPY

AD A 053516

DISTRIBUTION STATEMENT A

Approved for public release;
Distribution Unlimited



AD A 053516

AD No.
DDC FILE COPY

AN EXPLORATORY PHOTOELASTIC INVESTIGATION OF POST-TENSIONED
CONCRETE ANCHORAGE ZONE BURSTING STRESSES

①
SK

APPROVED:

John E. Green
Ching H. Yeh

DDC
RECEIVED
MAY 2 1978
A

DISTRIBUTION STATEMENT A
Approved for public release
Distribution Unlimited

6 AN EXPLORATORY PHOTOELASTIC INVESTIGATION OF POST-TENSIONED
CONCRETE ANCHORAGE ZONE BURSTING STRESSES

by

10 STEPHEN DONALD VAUGHN B.S., General

9 Master's THESIS,

Presented to the Faculty of the Graduate School of
The University of Texas at Austin
in Partial Fulfillment
of the Requirements
for the Degree of
MASTER OF SCIENCE IN ENGINEERING

12 106 p.

THE UNIVERSITY OF TEXAS AT AUSTIN

11 Aug 1977

347 800

ACCESSION FOR	
DTIC	When Searched <input checked="" type="checkbox"/>
DOC	Not Searched <input type="checkbox"/>
UNANNOUNCED	<input type="checkbox"/>
JUSTIFICATION	
Letter on file	
BT	
DISTRIBUTION/AVAILABILITY CODES	
Dist. Avail. and/or SPECIAL	
A	

nb

Dedicated to my parents, whose encouragement,
understanding, and constant support
are deeply appreciated.

ACKNOWLEDGMENTS

The author would like to express his sincere appreciation to Dr. John E. Breen, Chairman of the Supervisory Committee, for his guidance throughout the course of this study and his additional effort to help the author complete this investigation within a limited time frame imposed by external constraints. Special thanks are also due Dr. Ching-Hsie Yew, whose unselfish donation of time and expertise were essential to the completion of the photoelastic investigation.

Personal thanks are extended to fellow graduate students Bill Stone and Robert Holloway. They provided not only technical assistance during the course of this study, but also friendship and support when it was needed. Special thanks are also due Mr. James Steward, whose willingness to do more than was required of him in his position as machinist enabled the project to be completed on time and with a minimum of difficulty.

Like so many other graduate students before him, the author owes a special debt of gratitude to Maxine DeButts, who typed the report and provided tremendous assistance in the formulation of the final draft, and Tina Robinson, who during the entire period handled the procurement of all the materials required to conduct the investigation. Both of these special ladies were essential to the investigation's successful completion. Thanks are also extended to George Moden and Gorham Hinckley, who provided assistance and suggestions which greatly aided the author.

The research described herein was sponsored by the Texas Department of Highways and Public Transportation and the Federal Highway Administration.

S. D. V.

The University of Texas at Austin
May 1977

A B S T R A C T

✓ The use of post-tensioning prestressed concrete members is becoming increasingly popular in the United States. Span length requirements are becoming greater and the use of post-tensioned concrete members is the most economical solution for many of these longer spans.

Problems have arisen in the design of the anchorage zones of these members, however, as the post-tensioning force has caused cracking in several instances. The anchorage zone itself is a complicated stress region influenced by many different factors. While there have been numerous analytical studies of the stresses present in the anchorage zone, a general lack of insight into the nature of stresses present and the influence of various parameters on their distribution persists.

The exploratory investigation reported herein was undertaken to more closely examine the stresses found in the anchorage zone, utilizing the analysis method of photoelasticity. The investigation was to design an appropriate photoelastic model, develop appropriate testing procedures, and then conduct a series of tests varying anchorage zone parameters to determine their influence on the stresses created in the anchorage zone. K

After designing a photoelastic model to represent an existing post-tensioned concrete member anchorage zone and developing a testing procedure for the photoelastic analysis, a series of nine tests was conducted examining the effects of various parameters such as anchorage system type, load eccentricity, the use of multiple anchors, and tendon duct inclination. Recommendations were presented for the conduct of future photoelastic testing and for areas of

further investigation into the nature of stress distributions in anchorage zones. Conclusions were drawn concerning the effects of certain parameters on the stress distribution in the anchorage zone.

C O N T E N T S

Chapter		Page
1	INTRODUCTION	1
	1.1 General Discussion	1
	1.2 Objectives and Scope	2
	1.3 Problem Background	6
	1.4 Organization of This Investigation	12
2	PRINCIPLES OF TWO-DIMENSIONAL PHOTOELASTICITY	14
	2.1 Theory of Photoelasticity	14
	2.2 Photoelastic Testing Equipment and Procedures	27
	2.3 The Shear Difference Method of Stress Determination at an Interior Point	33
	2.4 Technique for Constructing Stress Trajectories from Isoclinic Patterns	38
	2.5 Methods of Confirming Photoelastic Results	41
3	TEST PROGRAM AND SPECIMEN DESCRIPTION	45
	3.1 Anchorage Models	45
	3.2 Concrete Anchorage Zone Model	52
	3.3 Loading System	64
	3.4 Problems Encountered	74
4	TEST RESULTS AND DISCUSSION	77
	4.1 General Discussion of Interpretation of Results	77
	4.2 Test #1--Symmetric Loading with Single Flat Bearing Anchor	80
	4.3 Test #2--Symmetric Loading with Single Inset Bearing Anchor	91
	4.4 Test #3--Symmetric Loading with Single Conical Anchor	100
	4.5 Test #4--Eccentric Loading with Single Flat Bearing Anchor	110
	4.6 Test #5--Single Flat Bearing Anchor with Inclined Tendon Duct	122
	4.7 Test #6--Web Cross Section with Single Tendon Duct	130

Chapter		Page
4.8	Test #7--Multiple Flat Bearing Anchors with Straight Tendons	139
4.9	Test #8--Multiple Flat Bearing Anchors with Inclined Tendons	152
4.10	Test #9--Web Cross Section with Two Tendon Ducts	157
5	DISCUSSION OF TESTING PROCEDURES AND RESULTS . . .	165
5.1	Testing Procedures	165
5.2	Test Results	169
6	RECOMMENDATIONS AND CONCLUSIONS	175
6.1	Recommendations for Further Photoelastic Testing	175
6.2	Recommendations for Further Anchorage Zone Investigations	177
6.3	Conclusions	177
APPENDIX A	SAMPLE CALCULATIONS FOR "SHEAR DIFFERENCE METHOD"	180
REFERENCES	188

L I S T O F T A B L E S

Table		Page
2.1	Summary of Polariscope Arrangements	31
3.1	Young's Modulus of Elasticity for Various Materials	46
A4.1	Test #1--Shear Stress	181
A4.2	Calculation of Normal Stresses--Test #1, Line 1 . .	182
A4.3	Calculation of Normal Stresses--Test #1, Line 2 . .	183
A4.4	Calculation of Normal Stresses--Test #1, Line 3 . .	184
A4.5	Calculation of Principal Stresses--Test #1, Line 1	185
A4.6	Calculation of Principal Stresses--Test #1, Line 2	186
A4.7	Calculation of Principal Stresses--Test #1, Line 3	187

LIST OF FIGURES

Figure		Page
1.1	Combination of end zone, radial and inclined wedge effect stresses	3
1.2	Two planes of reference for two-dimensional photoelastic analysis	5
1.3	Typical crack patterns developed in existing structures due to post-tensioning	7
1.4	Distribution of transverse and axial anchorage zone stresses as calculated by various investigations	9
2.1	Ether wave theory of light	16
2.2	The polarization of light	18
2.3	A representation of the effects of "circularly polarized light"	20
2.4	What happens in the plane polariscope	24
2.5	Transmission polariscope schematics	32
2.6	Determination of stress at interior points by Shear Difference Method	36
2.7	Construction technique for converting isoclinics to isostatics	40
3.1	Cooper's one-sixth scale model of anchorage systems	47
3.2	Flat bearing anchorage model	48
3.3	Inset bearing anchorage model	51
3.4	Conical bearing anchorage model	53
3.5	Cooper's one-sixth scale model of existing thin web prestressed bridge section	55

Figure		Page
3.6	Model for Test #1	58
3.7	Model for Test #2	58
3.8	Model for Test #3	60
3.9	Model for Test #4	60
3.10	Model for Test #5	61
3.11	Model for Test #6	61
3.12	Model for Test #7	63
3.13	Model for Test #8	63
3.14	Model for Test #9	65
3.15	Various boundary conditions for model and prototype	66
3.16	Test apparatus employed in investigation	68
3.17	Loading system elevation view	70
3.18	Loading system plan view	71
3.19	Photoelastic model frame	73
4.1	Test #1--Symmetric loading with single flat bearing anchor	81
4.2	Test #1--Isochromatic diagram, light field	82
4.3	Test #1 recorded isochromatics, light field	83
4.4	Test #1 stress trajectory	85
4.5	Test #1 isoclinic diagram	86
4.6	Test #1--Principal longitudinal stress Q	88
4.7	Test #1--Principal transverse stress P	89

Figure		Page
4.8	Test #2--Symmetric loading with single inset bearing anchor	92
4.9	Test Series #2 recorded isochromatics, light field	93
4.10	Test #2 isoclinic diagram	96
4.11	Test #2A isoclinic diagram	97
4.12	Test #2B isoclinic diagram	98
4.13	Test #2 stress trajectory	99
4.14	Test #3--Symmetric loading with single conical anchor	101
4.15	Test #3--Isochromatic diagram, light field	102
4.16	Test #3 recorded isochromatics, light field	103
4.17	Test #3 isoclinic diagram	105
4.18	Test #3 stress trajectory	106
4.19	Test #3--Principal longitudinal stress Q	107
4.20	Test #3--Principal transverse stress P	108
4.21	Test #4--Eccentric loading with single flat bearing anchor	111
4.22	Test #4 isochromatic diagram, light field	112
4.23	Test #4 recorded isochromatics, light field	113
4.24	Test #4 isoclinic diagram	114
4.25	Test #4 stress trajectory	116
4.26	Test #4--Principal longitudinal stress Q	117
4.27	Test #4--Principal transverse stress P	118

Figure		Page
4.28	Test #5--Single flat bearing anchor with inclined tendon duct	122
4.29	Test #5 isochromatic diagram, light field	123
4.30	Test #5 recorded isochromatics, light field	124
4.31	Test #5 isoclinic diagram	126
4.32	Test #5 stress trajectory	127
4.33	Test #5--Principal longitudinal stress Q	128
4.34	Test #5--Principal transverse stress P	129
4.35	Test #6--Web cross section with single tendon duct	131
4.36	Test #6 loading plan	132
4.37	Test #6 isochromatic diagram, light field	133
4.38	Test #6 recorded isochromatics, light field	134
4.39	Test #6 isoclinic diagram	135
4.40	Test #6 stress trajectory	137
4.41	Test #7--Multiple flat bearing anchors with straight tendons	139
4.42	Test #7 isochromatic diagram, light field	141
4.43	Test #7 recorded isochromatics, light field	142
4.44	Test #7 isoclinic diagram	143
4.45	Test #7 stress trajectory	144
4.46	Principal stress trajectories from Christodoulides' two-dimensional photoelastic test	146
4.47	Isochromatic fringes from Christodoulides' two-dimensional photoelastic test	147

Figure		Page
4.48	Isoclinic diagram from Christodoulides' two-dimensional photoelastic test	148
4.49	Test #7--Principal longitudinal stress Q	149
4.50	Test #7--Principal transverse stress P	150
4.51	Test #8--Multiple flat bearing anchors with inclined tendons	153
4.52	Test #8 isochromatic diagram, light field	154
4.53	Test #8 recorded isochromatics, light field	155
4.54	Test #8 isoclinic diagram	156
4.55	Test #8 stress trajectory	158
4.56	Test #9--Web cross section with two tendon ducts	159
4.57	Test #9 isochromatic diagram, light field	160
4.58	Test #9 recorded isochromatics, light field	161
4.59	Test #9 isoclinic diagram	162
4.60	Test #9 stress trajectory	164

CHAPTER 1

INTRODUCTION

1.1 General Discussion

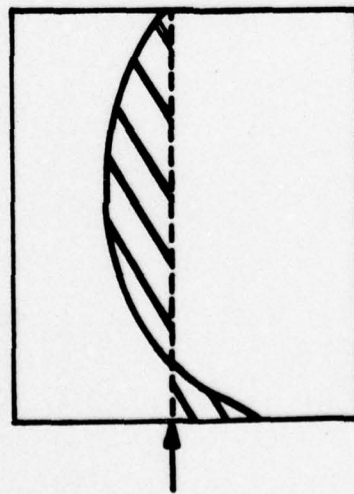
The use of post-tensioned prestressed concrete members in construction is becoming increasingly popular in the United States. Span-length requirements are becoming larger, and the use of post-tensioned concrete members in many cases offers the most economical solution for these larger spans. With this increased popularity, however, certain design problem areas have been identified. The proper design for the anchorage zones for these members is certainly one of these areas. The anchorage zone or end block of a post-tensioned concrete member is an extremely complicated area when considering the distribution of stresses. There is not a great deal of information for the proper design of anchorage zones provided the designer.¹ Recently problems have developed in several post-tensioned structures, due to cracking in the webs of their members, caused by stresses created in the anchorage zones.^{5,7} While there have been many analytical and some experimental investigations of the stresses created in anchorage zones, their results have not been widely published nor have they led to the generation of general design procedures. The problems encountered in these recently constructed structures indicate, however, the need for more exact design procedures and a better insight into the stresses created in the anchorage zone. Since this problem is associated with the cracking of the concrete and does not necessarily greatly affect the ultimate strength of the structure, the problem may be considered to be one of serviceability. Generally, prestressed concrete is considered

elastic until the formation of first cracking. In this case, since cracking occurs with essentially linear stress-strain relations, a method based on elastic analysis should provide insight into the problem. Photoelasticity has been used in the past with considerable success in the analysis of elastic regions with highly complex stress distributions,^{9,12,13,14,17} The study of the stresses created in the anchorage zone of a post-tensioned concrete member would appear to lend itself to a photoelastic investigation. This is not a new idea, and there have been limited photoelastic investigations of anchorage zones in the past.^{2,3,4} These investigations, however, have ignored many typical parameters and, thus, limited themselves to very unrealistic situations. This photoelastic investigation was initiated to go deeper into the subject by exploring numerous conditions typical of complex post-tensioning applications.

1.2 Objectives and Scope

The objectives of this study were:

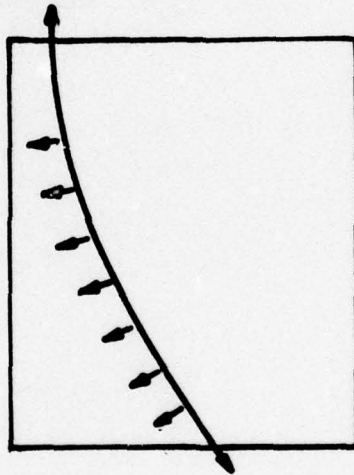
- (1) The development of a two-dimensional photoelastic model of the anchorage zone of a thin-web post-tensioned prestressed concrete member.
- (2) The development of a photoelastic testing procedure for these models.
- (3) The completion of a series of photoelastic tests to gain insight into the development of stresses in typical anchorage zones.
- (4) Identification of important parameters which affect the distribution of stress in the anchorage zone. (Figure 1.1 shows the variety of parameters which can affect the distribution of stresses and gives an indication of the complexity of the problem.)
- (5) Development of a source of directly measured data which could be used to verify other analytical or numerical methods of analysis.
- (6) Development of insight into the efficient and accurate conduct of future photoelastic studies in the same area.



END ZONE BURSTING STRESSES

influenced by

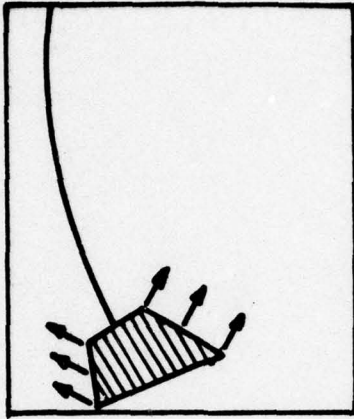
1. ANCHORAGE TYPE
2. ECCENTRICITY OF ANCHOR
3. NUMBER OF ANCHORS



RADIAL FORCES DUE TO TENDON CURVATURE

influenced by

1. TENDON LAYOUT



INCLINED WEDGE EFFECT

influenced by

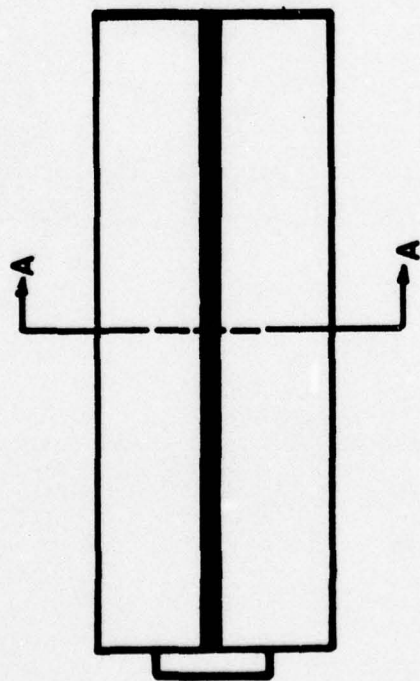
1. ANCHORAGE TYPE
2. TENDON LAYOUT

Fig. 1.1 Combination of end zone, radial and inclined wedge effect stresses

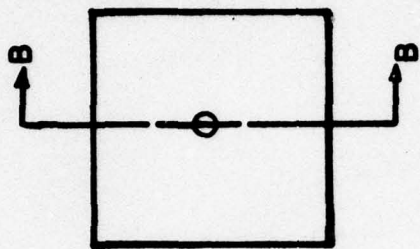
The scope of the study included a series of nine two-dimensional photoelastic tests. There were a variety of reasons why a two-dimensional study was selected as opposed to a three-dimensional study, even though the problem is in reality three-dimensional in nature. A three-dimensional test is much more difficult to conduct than a two-dimensional test and requires a great deal more in the way of facilities and specialized equipment.¹³ A three-dimensional investigation requires much more time than a two-dimensional investigation. The estimated time required to conduct a series of nine three-dimensional investigations would be prohibitive and would have taken two to three times the time required for a similar two-dimensional investigation. Since this was an exploratory investigation, the improvement in results expected from conducting a three-dimensional investigation as opposed to a similar two-dimensional investigation was not deemed critical enough to warrant the increase in time, equipment, and expense.

A major consideration in deciding on the scope of the testing program was the development of both an anchorage system model and an end block or anchorage zone model which reflected the proper dimensional relationships. An actual prototype post-tensioned concrete member would have to be selected and the models scaled and designed to reflect the existing prototype. Also, the models would have to be designed in such a manner that the actual methods which created stress in the prototype would be reflected in the model. The model would have to be versatile enough to show the effects of various parameters such as tendon duct geometry and anchorage system type.

The two-dimensional photoelastic study was conducted along two planes of reference through the prototype anchorage zone. The first plane of reference was the vertical plane running along the length of the tendon duct [see Fig. 1.2(a)], cutting through the web of the post-tensioned member. Christodoulides had shown in an



SECTION B - B



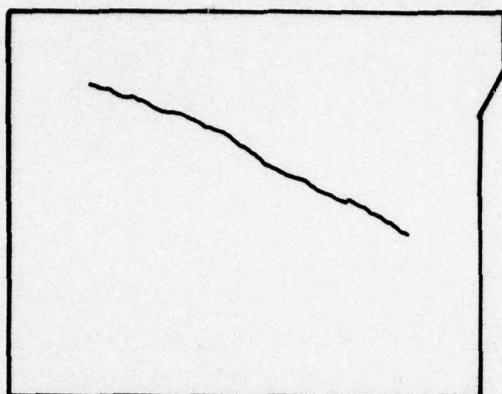
SECTION A - A
(TENDON CROSS SECT.)

Fig. 1.2 Two planes of reference for two-dimensional photoelastic analysis

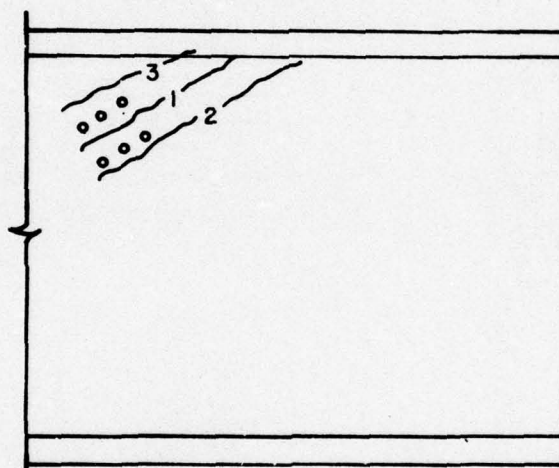
earlier two-dimensional study that this plane appeared to be the critical plane for creation of stresses in the member.^{2,4} The second plane of reference was a cross-sectional plane through the web of the member [Fig. 2.1(b)]. This plane was used to study the effects of the local tendon pressure due to the tendon duct in members with inclined or parabolic tendon duct geometries.

1.3 Problem Background

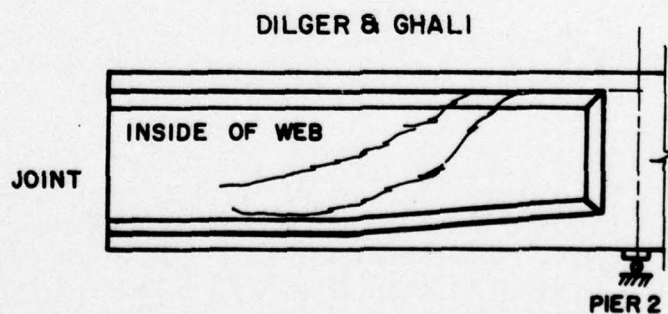
While extensive analytical and experimental investigations have been carried out in post-tensioned concrete, the behavior of anchorage zone stresses in post-tensioned concrete is still relatively unknown. Recently, several structures have developed problems with cracks forming in the webs of post-tensioned members near the anchorage zone. Figure 1.3(a) shows the cracking which developed in the web of a segmental box girder bridge on the John F. Kennedy Memorial Causeway in Corpus Christi, Texas, and Fig. 1.3(b) shows the cracking produced in a scale model of the same structure during an investigation conducted by Cooper.⁵ Dilger and Ghali⁷ made a study of the web cracking found in a post-tensioned prestressed box girder bridge, and Fig. 1.3(c) shows the typical crack patterns found in the webs of those post-tensioned members. Investigators, however, despite the need for design guidance indicated by these troubled structures, are not in agreement concerning the distribution of stresses in the anchorage zone. While several different analytical models have been developed by Ross,¹⁸ Gerstner and Zienkiewicz,¹⁰ Sievers,²² Douglas and Trahair,⁸ Bleich,²² Iyengar,^{22,23} Magnel,⁸ and Guyon²² (to name some of the more prominent), and some experimental work conducted by investigators such as Christodoulides,^{2,3} and Zielinski and Rowe,^{24,25} there is still no firm agreement on the distribution of stresses in the anchorage zone, nor is there any firm consensus on the effects of such variables as load eccentricity or tendon duct geometry.



(a) TYPICAL WEB CRACK CREATED DURING POST-TENSIONING OF JOHN F. KENNEDY MEMORIAL CAUSEWAY, CORPUS CHRISTI, TEXAS.



(b) TYPICAL CRACKING DUE TO POST-TENSIONING FOUND BY COOPER.



(c) TYPICAL WEB CRACKING FOUND BY DILGER AND GHALI.

Fig. 1.3 Typical crack patterns developed in existing structures due to post-tensioning

The analytical models all produce the same general distribution for both longitudinal and transverse stress, but they vary with respect to magnitude and specific orientation. Figure 1.4(a) through (f) shows the distribution and magnitude suggested for the transverse and longitudinal stresses produced in the anchorage zone by various investigators for similar loading conditions. Note that while all the investigators predict the same general shapes, there are marked differences in magnitude and orientation for the anchorage zone stresses predicted.

Another problem with the existing studies is that they deal with overly simplified models which depict unrealistic anchorage zone situations and neglect the effects of a broad range of variables such as tendon presence, anchorage eccentricity, and the presence of internal anchorage systems. Modern structures employ complex anchorage systems which may be offset, inclined, and consist of multiple systems which extend internally into the end block. The existing analytical and experimental investigations are not sufficient to predict the stresses created in the anchorage zones of these structures. The designer is left without guidance concerning the design of the anchorage zone. The American Concrete Institute Building Code (ACI 318-71) provides only the following extremely limited design guidance for end regions for prestressed concrete:¹

Reinforcement shall be provided when required in the anchorage zone to resist bursting, horizontal splitting, and spalling forces induced by the tendon anchorages. Regions of abrupt change in section shall be adequately reinforced.

End blocks shall be provided when required for end bearing or for distribution of concentrated prestressing forces.

Post-tensioning anchorages and the supporting concrete shall be designed to support the maximum jacking load at the concrete strength at time of prestressing and the end anchorage region shall be designed to develop the guaranteed ultimate tensile strength of the tendons at a ϕ of 0.90 for the concrete.

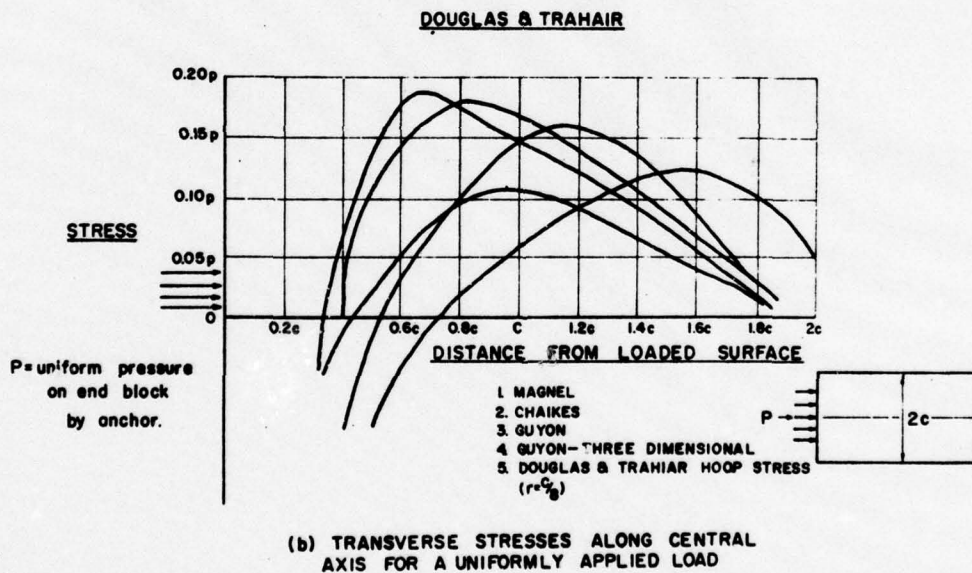
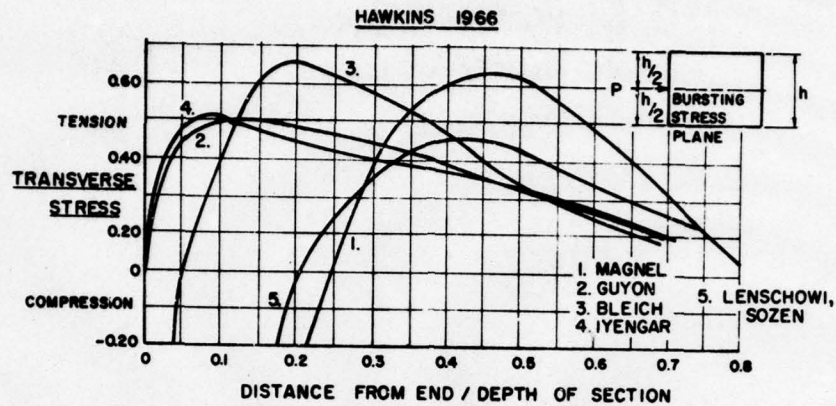
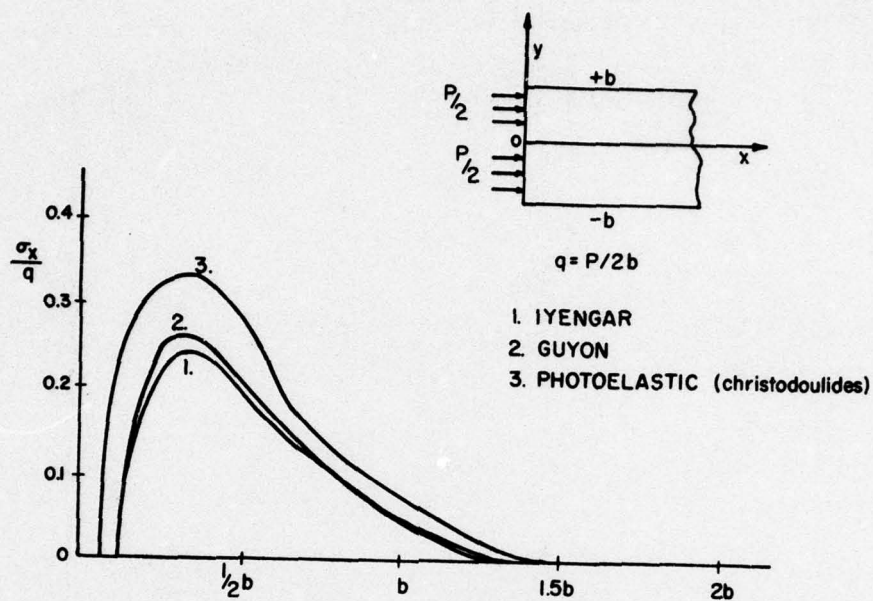
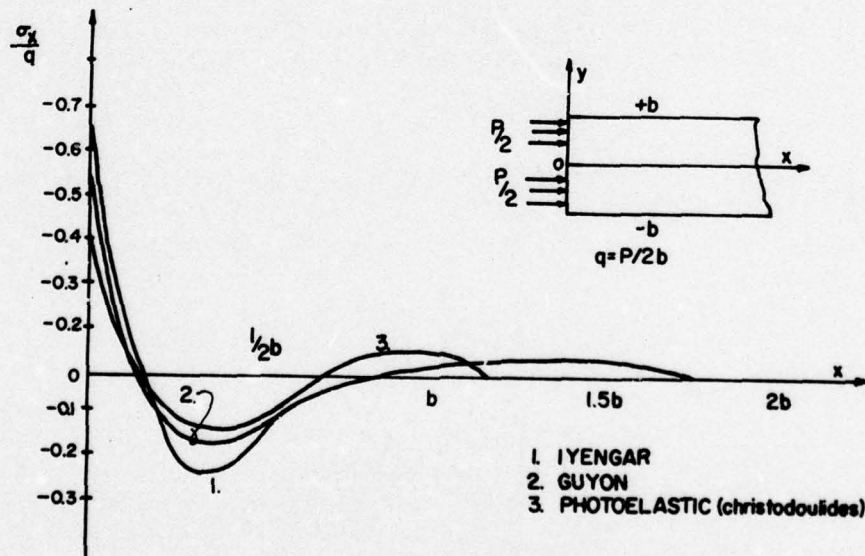


Fig. 1.4 Distribution of transverse and axial anchorage zone stresses as calculated by various investigations

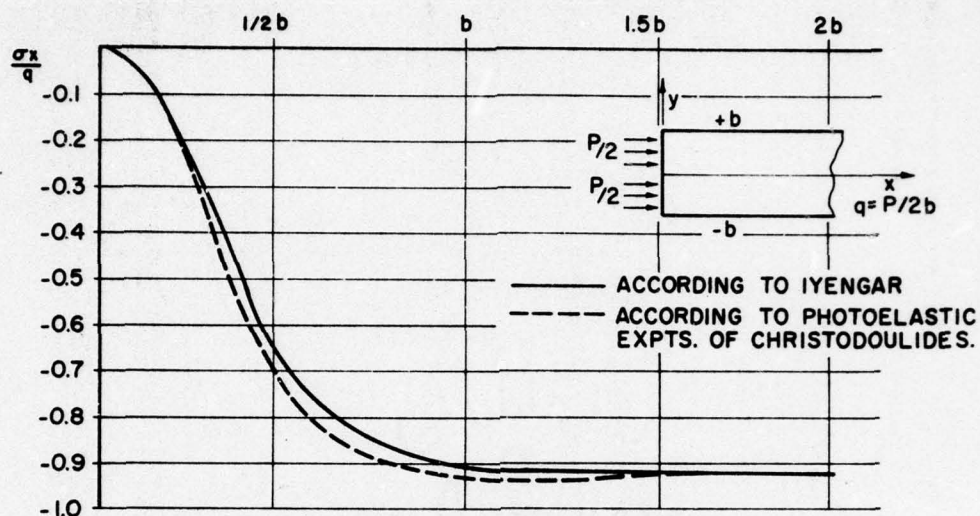


(c) DISTRIBUTION OF TRANSVERSE STRESS $+\sigma_y$ ALONG $y = b/2$ FOR TWO SYMMETRICAL FORCES

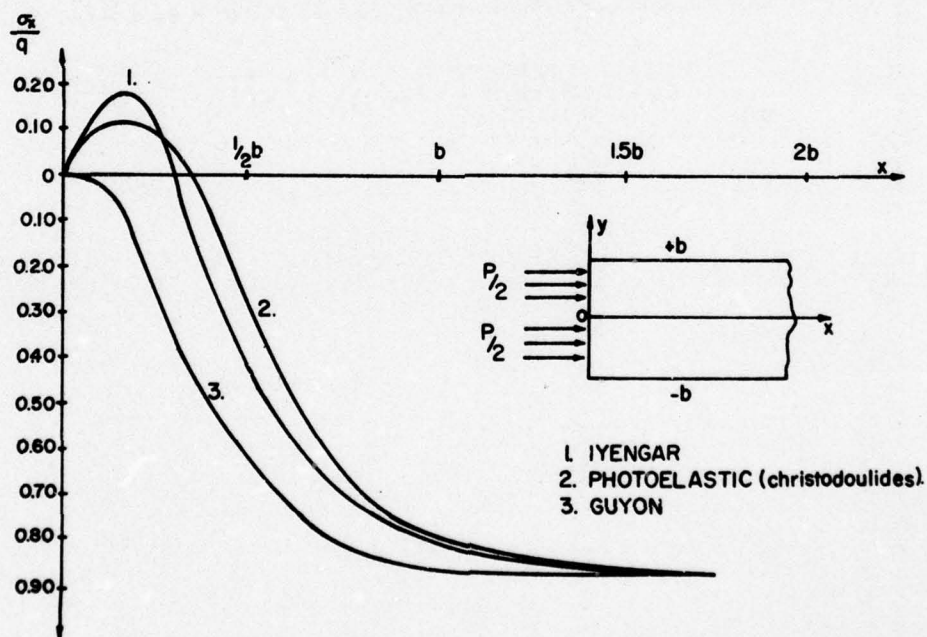


(d) DISTRIBUTION OF TRANSVERSE STRESS ALONG $y = 0$ FOR TWO SYMMETRICAL FORCES

Fig. 1.4 (Continued)



(e) DISTRIBUTION OF LONGITUDINAL STRESS σ_x ALONG $y=0$ FOR TWO SYMMETRICAL FORCES



(f) DISTRIBUTION OF LONGITUDINAL STRESS σ_x ON $y=b$ FOR TWO SYMMETRICAL FORCES

Fig. 1.4 (Continued)

These Code requirements offer no guidance in estimating the stresses created in the anchorage zone. Designers must consider stresses created by certain loading conditions when there is almost no agreement among current investigators as to the actual magnitude of the stresses created nor a method provided to calculate them. There is, therefore, a need for a comprehensive research program to investigate the nature of stress in the anchorage zone of typical post-tensioned concrete members, to provide insight into the distribution of stresses in the anchorage zone, and to generate design criteria to assist the designer.

1.4 Organization of This Investigation

This two-dimensional photoelastic investigation is included in a much larger research program which is underway at The University of Texas at Austin to determine typical post-tensioned concrete anchorage zone bursting stresses. The study includes these photoelastic studies as well as a finite-element analysis, and a comprehensive program of direct model testing. The photoelastic study was built upon the previous work of Cooper,⁵ who conducted an investigation into anchorage performance in post-tensioned thin-web box girder models. Cooper's models of an existing structure--the John F. Kennedy Memorial Causeway in Corpus Christi, Texas--were used as the basis for design of the photoelastic models, so that they would reflect an actual existing structure. The anchorage system models were also greatly influenced by Cooper's work so they would reflect prominent actual commercial anchorage systems. A series of nine separate tests was conducted to determine the feasibility of the photoelastic model designed, to develop good photoelastic testing procedures, and to study the effects of various parameters on the creating of stress in the anchorage zone.

The investigation is presented in the following manner. Chapter 2 consists of a discussion of the basic theory of

photoelasticity and the general procedures employed to conduct and analyze a photoelastic test. Chapter 3 discusses design considerations and the actual models used to represent the prototype anchorage systems and the anchorage zones for the nine-test series. Each test in the series is discussed separately. The loading system employed during the testing is explained, and a discussion of the problems encountered during the testing with respect to the models and the loading system is presented. Chapter 4 presents and discusses the test data from each of the nine tests in detail. Chapter 5 provides a discussion of the observations made concerning the design of the test models and procedures used to conduct the photoelastic investigation. Chapter 5 also analyzes the data presented in Chapter 4, with respect to various parameters which the tests were intended to investigate and presents conclusions concerning those parameters. Chapter 6 gives the final recommendations for the conduct of further photoelastic tests, and for further investigation into the distribution of anchorage zone stresses. Chapter 6 also includes a summary of results obtained from the photoelastic investigation concerning the distribution of stresses in the anchorage zone.

CHAPTER 2

PRINCIPLES OF TWO-DIMENSIONAL PHOTOELASTICITY

2.1 Theory of Photoelasticity

Relatively simple stress distribution problems can be handled successfully by mathematical methods. There are, however, many more complicated practical problems for which mathematical methods are inadequate. These more complicated problems require the use of experimental procedures. The photoelastic method is one of the best known and most useful of these experimental stress analysis methods and is widely used to solve for stress distributions in more complicated members.^{9,12,13,14} The photoelastic method is based upon the fact that, when certain transparent materials are stressed, their optical properties are changed and this change is measurable and can be directly related to the change in stress in the material. A model is constructed from a suitable material and is loaded in the same manner as the prototype. By a study of the optical properties of the model, the stress distribution in the model can be determined. Depending on the accuracy of the modeling process, the distribution can be related to the prototype. In this manner the actual state of stress in the prototype can be approximated and a better understanding of what stresses actually exist and are created in the prototype can be obtained.

Since the theory of photoelasticity is related very closely to many principles of optics, it is necessary to briefly review a few of these principles. Photoelasticity can be explained satisfactorily by means of the ether-wave theory of light. This theory states that light is the result of transverse vibration in a plane containing the ray of light, of all the particles lying along the

ray. It is further assumed that all these particles lie along a sinusoidal curve, the amplitude of which is $2a$ and the wavelength of which is λ (see Fig. 2.1). Assume that there are two particles m and n which vibrate between points A and B and C and D, respectively. Also, at time, $t = 0$, these particles are assumed on the solid curve in Fig. 2.1. Suppose that at some other time t_1 these particles have moved to positions m_1 and n_1 and now lie on the dashed curve. The effect of this transverse vibration of the particles has been to cause the curve connecting them to move to the right along the ray a distance ΔZ .

The rate of the apparent movement of the curve along the ray is called the velocity of light and is constant for the given medium through which the light is passing. For the sinusoidal curve to pass one point entirely, it is necessary that the particles of the wave undergo one complete cycle of vibration. The frequency of the particle vibrations is, therefore, the same as the frequency of the harmonic curve as it passes a given point. It is this frequency of vibration, f , which determines the color of light and is constant for any given color regardless of the medium through which the ray is passing. White light is light composed of waves of all frequencies. The velocity of light is equal to the product of the length of one complete wave and the frequency with which the waves pass a given point, or

$$v = \lambda f$$

Since the frequency for any given color of light is constant, the wavelength of that color varies directly with the velocity which is dependent on the medium through which the light is passing.

Since light is composed of waves, its individual components may be represented mathematically in the form

$$S = a \cos \frac{2\pi}{\lambda} (Z - \Delta Z + Z_0)$$

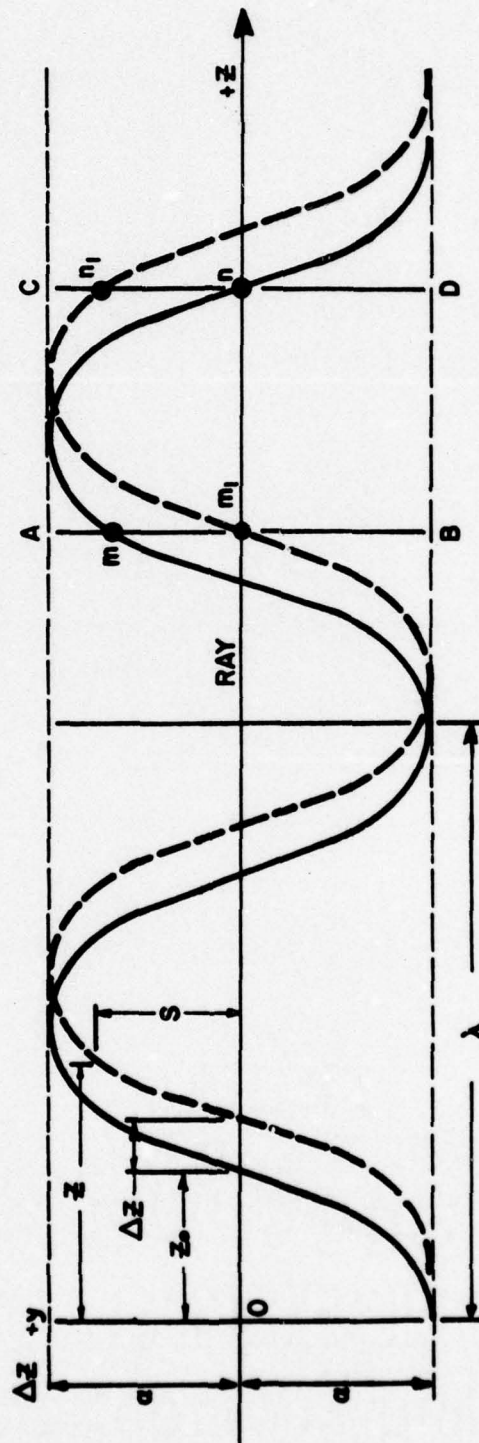


Fig. 2.1 Ether wave theory of light

where S = magnitude of vertical displacement of vibrating particle

Z = distance along the light ray from some reference point

$$\Delta Z = vt = \lambda ft$$

a = amplitude of vibration

Z_0 = a constant which shows initial horizontal displacement

In the case of light with just one frequency (monochromatic light) and in which both Z and Z_0 are equal to zero, the equation above may be reduced to the following expressions:

$$S = a \cos \frac{2\pi}{\lambda} (vt)$$

$$S = a \cos \frac{2\pi}{\lambda} (\lambda ft)$$

$$S = a \cos (2\pi f)t$$

$$S = a \cos pt, \text{ where } p = 2\pi f$$

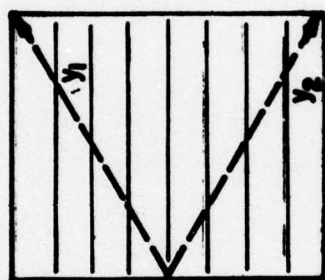
This final form shows that the magnitude of displacement varies harmonically with time, and that the light has a color dependency on the frequency, as indicated by the proportionality factor p .

The concept of polarized light is important to photoelasticity and should be defined. Ordinary light consists of waves vibrating in all planes which can be passed through the ray. If these vibrations are controlled in some manner or restricted to certain planes passing through the ray, then the light is said to be polarized. If the vibrations are restricted to one plane only, the light is said to be "plane polarized". Such light need not be monochromatic and may be produced by passing ordinary light through a Nicol prism, a Polaroid sheet, or some other device known as a "polarizer" (see Fig. 2.2).

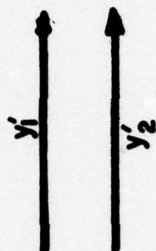
If, however, after passing through the polarizer, the light consists of two waves of equal amplitude and wavelength but is vibrating in perpendicular planes and is one-quarter of a wavelength out of phase, it is said to be "circularly polarized". This light



ACTUAL LIGHT



POLARIZER



PLANE POLARIZED LIGHT

Fig. 2.2 The polarization of light

is the product of passing plane-polarized monochromatic light through a "quarter-wave plate". The "quarter-wave plate" is some permanently doubly refractive material, the axes of which are set at 45° to the plane of polarization of the entering light. The thickness of the plate is such that one of the two component waves is slowed up a quarter of a wavelength with respect to the other. The component waves emerge on the far side of the quarter-wave plate one-quarter wavelength out of phase, equal in amplitude, and vibrating in perpendicular planes (see Fig. 2.3).

These fundamental concepts of the theory of light are needed to understand the actual theory of photoelasticity. Photoelasticity is the study of the stress distribution in a transparent material which is supporting an induced load and which remains in the elastic state. This study is accomplished by polarizing light and passing it through the material and then bringing this light back into the same plane of action by passing it through a final polarizer called an "analyzer". The patterns created by the interference and relative phase differences in this light as it is brought together give the necessary information to reconstruct the stress distribution in the model due to the loading. The entire concept of photoelasticity is founded on two fundamental optics laws of photoelasticity concerning what happens to light as it passes through a material which has induced stresses.¹³

- (1) Light passing through a material containing stresses is polarized in the directions of the principal stress axes and is transmitted only on the planes of principal stress.
- (2) The velocity of transmission in each principal plane is dependent on the intensities of the principal stresses in these two planes and obeys the following equations which have been simplified from a general case to represent situations of plane stress and normal incidence of light

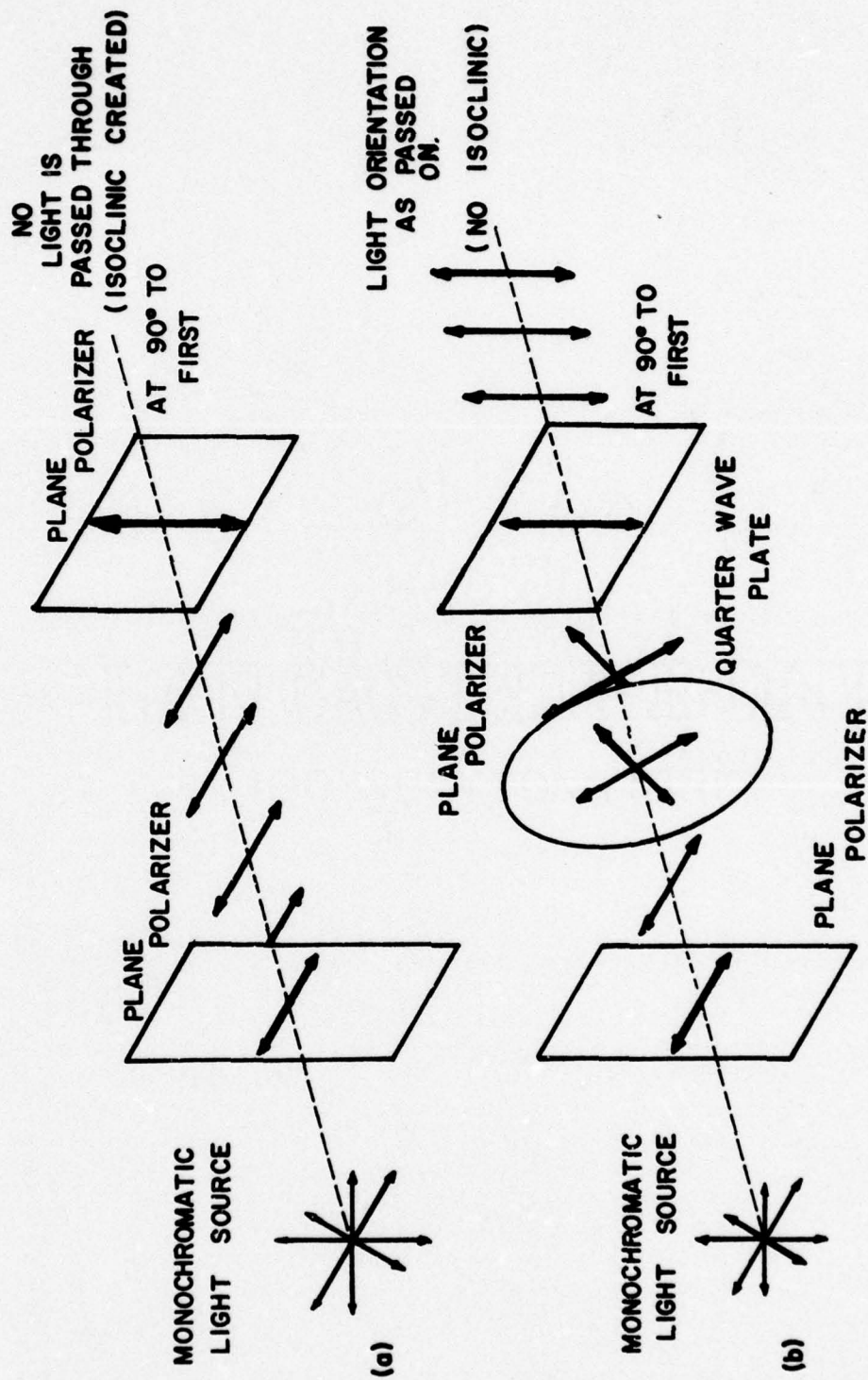


Fig. 2.3 A representation of the effects of "circularly polarized light"

$$\delta_1 = N_1 - N_0 = A\sigma_1 + B\sigma_2$$

$$\delta_2 = N_2 - N_0 = B\sigma_1 + A\sigma_2$$

where δ_1 = change in refractive index on No. 1 principal plane

δ_2 = change in refractive index on No. 2 principal plane

N_0 = refractive index of unstressed material

N_1 = refractive index of No. 1 principal plane
= V/V_1

N_2 = refractive index of No. 2 principal plane
= V/V_2

σ_1, σ_2 = principal stresses in material where the light is passing through the medium

A, B = photoelastic constants of the material

The refractive index is the ratio of the respective velocities of light as it passes through two separate mediums

$$\text{Index of Refraction} = \frac{\text{Velocity in 1st Medium}}{\text{Velocity in 2nd Medium}}$$

A direct relationship can be derived using the second optics law of photoelasticity between the properties of the propagated light and the internal stresses of the medium through which the light passes.

$$\delta_1 - \delta_2 = N_1 - N_2 = (A - B)(\sigma_1 - \sigma_2)$$

$$\delta_1 - \delta_2 = C(\sigma_1 - \sigma_2) \text{ where } C = (A - B)$$

From the definition of the refractive index

$$\delta_1 - \delta_2 = \frac{V}{V_1} - \frac{V}{V_2} = \frac{V(V_2 - V_1)}{V_1 V_2}$$

where V = velocity of light in unstressed material

V_1 = velocity of light along stress plane No. 1

V_2 = velocity of light along stress plane No. 2

$$\frac{v(v_2 - v_1)}{v_1 v_2} = C(\sigma_1 - \sigma_2) \quad (1)$$

If h represents the thickness of the photoelastic material along the path of the light, then

$$\left. \begin{aligned} t_1 &= \frac{h}{v_1} \\ t_2 &= \frac{h}{v_2} \end{aligned} \right\} \text{where } t_1 \text{ and } t_2 = \text{respective times of} \\ \text{passage of light through} \\ \text{the medium}$$

and

$$t_1 - t_2 = h \left(\frac{1}{v_1} - \frac{1}{v_2} \right) = h \left(\frac{v_2 - v_1}{v_1 v_2} \right)$$

Therefore

$$\frac{v_2 - v_1}{v_1 v_2} = \frac{t_1 - t_2}{h} \quad (2)$$

Substituting Eq. (2) into Eq. (1)

$$v \left(\frac{t_1 - t_2}{h} \right) = C(\sigma_1 - \sigma_2)$$

and

$$t_1 - t_2 = \frac{C h}{v} (\sigma_1 - \sigma_2) \quad (3)$$

and

$$\rho(t_1 - t_2) = \rho \left[\frac{C h}{v} (\sigma_1 - \sigma_2) \right]$$

Equation (3) shows that the phase difference of light waves emerging from the model, $\rho(t_1 - t_2)$, is directly proportional to the difference between the principal stresses. It is also proportional to the model thickness h and an optic constant for the material and surrounding medium C/v . "Thus any method that can be employed to determine this phase difference can be used as a measure of the difference between the principal stresses."¹³

Figure 2.4 shows a schematic representation of the photoelastic principle. Below the schematic path of the light are vector representations of the light displacement and its appropriate mathematical expression during the course of the light's journey from the source through the polarizer and model until it is brought into the same plane by the analyzer. Note that as the light travels through the model it is oriented along the principal stress axes and goes through phase modification. If the analyzer's plane of transmission is at right angles to the polarizer's plane of transmission, the components of the two vibrations emerging from the model which will be transmitted by the analyzer are represented by

$$\begin{aligned} & a \cos \alpha \sin \alpha \cos \rho(t - t_1) \\ \text{and} \quad & a \sin \alpha \cos \alpha \cos \rho(t - t_2) \end{aligned}$$

After passing through the analyzer, these components will lie in the same plane and they may be added algebraically to give the expression for the resulting vibration.

$$\begin{aligned} & a \cos \alpha \sin \alpha [\cos \rho(t - t_1) - \cos \rho(t - t_2)] \\ \text{Resultant} = & a \sin 2\alpha \sin \rho\left(\frac{t_1 - t_2}{2}\right) \sin \rho\left(t - \frac{t_1 + t_2}{2}\right) \end{aligned} \quad (4)$$

The resultant light amplitude leaving the analyzer is a function of the angle α (principal stress axes) and the phase difference $\rho(t_1 - t_2)$ and, thus, is influenced by the direction of principal stress and the difference in principal stress.

By examining Eq. (4) it may be shown that a dark spot will occur on the light emerging from the analyzer at every point where

$$a \sin 2\alpha \sin \rho\left(\frac{t_1 - t_2}{2}\right) = 0$$

These dark spots are usually linked together to form loci representing one of two conditions. The first condition is when $\alpha = 0$,

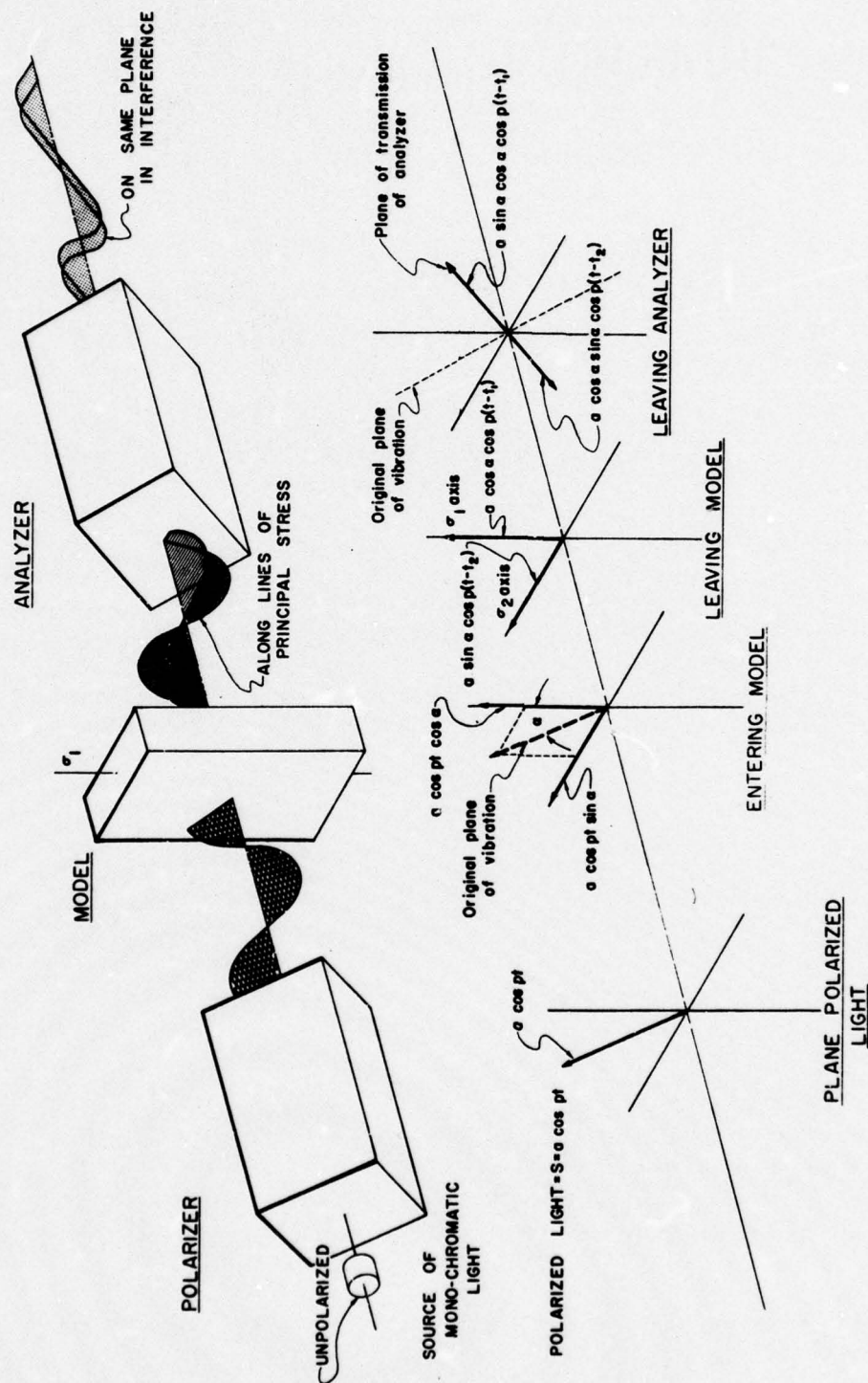


Fig. 2.4 What happens in the plane polariscope

or 90° . The loci of such points are called "isoclinics" and they are the locus of points where the principal axes of stress all have the same orientation with some reference axes, such as the axes of the plane of propagation of the polarizer. This is a very useful fact, since by rotating the polarizer through a series of known orientations with a reference axes and recording the isoclinics for each orientation of the polarizer, the orientation of the principal axes of stress at any point in the model may be determined.

The second condition creating a locus of dark spots is when

$$\sin \rho\left(\frac{t_1 - t_2}{2}\right) = 0$$

This condition will take place at all locations where

$$\rho\left(\frac{t_1 - t_2}{2}\right) = 0 \text{ or } n\pi \text{ where } n = \text{any integer}$$

Conversely, a maximum intensity will take place at all locations where

$$\rho\left(\frac{t_1 - t_2}{2}\right) = \frac{\pi}{2} \text{ or } (n + 1/2)(\pi) \quad n = \text{any integer}$$

A series of light and dark contours are created which are known as "isochromatics". Since it has previously been shown that phase difference in light waves is directly proportional to principal stress difference, then these isochromatic fringes relate points of equal difference in principal stress.

$$\rho\left(\frac{t_1 - t_2}{2}\right) \text{ is proportional to } (\sigma_1 - \sigma_2)$$

and

$$\sigma_1 - \sigma_2 = \frac{V}{C h} (t_1 - t_2) \quad \text{Eq. (3)}$$

Therefore

$$(\sigma_1 - \sigma_2) = \frac{f}{h} \times n \quad (5)$$

where $f = V/C = \text{a material constant determined experimentally}$

$h = \text{thickness of material light passes through}$

n = order of interference of isochromatic line since n is directly related to $\rho(\frac{t_1 - t_2}{2})$

Thus, through photoelasticity and the laws of optics, for any given point on a model, two very important properties of the stress at that point can be determined. One property is the value of the angle of the axes of principal stress with a predetermined axis of orientation. The second property is the value of the difference in the principal stresses at a point. The difference in principal stresses will give directly the maximum shear stress at any point in the model and will give the actual stress at the boundary of the model, since one of the principal stresses at a free edge is equal to zero. From the isoclinic parameters recorded, the stress trajectories may be plotted which give an overall graphic representation of the directions of the principal stresses (see Sec. 2.4). Also, the value of stress at any interior point may be calculated from the data obtained by a photoelastic analysis. There are several methods available for the determination of stress at interior points. The "Shear Difference Method" of stress determination at interior points was employed in this study and will be discussed later in greater detail.

There is one problem in photoelasticity which must be carefully avoided. Since both isoclinics and isochromatics are created at the same time, great care must be taken to know which is which. To eliminate isoclinics from isochromatics, the use of circularly polarized light and a quarter-wave plate is employed. The circularly polarized light will not disrupt the phase difference of light as it passes through the model, but it will reorient the planes of propagation of the light from the polarizer to the analyzer in such a manner as to eliminate the creation of isoclinics (see Fig. 2.3). To prevent isochromatics from interfering with isoclinics, a small load is applied to the model which creates very small stresses and, hence, few isochromatics, but still will properly align the axes of

principal stress and produce the required isoclinics which are independent of magnitude of stress.

2.2 Photoelastic Testing Equipment and Procedures

The principal piece of equipment in a photoelastic study is the polariscope. The polariscope is an arrangement of optical equipment which when employed together transmit, polarize, and record light waves in such a manner as to make use of the optical laws of photoelasticity and allow for the determination of and orientation of the stresses within the model being studied. The components of a polariscope will vary with the type of polariscope being used. There are two basic types of polariscopes, transmission and reflection. This discussion will be limited to the transmission polariscope, as it was the type employed for the study.

The transmission polariscope works by actually passing light through a transparent medium as opposed to reflecting the light from the surface of a nontransparent medium which is how the reflection polariscope works. The transmission polariscope may be further broken down into a plane polariscope or a circular polariscope. The plane polariscope does not employ the quarter-wave plates and, hence, is used in the recording of isoclinics. The circular polariscope does employ the quarter-wave plates and by circularly polarizing the light, eliminates the creation of isoclinics and allows only isochromatics to be formed (see Fig. 2.3).

The basic components of the transmission polariscope consist of the following (see Fig. 2.5):

- (1) light source and collimator
- (2) polarizer
- (3) quarter-wave plate
- (4) analyzer
- (5) photoelastic specimen and loading apparatus
- (6) method of recording data

The light source for the polariscope should have the capability of being either a white light source or a monochromatic source (only one frequency of light produced). This will require the necessary filters to remove all light frequencies but the single desired frequency for the monochromatic light. The lamp itself should be very powerful and it is suggested that a mercury vapor lamp or a lamp of equivalent strength be employed. A collimator should be used to direct and focus the light into the desired region. The polarizer and analyzer are both used to polarize the light from the source onto one plane of propagation. The polarizer orients the light prior to its passing through the model and the analyzer takes the light after it has passed through the model and reorients it into one common plane for analysis. The quarter-wave plates, as mentioned before, are used to circularly polarize the light from the polarizer so that light will be transmitted through the analyzer even if the polarizer and analyzer are set at right angles to one another and would fail to transmit light without the quarter-wave plates (a common setup). The photoelastic specimen and loading apparatus are designed to simulate the prototype being studied and to approximate its actual loading conditions as closely as possible. The experimenter should determine what method of recording the formation of the isoclinics and isochromatics he desires to utilize. He may employ a camera and take photographs of the data or he may just use a screen to observe what is formed. It should be remembered, however, that most solutions for photoelastic studies require hours of analysis and the method of recording the data should in most cases be permanent if it is to be useful.

The polarizer and analyzer may be thought of as slots which will only pass the components of the light wave which are parallel to the slot. If the transmission planes of the polarizer and analyzer are at right angles to each other and no stressed model is present, then the light will be completely extinguished. If a

stressed model is placed in the light's path between the polarizer and analyzer, it will break the light into two components along its axes of principal stress and the analyzer will pass that component of the light which is parallel to its slot. This situation is known as a "dark field polariscope," since only the model appears light and the surrounding field is dark. The isoclinics will appear as dark lines, since the polarizer and axis of principal stress are the same and no component of light passing through the model is created which the analyzer will transmit. Black isochromatic fringes will represent integral orders of interference. If, on the other hand, the polarizer slot and analyzer slot are parallel to each other, then all light will be passed and the opposite situation is created, in that isoclinic lines are now light and black isochromatic fringes now indicate half orders of interference. Such a situation is described as a "light field polariscope," since the background to the model is now light.

The quarter-wave plate may be thought of as a slot which transmits light waves at a 45° angle to the polarizer and analyzer (Fig. 2.3). One is usually placed before and after the model to eliminate the transmission of isoclinics by not allowing light transmitted along a principal axis of stress in a model to orient itself with the analyzer in such a manner that no component of it can be transmitted by the analyzer. Since there are two quarter-wave plates, they may either augment each other by being oriented along the same 45° axis or they may be in opposition by being oriented along opposite 45° axes or 90° apart from each other.

During the course of the photoelastic study, the polarizer and analyzer and the quarter-wave plates will be rotated through various orientations to properly record the isoclinics for various angular changes from the reference axis and to properly record the isochromatic pattern. The experimenter must constantly keep in mind

the orientation of his polariscope and the type of field being used to produce his data, if he is to properly analyze his data.

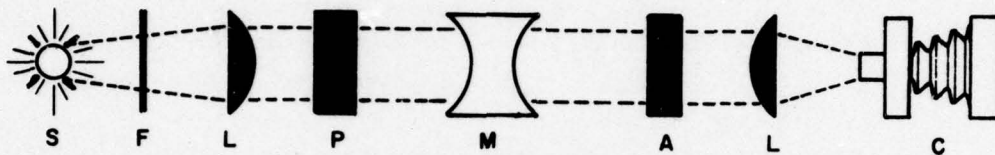
Table 2.1 discusses the basic polariscope orientations and gives the type of field produced, along with the integral values for the fringe constants in each case.¹³

The basic procedures to conduct a photoelastic study of a test specimen are not complicated. Once the proper model and loading system have been designed, the process is identical for almost every two-dimensional photoelastic study. The polariscope is positioned and the optics are checked to ensure the proper settings and focal distances for all lenses, so that clear, precise pictures are created. Orientations are checked to ensure the light rays are normal to the plane of the model. The unloaded model is checked to assure no residual stresses are present which would confuse the actual data from the loading. If residual stresses are present, then corrective action must be taken to remove them prior to testing. If the model is clear of residual stresses, then load is introduced to the model. Using a circular polariscope to eliminate isoclinics and recording the type field employed (Table 2.1), the development of isochromatic fringes are carefully observed so that the proper fringe order of interference (n) can be given to each fringe. When sufficient isochromatic fringes have been developed and ensuring the model is still elastic (no cracking), then the isochromatic pattern is recorded, usually using a camera. The picture is properly indexed and the values of applied load and pertinent data are properly tabulated. The load is then reduced on the model and the quarter-wave plates are removed from the polariscope creating a plane polariscope. Sufficient load is left to create isoclinic lines, but to minimize isochromatic interference. Also, the use of white light will facilitate this separation, since isochromatics (except for zero order isochromatics) will be of varying colors and isoclinics will be black as long as a dark field

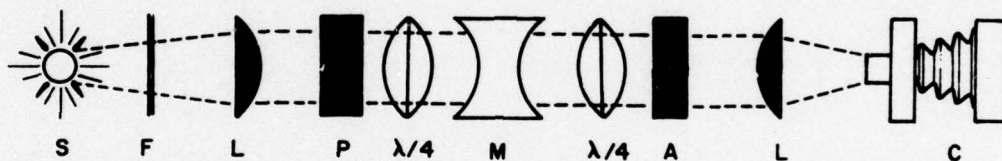
TABLE 2.1 SUMMARY OF POLARISCOPE ARRANGEMENTS

Type of polariscope	Arrangement	Field	Isoclinics	With monochromatic light, black isoclinic represents
Plane	Polarizer and analyzer crossed at 90°	Dark	Black	Integral orders of interference
	Polarizer and analyzer parallel	Light	Light	Half orders of interference
Circular	Equivalent of crossed polarizer and analyzer with $\lambda/4$ plates in opposition	Dark	Not shown	Integral orders of interference
	Equivalent of crossed polarizer and analyzer with $\lambda/4$ plates augmenting each other	Light	Not shown	Half orders of interference
	Equivalent of parallel polariscope and analyzer with $\lambda/4$ plates augmenting each other	Dark	Not shown	Integral orders of interference
	Equivalent of parallel polariscope and analyzer with $\lambda/4$ plates in opposition	Light	Not shown	Half orders of interference

PLANE TRANSMISSION POLARISCOPE



CIRCULAR TRANSMISSION POLARISCOPE



- S = MONOCHROMATIC LIGHT SOURCE
- F = LIGHT FILTER
- L = LENSE AND COLLIMATOR
- P = POLARIZER(WITH VARIABLE PLANE OF TRANSMISSION)
- $\lambda/4$ = QUARTER WAVE PLATE
- A = ANALYZER(WITH VARIABLE PLANE OF TRANSMISSION)
- C = CAMERA OR RECORDING DEVICE
- M = MODEL

Fig. 2.5 Transmission polariscope schematics

orientation is used. The planes of propagation of the polarizer and analyzer are kept crossed and are calibrated to a set of reference axes. Pictures are then recorded from the isoclinic patterns created as the axes of the polarizer and analyzer are rotated through 90° at set increments, so that the corresponding orientation of the principal axes of stress to the reference axes may be recorded. Care is taken to record the orientation of the axes of the polarizer and analyzer with the chosen reference axes for each recorded drawing, in order that all data may eventually be placed on one drawing containing all the isoclinic parameters for each angular rotation of the polarizer and analyzer. Once this has been completed, all necessary data have been recorded. For all points on the model, the directions of the principal stresses, the difference between the principal stresses, and the individual values of the principal stresses along free boundaries are now known.

2.3 The Shear Difference Method of Stress Determination at an Interior Point

The final data necessary for a complete photoelastic study is the determination of the value of stress at interior points within the model. While there are various methods to accomplish this task, one of the simplest, and the one employed in this study, is the Shear Difference Method.^{6,9,12,13,14} This method is derived quite readily from the theory of elasticity. The theory of elasticity gives the following relationship

$$\frac{\partial \tau_x}{\partial x} + \frac{\partial \tau_{xy}}{\partial y} + x = 0 \quad (6)$$

$$\frac{\partial \sigma_y}{\partial y} + \frac{\partial \tau_{xy}}{\partial x} + y = 0 \quad (7)$$

where σ_x, σ_y = normal stresses on the x and y planes
 τ_{xy} = shearing stress intensity on the x and y planes
 x, y = body forces per unit volume in the x and y directions

If the above equations are integrated and the body forces are set equal to zero since their influence is usually very small in comparison with the effect of the applied load, Eqs. (6) and (7) may be rewritten in the form below:

$$\sigma_x = (\sigma_x)_o - \int \frac{\partial \tau_{xy}}{\partial y} dx \quad (8)$$

$$\sigma_y = (\sigma_y)_o - \int \frac{\partial \tau_{xy}}{\partial x} dy \quad (9)$$

where $(\sigma_x)_o, (\sigma_y)_o$ = values of σ_x and σ_y at a given location which is known or can be obtained

These integrals may be closely approximated by using small finite particles and summing finite increments. The resulting expressions are approximations which, depending on the size of the increments between elements, can be quite accurate.

$$\sigma_x = (\sigma_x)_o - \sum \frac{\Delta \tau_{xy}}{\Delta y} \Delta x \quad (10)$$

$$\sigma_y = (\sigma_y)_o - \sum \frac{\Delta \tau_{xy}}{\Delta x} \Delta y \quad (11)$$

These final expressions may be used to determine the value of stress at internal points in the model using only the data obtained from the polariscope and photoelastic study. The value of τ_{xy} is related to the principal stresses by the following equation:

$$\tau_{xy} = \frac{(\sigma_1 - \sigma_2)}{2} \sin 2\theta \quad (12)$$

where θ = acute angle between the direction of the principal stress σ_1 and the plane on which τ_{xy} acts

The value of $(\sigma_1 - \sigma_2)$ is obtained from the isochromatic fringe orders and the value of θ may be determined from the isoclinics by correcting the angle of rotation ϕ by an amount equal to the difference in orientation between the direction of τ_{xy} and the reference axis used to determine ϕ initially. It is important to keep the proper algebraic sign for τ_{xy} , since it can change (especially during a graphical integration).

Hetényi gives a step-by-step procedure using Eqs. (10) through (12) to solve for the stress at interior points in a photo-elastic model. The following steps are Hetényi's suggested procedure:¹³

(1) On a large-scale drawing of the model, draw in the line A-A along which it is desired to determine the distribution of the stresses (Fig. 2.6). Divide A-A into a number of equal parts and arrange the coordinate axes and origin conveniently, so that the origin falls at one end of A-A (at the edge of the model) and on one of the axes along it.

(2) On either side of A-A draw B-B and C-C at equal distances from A-A and separated by a total distance equal to the length of the uniform intervals already marked off along A-A. This makes $\Delta x = \Delta y$ and

$$\sigma_y = \sigma_y|_0 - \int \Delta \tau_{xy} \quad \text{from Eq. (11)}$$

$\Delta \tau_{xy}$ = difference in τ_{xy} at elementary particle on A-A from B-B to C-C

$$\sigma_y|_0 = 0 \text{ at boundary}$$

(3) Determine the positions at which the isochromatic and isoclinic lines intersect sections B-B and C-C, and for each

[illegible]

Fig. 2.6 Determination of stress at interior points by Shear Difference Method

section plot separate curves for fringe order and angle of orientation θ , both as functions of distance along the section (y in this case). Attempt to make smooth fit curves in order to minimize error for mean values of observations.

(4) From the curves in step 3 scale off ordinates at the midpoints of the intervals chosen on A-A and compute the values for τ_{xy} from the corresponding values for n and θ at these midpoints. These values are then plotted along the y-axis for sections B-B and C-C and these curves represent the distributions of the shear stress along the rectangular elements formed by marking off A-A and sections B-B and C-C.

(5) The difference in shear stress from B-B to C-C at points corresponding to the middle of each interval represents $\Delta\tau_{xy}$ in Eq. (11) in step 2 and is numerically equal to $\Delta\sigma_y$, the change in normal stress in the y direction along A-A from one station to another. By starting at the boundary $(\sigma_y)_0 = 0$, the summation of the values of $\Delta\tau_{xy}$ will give the value of σ_y at an interior point as indicated by the equation.

(6) A more exact procedure for finding the increment $\Delta\sigma_y$ would be to employ the equation directly and find the area enclosed between two intervals along y between τ_{xy} on B-B and C-C, which is equal to $\Delta\tau_{xy} \cdot \Delta y$ for the interval and then divide by the constant Δx for the change σ_y between the points

$$\frac{\text{Area EFJK}}{\Delta x} = \Delta\sigma_y \text{ from point 1 to point 2}$$

(7) When σ_y at all the desired points along A-A has been calculated, then σ_x , the normal stress at right angles to A-A, can be calculated from the following relationship:

$$\sigma_x = \sigma_y + (\sigma_1 - \sigma_2) \cos 2\theta \quad (13)$$

Once σ_x is known, then the principal stresses at the selected points along line A-A may be calculated using these final relationships:

$$\sigma_1 = \frac{\sigma_x + \sigma_y}{2} + \frac{\sigma_1 - \sigma_2}{2} \quad (14)$$

$$\sigma_2 = \frac{\sigma_x + \sigma_y}{2} - \frac{\sigma_1 - \sigma_2}{2} \quad (15)$$

While in principle the Shear Difference Method is quite simple, there should be a note of caution for any person who intends to use it. The first consideration is that an approximate solution is being employed. If the data are of sufficient precision, then accurate results may be obtained. However, it is not an exact solution. Also, the error using this solution is additive in nature and appreciable errors may develop. Since the value of σ_y determined by this method may represent the evaluation of a small difference between two relatively large quantities, the percentage error may be great. Also, for cases in which the results largely depend on σ_y , one should be prepared to expect appreciable errors. If σ_y is small relative to $(\sigma_1 - \sigma_2) \cos 2\theta$, then relatively precise results for σ_x may be expected; but, if the opposite case is true, then σ_x may have sizable error. Decreasing the size of Δx and Δy will decrease error considerably, but the experimenter must be careful to have data which are precise enough to warrant reductions in the size of Δx and Δy . In essence, the more precise the data and the smaller the intervals of integration, then the more precise the results.

2.4 Technique for Constructing Stress Trajectories from Isoclinic Patterns

Isoclinic parameters unfortunately give the direction of principal stresses in a form which is extremely difficult to interpret. Due to this fact, it is popular to use the isoclinic

parameters to construct a stress trajectory diagram or isostatic diagram. Chapter 4 of this study contains isostatic or stress trajectory diagrams for all nine photoelastic tests conducted (see Fig. 4.4). These stress trajectories are lines where the principal stresses are normal and tangent at each point. The isostatic diagrams give a more easily understood picture of the flow of stress in an area. They do not, however, relate intensity of stress nor should they be interpreted as lines of equal stress. They show orientation of principal stress only.

The first step in the construction of a stress trajectory diagram is to produce a consolidated isoclinic diagram which consists of a composite drawing showing all the isoclinic parameters. There are certain rules concerning the drawing of isoclinics which must be remembered when drawing the composite isoclinic diagram.⁶ These rules are:

- (1) Isoclinics of all parameters must pass through isotropic or singular points.
- (2) An isoclinic of one parameter must coincide with an axis of symmetry in the model if an axis of symmetry exists.
- (3) The parameter of an isoclinic intersecting a free boundary is determined by the slope of the boundary at the point of intersection.
- (4) Isoclinics of all parameters pass through points of concentrated load.

Once the composite isoclinic diagram has been drawn, the stress trajectories may be drawn from it. It is easiest to use tracing paper as an overlay to draw the stress trajectories. Placing the tracing paper over the isoclinic drawing allows the outline of the model to be traced and the outline of the individual parameters to be seen. The correct procedure to use is outlined below and shown graphically in Fig. 2.7. The stress trajectories are initiated on a zero degree isoclinic from arbitrarily spaced points. It is usually best to select a boundary as the zero degree isoclinic if at all possible. Lines labeled 1 in Fig. 2.7 and

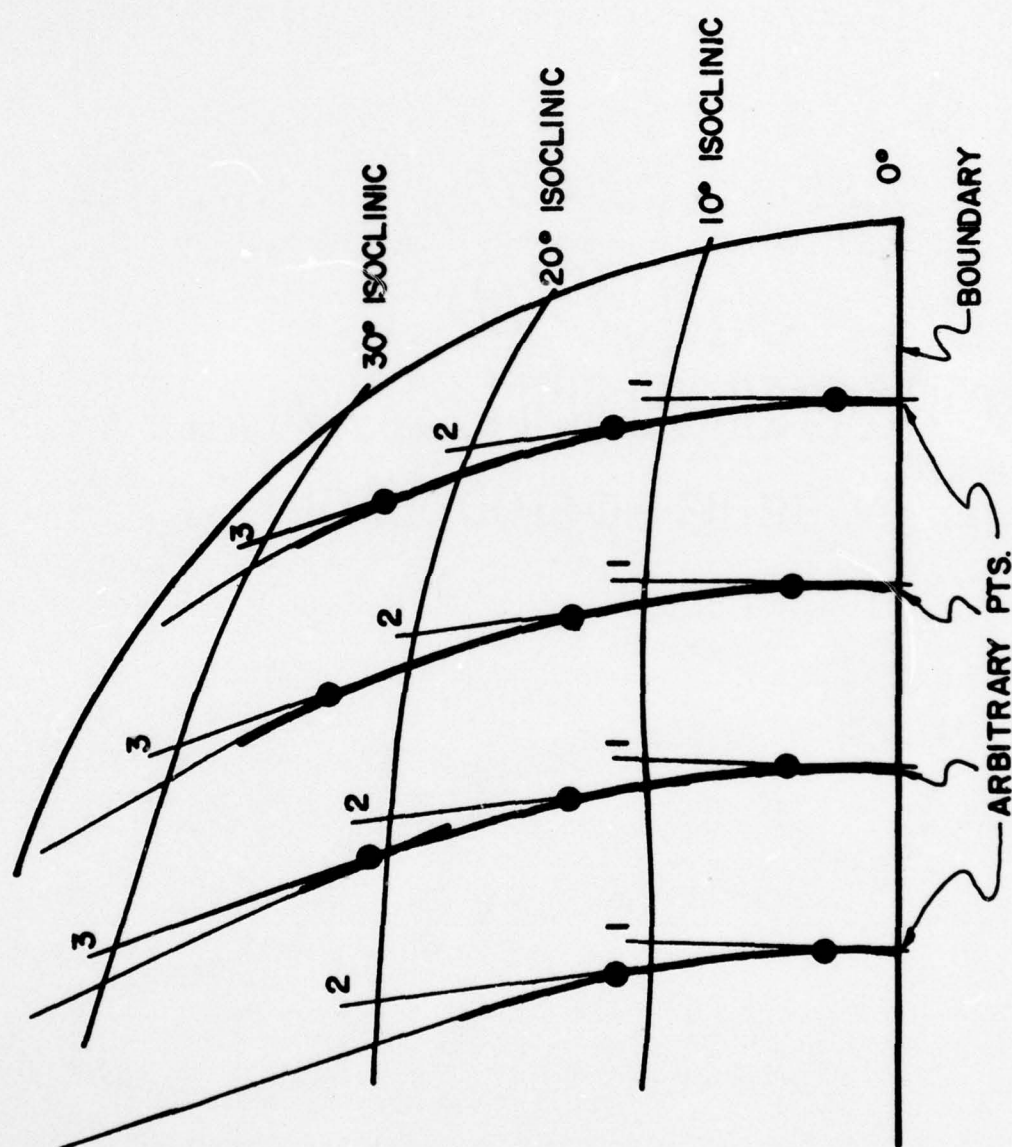


Fig. 2.7 Construction technique for converting isoclinics to isostatics

oriented 0° from the normal are drawn through each arbitrary point and continued until they intersect the 10° isoclinic line. The lines (1) are bisected, and a new set of lines (2) is drawn inclined at 10° to the vertical to the next isoclinic parameter. Again, these lines are bisected and another set of construction lines (3) is drawn at 20° to the normal until the next isoclinic is reached. This process is repeated until the entire field is covered. The stress trajectory may then be traced by using lines 1, 2, 3, etc., as a guide. The entire process may then be redone working from a boundary or isoclinic oriented at 90° to the original starting line, thus producing a network of isostatics which must intersect each other at right angles by definition. The network of stress trajectories allows a more easily understood picture of the actual stress orientation to be produced.

2.5 Methods of Confirming Photoelastic Results

Photoelasticity is a very powerful tool in that it tells you what is actually taking place in the model. However, the person conducting the test must properly analyze the test data and correctly interpret what it is telling him. Even with the Shear Difference Method there must be known data before the internal stresses may be calculated. It is important, therefore, to have methods of confirming calculated data and to have ways of checking assumptions or theories used in analyzing the distribution of stress.

One of the best checks for solving for stresses is working toward a free surface. The state of stress at a free edge is known from the isochromatic diagram. The normal stress at a free edge must be zero. The orientation of the principal stresses at a free edge is also known since the boundary itself is an isoclinic parameter. Therefore, since

$$\sigma_1 - \sigma_2 = nf$$

where n is the fringe order and f is derived from the properties and geometry of the model and $\sigma_2 = 0$ (free edge). $\sigma_1 = nf$ and is directly calculable from the isochromatic diagram. If one works toward a free edge and finds that the calculations do not give the value of stress indicated by the isochromatic diagram, then some error exists. The Shear Difference Method is extremely tedious and lends itself to numerical errors, so this type of check is very useful.

Another valuable check is based on the fact that compressive forces applied through anchorage systems will become uniform at some depth for symmetrically loaded members. It is this uniform compression which is so valuable to prestressed concrete. For uniform compression to develop, however, the isochromatic diagram must eventually reflect a constant fringe order for the region in question. Also, since the difference in shear stress is used to calculate changes in the normal stresses, for uniform stress to exist, τ_{xy} must equal zero or be a constant value so that $\Delta\tau_{xy} = 0$. Since $\tau_{xy} = \frac{(\sigma_1 - \sigma_2)}{2} \sin 2\theta$ and $(\sigma_1 - \sigma_2) \neq 0$ at uniform compression, then θ must equal 0° or 90° so that $\tau_{xy} = 0$ and uniform axial compression is indicated. Since $\tau_{xy} = 0$, this uniform axial compression indicated is a principal stress. This region will be marked by a zero or ninety degree isoclinic. If the isoclinic diagram shows an area of constant θ ($\theta \neq 0^\circ, 90^\circ$), this area also has a uniform value of stress, since $\Delta\tau_{xy} = 0$; but they are not necessarily principal nor is one of them equal to zero as is the case for transverse stresses equalling zero at uniform compression in prestressed concrete. In a region of uniform axial compression in a photoelastic model simulating a prestressed beam, the compressive stress should be equal to P/A , where P is the uniform axial load and A is the area over which the load is applied. In a

two-dimensional photoelastic analysis, this stress is found by realizing that there really is a third dimension, the thickness of the model.

A = model thickness \times model width

P = load applied over area

Stress (uniform) = P/A

This known value of stress provides an excellent check for calculations and gives greater insight into the photoelastic tests conducted in this study.

Isotropic points provide valuable knowledge to the distribution of stresses in a model. An isotropic point is a location at which the two principal stresses are equal ($\sigma_1 = \sigma_2$).¹³ As was mentioned earlier, an isotropic point has the property of having the stress oriented equally in all directions so all isoclinic parameters intersect at an isotropic point. If, in addition to being equal, the principal stresses are zero at the isotropic point, then it marks a change in the sign of the shear stress and indicates a change from either compression or tension to the other type of stress. Isotropic points, therefore, are extremely helpful to the analysis of photoelastic models.

Symmetry is the final tool to be discussed in interpreting photoelastic models. Symmetry of loading and geometry should create symmetrical isochromatic and isoclinic diagrams and, hence, symmetrical distributions of stresses. Symmetry is demonstrated also by having the axis of symmetry coincide with an isoclinic parameter. By properly interpreting symmetry, the investigator can save himself a great deal of work by using it to reduce the required calculations by one-half. Symmetry also provides a check to ensure your loading conditions are uniform and what you initially desired.

One final thought on photoelasticity should be brought out. The process is not intended to give exact answers. There are a

great number of variables which come into play which cannot be exactly accounted for. What photoelasticity does do is to provide an overview of the distribution of stresses which are actually created in the model. It gives a visual means of observing what takes place in the model. Photoelasticity in itself does not give final answers, but it does give insight which is of value to the investigator and gives him a starting place for more detailed studies. Photoelasticity is used when stress distributions are complicated and not easily understood.

CHAPTER 3

TEST PROGRAM AND SPECIMEN DESCRIPTION

3.1 Anchorage Models

3.1.1 General. One of the major objectives of this study was to develop a two-dimensional photoelastic model which accurately reflected the loading conditions found in the anchorage zone of a post-tensioned concrete member. This required that an anchorage system model be developed. Previous photoelastic tests had externally loaded a flat plate resting on the photoelastic model.² While there are anchorage systems that can readily be simulated by flat plates, there are also commercial anchorage systems which extend internally into the concrete member. It was felt that a series of anchorage system models should be developed which accurately reflected the loading conditions created by the general types of commercial anchorage systems available. A preliminary investigation was conducted at The University of Texas at Austin concerning types of commercial anchorage systems available. They were divided into three broad categories: flat bearing, inset bearing, and conical. Furthermore, the previous work of Cooper⁵ on anchorage performance in post-tensioned box girder bridge models had developed one-sixth scale models of the inset bearing and conical type end anchorages, which were scaled directly from actual anchorage systems employed on the United States' first segmental precast prestressed concrete box girder bridge, the John F. Kennedy Memorial Causeway in Corpus Christi, Texas (see Fig. 3.1). This existing work provided the basis for the dimensions for the photoelastic anchorage models. It was felt the models should be scaled to typify actual existing systems. The

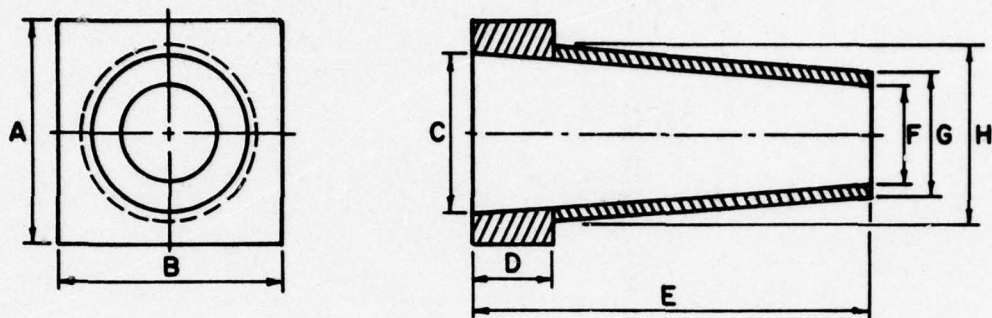
third anchorage system (flat bearing), while not employed by Cooper, was scaled to reflect his dimensions for the inset bearing type anchor so that it would reflect existing prototype dimensions (see Fig. 3.2).

A material had to be selected from which to construct the anchorage models. There were two considerations for the selection of the material. First of all, it was felt that every attempt should be made to approximate the modular ratio of steel to concrete so that the photoelastic tests would more accurately reflect the relationship between the steel anchors and the surrounding concrete. While exact similitude could not be attained due to the interior structure of the actual anchorage system which is very different from the crude representation of the model, it was felt an attempt should be made to approximate the actual relationship as closely as possible. Table 3.1 shows the materials considered and their respective values of Young's Modulus of Elasticity.

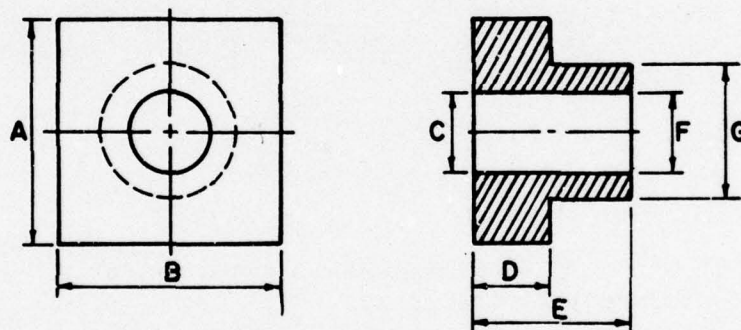
TABLE 3.1 YOUNG'S MODULUS OF ELASTICITY FOR VARIOUS MATERIALS

Possible Materials	Young's Modulus of Elasticity
<u>Anchor Materials:</u>	
Aluminum	10×10^6
Brass	$13-15 \times 10^6$
Copper	16.5×10^6
Iron	30×10^6
Lead	2.3×10^6
Steel	29×10^6
Tin	6×10^6
<u>Photoelastic Materials:</u>	
Bakelite (cast)	620×10^3
Catalin (cast)	200×10^3
Columbia Resin (cast)	350×10^3
Glass (sheet)	10×10^6
Lucite (sheet)	300×10^3
PSM-5 (sheet)	450×10^3

CONICAL

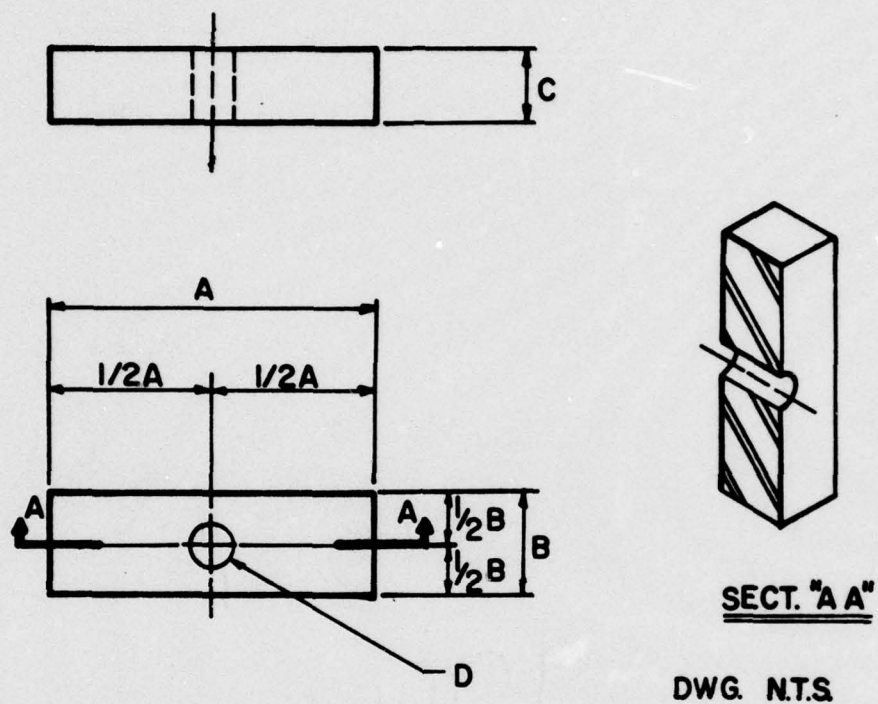


INSET BEARING TYPE



Anchorage Type	A	B	C	D	E	F	G	H
Conical	1.42"	1.42"	0.95"	0.50"	2.5"	0.55"	0.80"	1.10"
Inset Bearing	2.20"	1.42"	0.50"	0.50"	1.0"	0.50"	0.85"	—

Fig. 3.1 Cooper's one-sixth scale model of anchorage systems



ANCHOR	A	B	C	D
LB BEARING	1.1	0.375	0.25	0.125

NOTES:
ALL DIMS. IN INCHES

Fig. 3.2 Flat bearing anchorage model

An approximate value for the modular ratio of steel to concrete can be determined as follows:

$$\begin{aligned}
 E_c &= 57000 \sqrt{f'_c} \\
 E_c &= 57000 \sqrt{6000} && \text{Assume } f'_c = 6000 \text{ psi for} \\
 &= 4.42 \times 10^6 && \text{prestressed concrete} \\
 E_s &= 29.0 \times 10^6 \text{ psi}
 \end{aligned}$$

$$\frac{E_s}{E_c} = \text{Modular Ratio} = \frac{29.0}{4.42} = \underline{\underline{6.56}}$$

Assuming the use of a commercial photoelastic material such as PSM-5 (Photoelastic Inc., Malvern, PA) and examining Table 3.1, lead can be seen to be the material which provides the closest modular ratio.

$$\begin{aligned}
 E &= 450 \times 10^3 \text{ psi (PSM-5)} \\
 E_{\text{lead}} &= 2.3 \times 10^6 \\
 \frac{E_{\text{lead}}}{E_{\text{photo}}} &= \frac{2.3 \times 10^6}{450 \times 10^3} = \underline{\underline{5.11}}
 \end{aligned}$$

The second consideration for the selection of the material for the anchorage models was ease of manufacture. Due to the number of tests proposed (nine) and the small dimensions required for photoelastic tests, if each anchor were constructed from a material which required machining, considerable time and expense would be required. If lead were used, molds could be constructed and then lead models cast from the molds. This would be extremely convenient if a sizeable number of anchorage models were required. It was felt that by using the same molds to make the anchors, each anchorage would very closely reflect the previous one and make comparisons between tests valid.

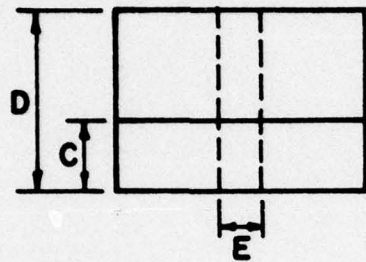
One drawback to the use of lead was the fact that lead has high creep tendencies. It was felt, however, that since the

photoelastic tests were to be conducted at comparatively low loads, and for short time durations, this creep would not greatly affect the test results. Lead was chosen to be the material from which the anchorage models would be constructed.

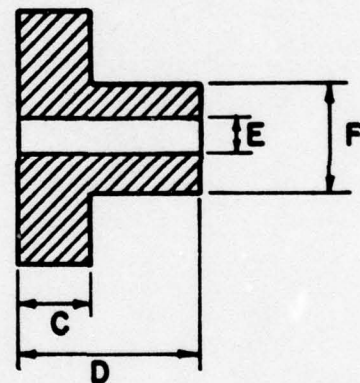
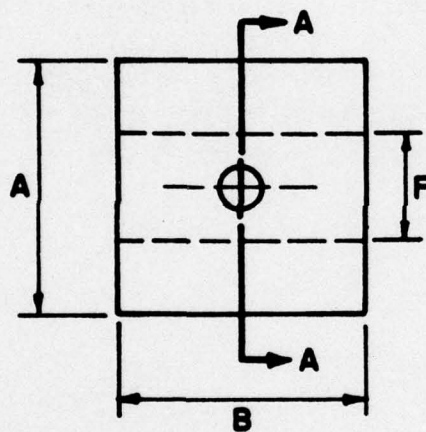
The anchorage models are at best crude approximations of very complex systems. The classification of existing commercial systems into three groups leads to further approximations and simplifications. However, the small dimensions required by photoelasticity rule out more complex models. Increased complexity would not increase the value of the results obtained from photoelasticity, since photoelasticity itself has limits of accuracy. The ultimate goal is to be able to draw general comparisons between systems and not highly precise comparisons.

3.1.2 Flat Bearing Anchorage Model. The flat bearing anchorage model shown in Fig. 3.2 was selected to represent commercial anchorage systems which have no bearing portions extending into the anchorage zone of the post-tensioned prototype. This model very closely approximates the anchorage models used by Christodoulides in his photoelastic investigations.^{2,3,4} The dimensions of the model come directly from Cooper's bearing type anchor and are one-half his scale, which makes them one-twelfth scale models of prototype anchorage systems.⁵ While Cooper ran no tests with this type of system, the current study did show commercially available anchorage systems which are closely approximated by this type of system.

3.1.3 Inset Bearing Anchorage Model. The inset bearing anchorage reflects a series of commercial anchorage system which are inset into the concrete anchorage zone and in which load transfer is carried out by this inset portion as well as external portions of the anchor. Dimensions for this model came directly from Cooper's model and are one-half his scale, or one-twelfth scale of the actual prototype. Figure 3.3 gives the actual dimensions used for the photoelastic model.



SECTION "A-A"



ANCHOR	A	B	C	D	E	F
INSET BEARING	1.1"	0.375"	0.25"	0.50"	0.125"	0.425"

Fig. 3.3 Inset bearing anchorage model

3.1.4 Conical Bearing Anchorage Model. The conical bearing anchorage model reflects a series of commercial anchorage systems which are inset into the concrete anchorage zone and are tapered to some reduced dimension. This inset tapered section is employed to transfer load from the anchorage system to the anchorage zone. As with the previous models, this model is one-half the scale of the Gooper model and thus becomes one-twelfth the scale of the prototype system. Figure 3.4 shows the dimensions used for the photoelastic model.

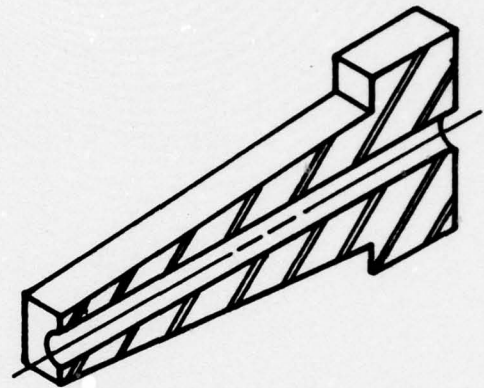
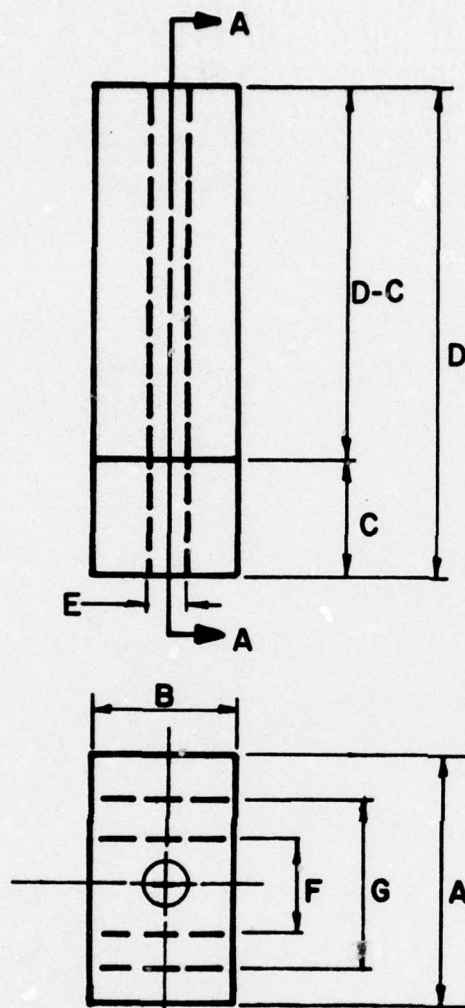
3.2 Concrete Anchorage Zone Model

3.2.1 General Considerations. To design a photoelastic model to represent the anchorage zone of a post-tensioned concrete member, a number of factors must be considered, including:

- (1) The choice of photoelastic material
- (2) The dimensions of the model
- (3) The parameters to be studied in the model
- (4) The construction methods employed to build the model

Each of these considerations must be examined in light of the desired results and goals of the investigation. The final objective is to develop a model which is usable and reflects accurately the prototype situation.

The choice of photoelastic material is closely related to the construction technique to be employed for the model. The model may either be cast using a mold and photoelastic material which, when mixed with certain additives, goes from a liquid to a solid state. This method of construction requires a great deal of effort as the process is long, time-consuming, and complicated. Controlled temperatures and environment are required and substantial time is required for the hardening process to take place. A second choice is to purchase prepared photoelastic sheets of specified thickness and machine these sheets to the specific shapes required for



SECT. "AA"

DWG. N.T.S.

ANCHOR	A	B	C	D	E	F	G
CONICAL TYPE	0.71	0.375	0.25	1.25	0.125	0.40	0.55

NOTES:
ALL DIMS. IN INCHES

Fig. 3.4 Conical bearing anchorage model

the model. This method has the disadvantage of requiring machining, which can produce residual stresses in the plastic caused by the heat produced during the machining process. These residual stresses remain in the plastic and cause problems in analyzing test results. The photoelastic material selected for the two-dimensional photoelastic analysis was a commercially produced photoelastic sheet known as PSM-5. This material had good sensitivity, very low creep, and time-edge effects, and supposedly machined well.¹⁵ Also, this material was precalibrated and had a known stress-optical constant which greatly aided calculations for material constants to be used in the analysis portion of the investigation. The selection of plastic sheet for the material also determined the construction technique since the sheet required machining to the shape of the model. It was felt that the machining process would greatly expedite the preparation of the models for testing as opposed to longer time required for the casting method.

To determine the dimensions for the model, the existing work of Cooper⁵ was employed. Cooper had already generated a model for a post-tensioned thin-web concrete member from an existing structure. This model provided an excellent vehicle from which to develop the photoelastic model (see Fig. 3.5). Since the photoelastic analysis was to be two-dimensional, the main concern was for the dimensions for the planes of action being considered. These planes of action have already been discussed in Sec. 1.2 and will not be repeated here. Since the anchorage system models had also come from Cooper's model and were at one-half of his scale, or one-twelfth prototype scale, the same scale was employed for the anchorage zone model, so that the entire test arrangement would reflect a scaled model of an existing real world situation. The dimensions for each existing test will be discussed in greater detail in following sections.

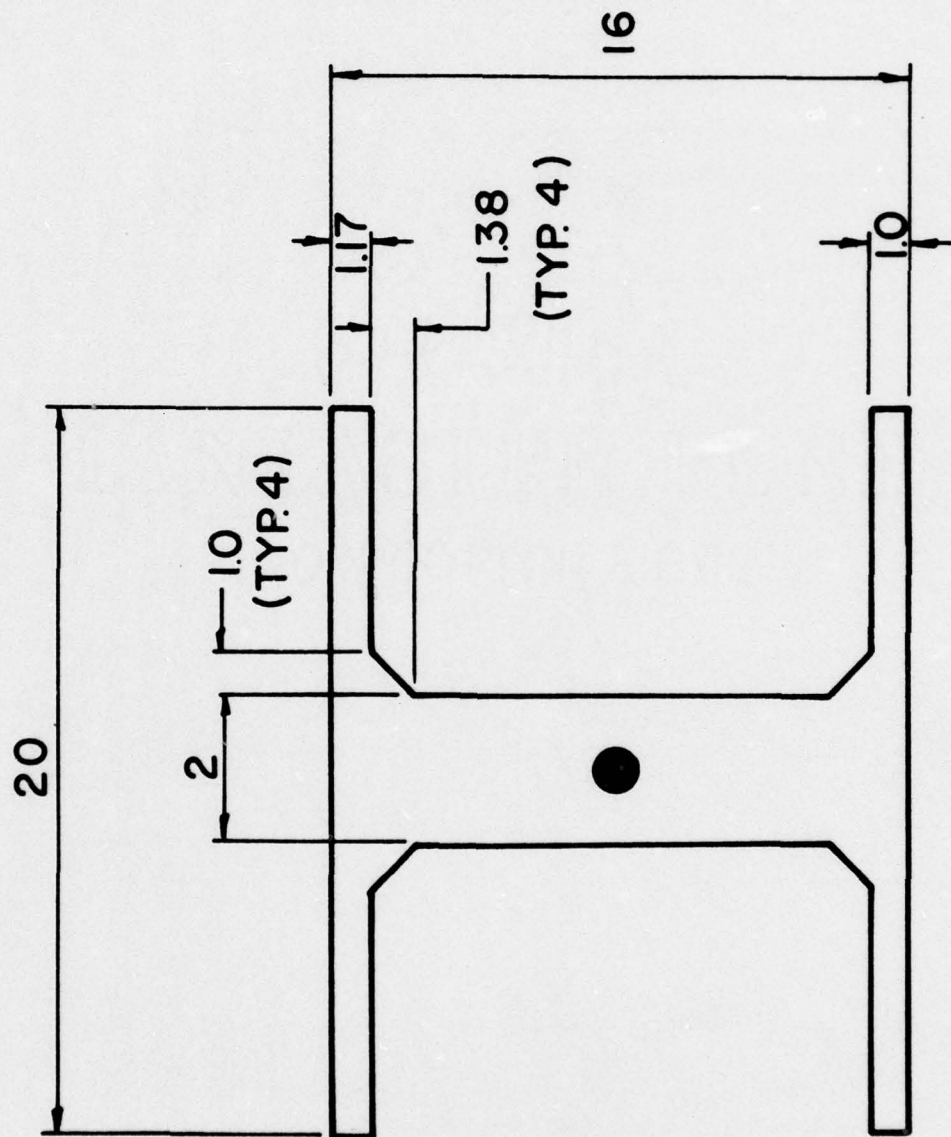


Fig. 3.5 Cooper's one-sixth scale model of existing thin web prestressed bridge section

The final consideration for the design of the anchorage zone model was to construct it in such a manner that parameters such as various types of anchorage systems, the presence of a tendon duct, and variations in geometric orientation of the duct and anchorage systems could be taken into account. Many of these parameters are not considered in earlier studies and it was felt that their effects should be included in any series of tests. By using photoelastic sheet and machining it to any desired configuration, a great deal of flexibility was introduced into the model design and by carefully designing the model all of the above parameters could be examined. Also, using this type of model allowed a loading system to be employed which actually introduced load by tension through a tendon which runs through the duct to the anchorage system. This load system, which reflects the actual loading condition in post-tensioned concrete members, was not used by Christodoulides in his two-dimensional photoelastic analysis.² It was hoped by using this type of a model the effects of tendon loading and duct presence could be examined.

The model was designed to simulate as closely as possible typical boundary conditions found in the prototype anchorage zone. Figure 3.15 shows the respective boundary conditions considered to exist in the actual prototype, the photoelastic model, and what would be used in an analytical model of the prototype. Both symmetrical and unsymmetrical loading cases are examined. Across the tendon duct in the prototype, there is actually restraint due to side cover and stiffness of the concrete for both the symmetrical and unsymmetrical loading cases. The photoelastic model, however, does not reflect this restraint, since it is a two-dimensional model with a free edge simulating the tendon duct. The photoelastic model tendon duct boundary conditions, therefore, do not accurately reflect the prototype duct boundary conditions. In the analytical model, however, these restraints in the prototype shown as springs

across the duct in both Figs. 3.15(a) and (b) can be represented. For the symmetrical loading condition, since the duct runs along an axis of symmetry where shear is zero and lateral displacements are zero, the condition may be shown as a series of rollers [see Fig. 3.15(a)]. For the unsymmetrical case, the shear is no longer zero along the duct and the restraint may be shown as a free boundary with spring linkage [Fig. 3.15(b)]. In a finite element analysis, these spring forces are generated from the element stiffness and nodal connectivity. In the prototype, there are friction forces which exist between the steel anchor and the concrete. These friction forces also exist in the photoelastic model between the lead anchor and the photoelastic plastic. In both loading cases for Fig. 3.15, these friction forces are shown as roller supports at B for the photoelastic model. They are also reflected in the analytical model in the same manner. The end of the photoelastic model is shown as a series of roller connections. This case exists as long as uniform compression has been reached in the model. Most designers feel safe to assume this uniform compression exists at a depth equal to the width of the model. The photoelastic model, however, was only 5 in. deep and its width was 8 in. For certain loading cases, therefore, it is possible uniform compression may not have been reached, and the assumption of roller supports along the end would not be correct.

3.2.2 Specimen 1 (Fig. 3.6). Specimen 1 was the first test. The specimen was made from 0.375 in. thick PSM-5 sheet material. The anchorage system employed was the flat bearing anchor and the tendon duct was straight. The anchorage system was centered symmetrically on the test specimen, as shown in Fig. 3.5. The specimen is actually composed of two pieces of photoelastic sheet which were placed in the model frame and placed 0.125 in. apart to simulate the tendon duct. The loading system will be discussed in detail in succeeding sections. The test was designed to examine end anchorage

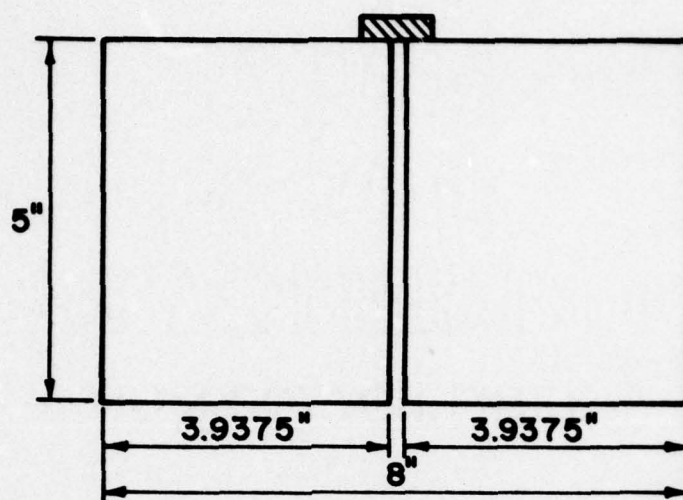


Fig. 3.6 Model for Test #1

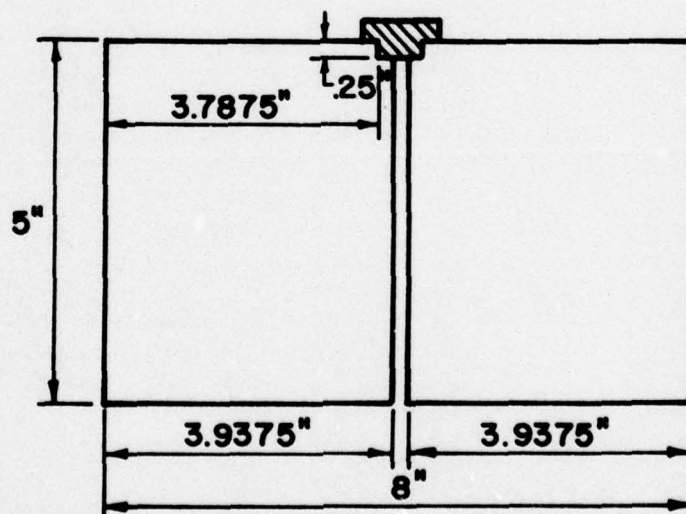


Fig. 3.7 Model for Test #2

zones which were symmetrically loaded with flat bearing anchorage systems and straight tendons.

3.2.3 Specimen 2 (Fig. 3.7). Specimen 2 was designed to be a symmetrically loaded end anchorage zone employing a straight tendon and an inset bearing anchor. The specimen consisted of two pieces of photoelastic sheet 0.375 in. thick, which were notched to a sufficient size so that the inset bearing anchor would fit snugly. The model was placed in the model frame so that the duct separating the two pieces would be 0.125 in. wide. The test was designed to examine the effects of the inset bearing anchorage system on symmetrically loaded anchorage zones with straight tendons.

3.2.4 Specimen 3 (Fig. 3.8). Specimen 3 was designed to be a symmetrically loaded end anchorage zone employing a straight tendon and a conical anchorage system. The specimen consisted of two pieces of 0.375 in. thick photoelastic sheet with an inclined wedge machined out so that a conical anchorage model would fit snugly. The model was placed in the model frame so that the tendon duct separating the two pieces would be 0.125 in. apart. The test was designed to examine the effects of the conical anchorage system on the symmetrically loaded anchorage zone with straight tendons.

3.2.5 Specimen 4 (Fig. 3.9). Specimen 4 was designed to be an eccentrically loaded end anchorage zone employing a straight tendon and a flat bearing anchor. The specimen consisted of two pieces of 0.375 in. thick photoelastic sheet placed in the model frame so that the tendon duct would be 0.125 in. wide. The test was designed to examine the effects of eccentricity on the anchorage zone with straight tendons without the bias of internal anchorage systems.

3.2.6 Specimen 5 (Fig. 3.10). Specimen 5 was designed to be an anchorage zone loaded by an inclined tendon and a flat bearing anchor. The specimen consisted of two pieces of 0.25 in. thick

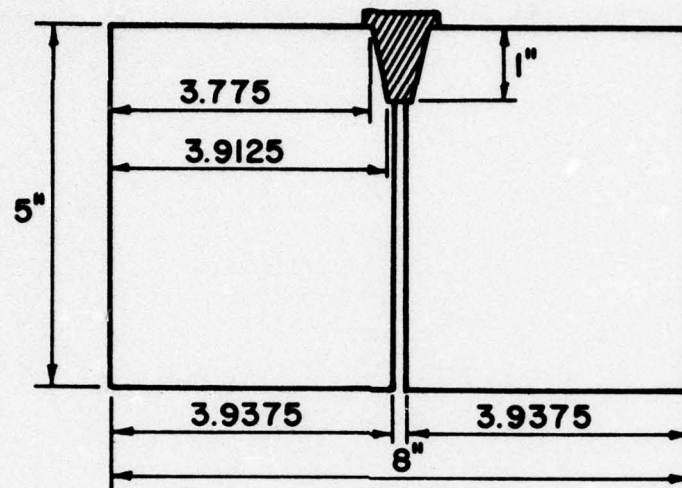


Fig. 3.8 Model for Test #3

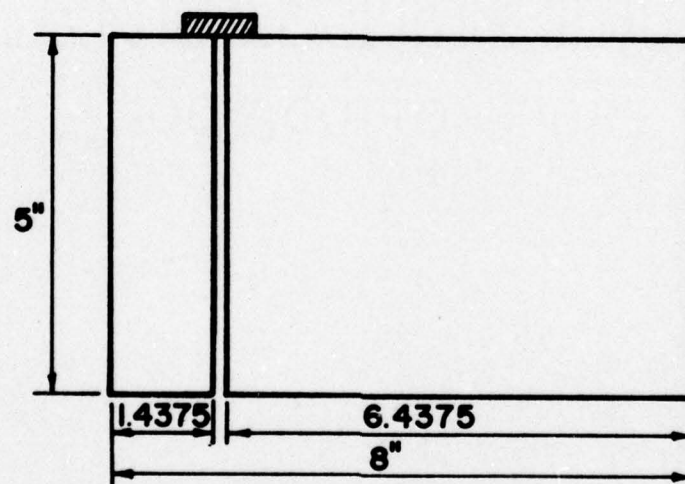


Fig. 3.9 Model for Test #4

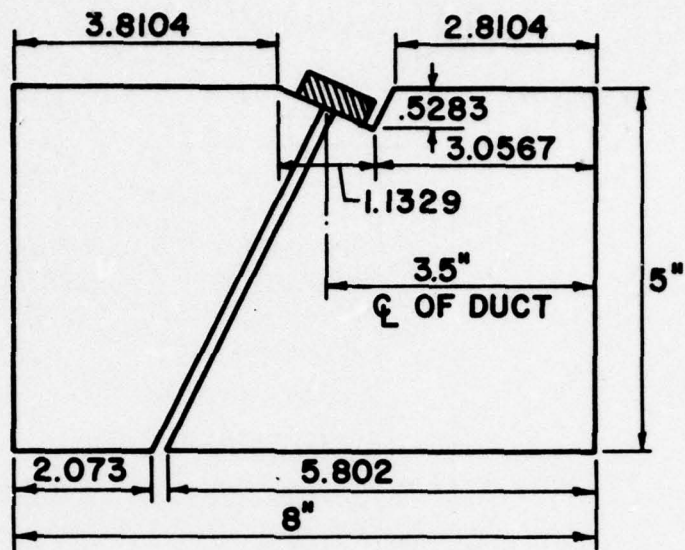


Fig. 3.10 Model for Test #5

NOTE: DIAMETER
OF DRILLED HOLE
IS 0.25"

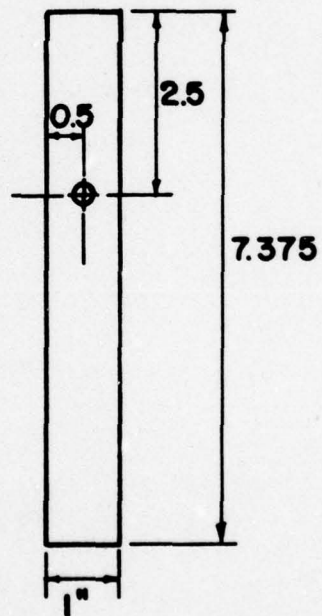


Fig. 3.11 Model for Test #6

photoelastic sheet with a notch machined along the top for a flat bearing anchor to rest at an angle normal to the inclined tendon duct. The angle of inclination of the tendon duct is 25° from the vertical. This angle was selected after examining highway bridge plans for a post-tensioned highway bridge from the State of Illinois Department of Transportation and the segmental box girder members of the John F. Kennedy Memorial Causeway.^{5,21} The angle was found to be representative and quite common. The common angle found on Cooper's specimens was 28° and this compared nicely with the 25° angle chosen.⁵ The tendon duct was designed to be 0.125 in. wide. The test was designed to examine the effects of inclined tendon geometry on the stress distribution of anchorage zone regions. Flat bearing anchorage systems were used so that effects of the tendon geometry could be more easily observed.

3.2.7 Specimen 6 (Fig. 3.11). Specimen 6 was designed to be a cross-sectional representation of the web of a post-tensioned member. The tendon duct was simulated by a 0.25 in. diameter drilled hole and the load was applied by running a tendon through the hole and loading it. The scale of this specimen was one-half of Cooper's model to include the size of the tendon duct.⁵ This duct may be slightly larger than what would be expected in the full-scale prototype, but the difference should not be great. The specimen consisted of one piece of 0.25 in. thick photoelastic sheet. The test was designed to examine the effects of tendon pressure on the duct in draped and inclined tendon duct geometric situations.

3.2.8 Specimen 7 (Fig. 3.12). Specimen 7 was designed to be a symmetrically loaded anchorage zone with multiple anchors with straight tendon geometry. The specimen consisted of three pieces of 0.25 in. thick photoelastic sheet. The specimen was placed in the model frame so that each duct would be 0.125 in. wide. Two flat bearing anchorage systems were employed to introduce the load to the model. The test was designed to examine the effects of multiple

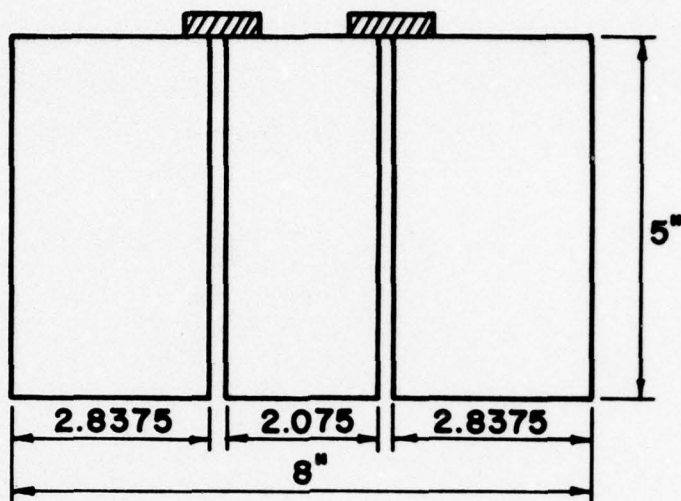


Fig. 3.12 Model for Test #7

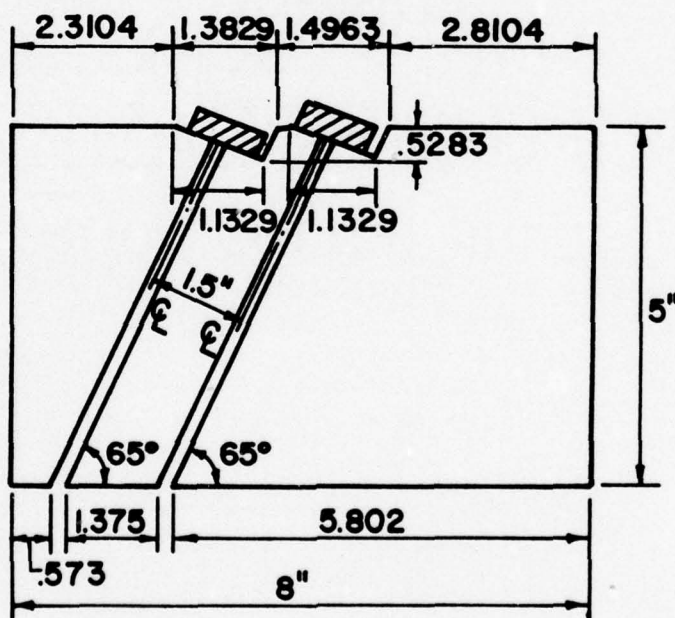


Fig. 3.13 Model for Test #8

anchorage systems with straight tendon geometrics. Pure bearing anchors were used so that the effects of the multiple anchors could be observed.

3.2.9 Specimen 8 (Fig. 3.13). Specimen 8 was designed to be an anchorage zone loaded by multiple inclined tendons with flat bearing anchors. The specimen consisted of three pieces of 0.25 in. thick photoelastic sheet and the tendon orientations were identical to the tendon orientation used in Specimen 5. The test was designed to gain insight into the effects of multiple anchorage systems along with inclined tendon geometry. The tendon ducts were adjusted to be 0.125 in. wide.

3.2.10 Specimen 9 (Fig. 3.14). Specimen 9 was designed to be a cross-sectional representation of the web of a post-tensioned member with multiple tendons. The specimen consisted of one piece of 0.25 in. thick photoelastic sheet with two drilled holes with 0.25 in. diameters. The dimensions for the tendon spacings and the entire model are taken from Cooper's model and are one-half his scale.⁵ This test was designed to examine the effects of tendon pressure on multiple ducts in draped or inclined tendon duct geometric situations.

3.3 Loading System

One of the major objectives of this investigation was to develop a photoelastic loading system so that two-dimensional photoelastic tests could be conducted. The loading system had to be designed to simulate the loading of the anchorage zone in an actual post-tensioned concrete member. The system had to be designed to meet the constraints of the photoelastic material selected and the modeling methods employed for the anchorage zone (see Fig. 3.15 for various boundary conditions). The loading system which was finally decided upon consisted of two parts which interacted together, the

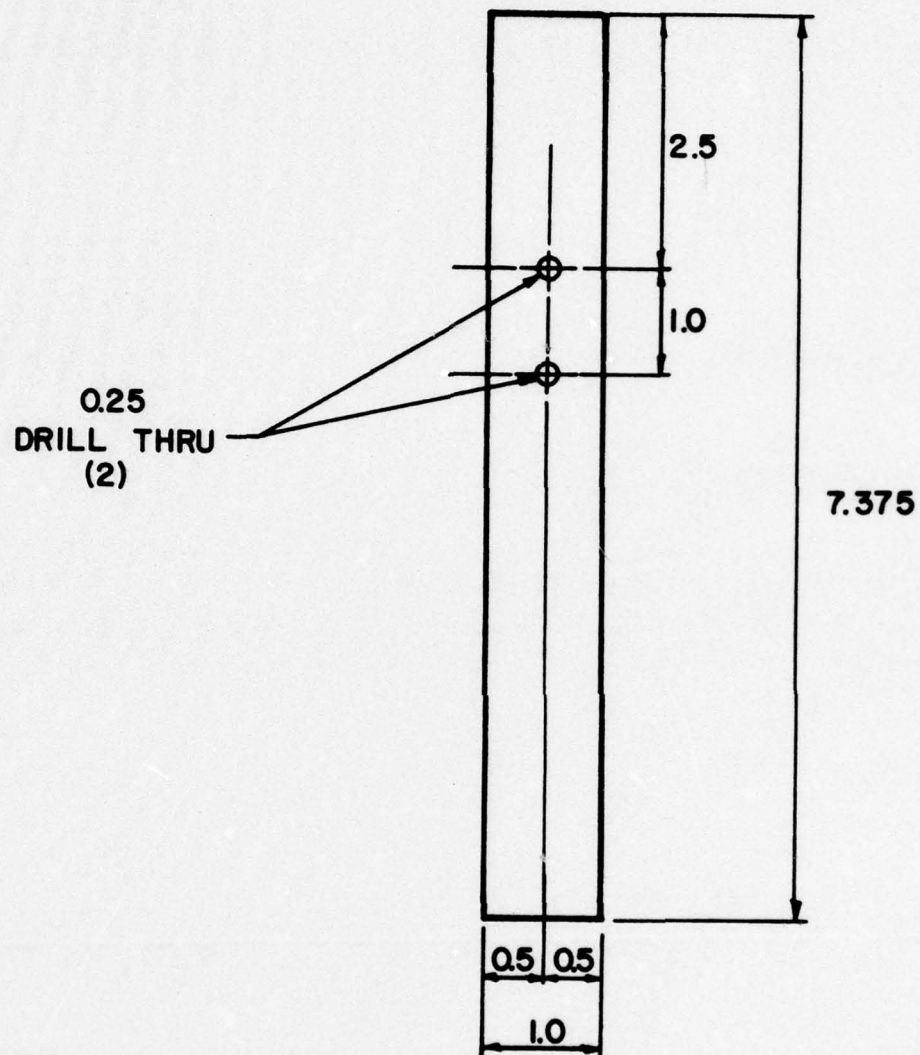
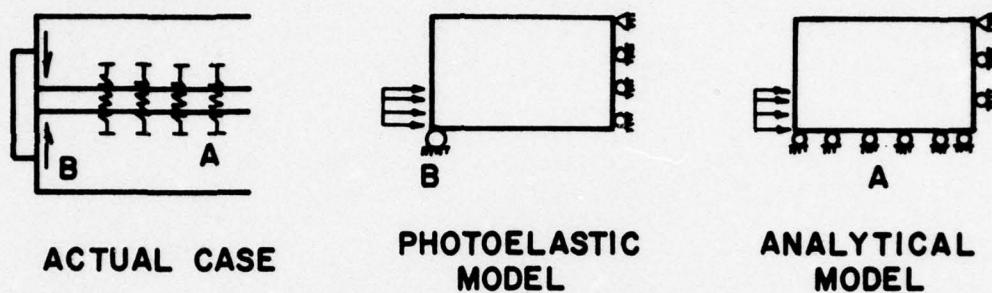
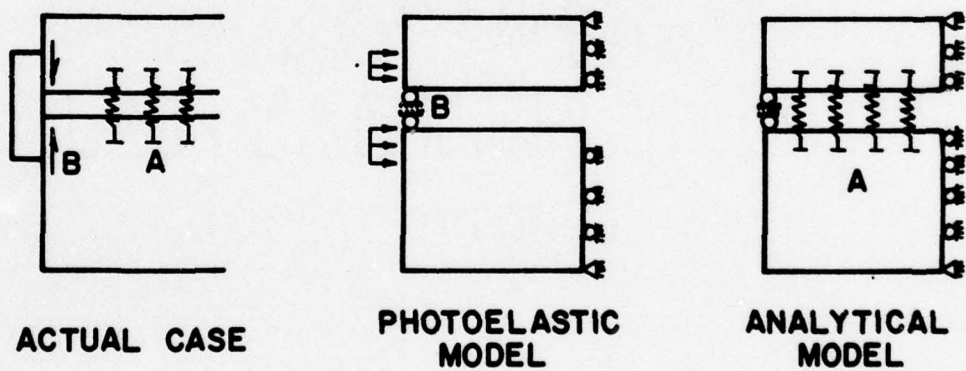


Fig. 3.14 Model for Test #9



(a) Boundary conditions for symmetrical loading

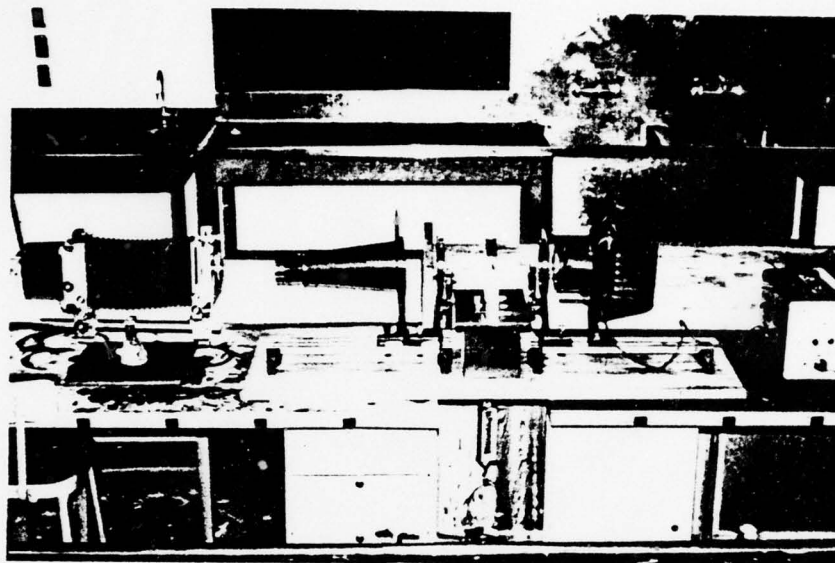


(b) Boundary conditions for unsymmetrical loading

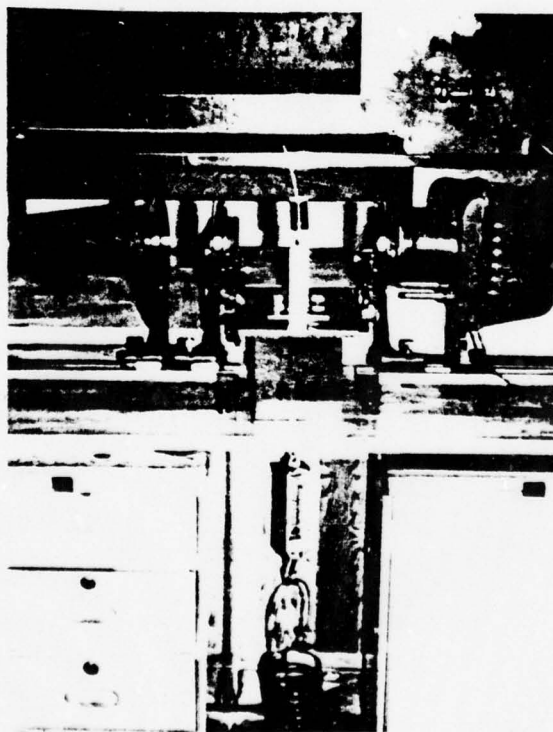
Fig. 3.15 Various boundary conditions for model and prototype

load platform and the model frame. Figure 3.16 shows the actual system employed.

3.3.1 Load Platform. In a prestressed, post-tensioned concrete member, the prestressing force is transferred from the post-tensioning tendon to the anchorage system, which, in turn, introduces a compressive stress to the concrete member through the anchorage zone. The loading system for the photoelastic tests would have to work in approximately the same manner, if an accurate representation of the anchorage zone stresses was to be obtained. It was decided to load the model through a tendon which had an applied tensile load and which ran through the model's tendon duct to the anchorage system, where it was secured. This tensile force would then be transferred to the photoelastic model's anchorage zone as a compressive force in much the same manner as in the actual concrete member. Figure 3.17 shows a representation of the loading system and how it operated. The primary component of the loading system was the load platform. This platform consisted of 0.5 in. steel plate which had slots cut through it, so that an adjustable securing device consisting of two $1\frac{1}{4} \times 1\frac{1}{4} \times \frac{1}{4}$ in. angles attached to the platform by $\frac{3}{8}$ in. bolts passing through these slots could be used to secure the model in place. In addition, there was a slot cut through the platform running between the two angles wide enough to allow a seven-strand prestressing wire to pass through the platform and up the model's tendon duct to the end anchor (see Fig. 3.17). Force could then be applied to the tendon below the platform in the form of weights and the load would be transferred to the model in the desired manner. The loading platform, therefore, almost directly approximated the loading conditions in the concrete member. The load was initially applied to the tendon by securing buckets to the tendon and adding lead shot to the bucket until the desired weight was reached. Figure 3.18 shows a plan view of the loading platform.

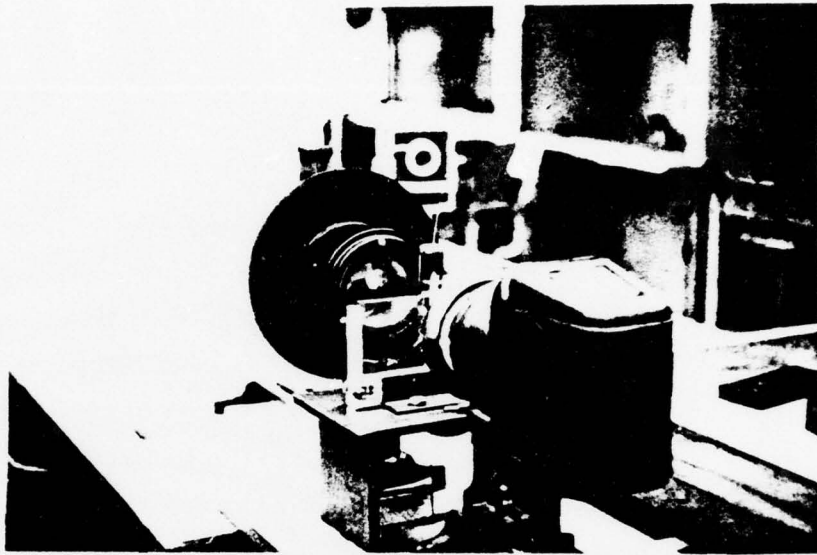


(a) Actual loading system with photoelastic equipment

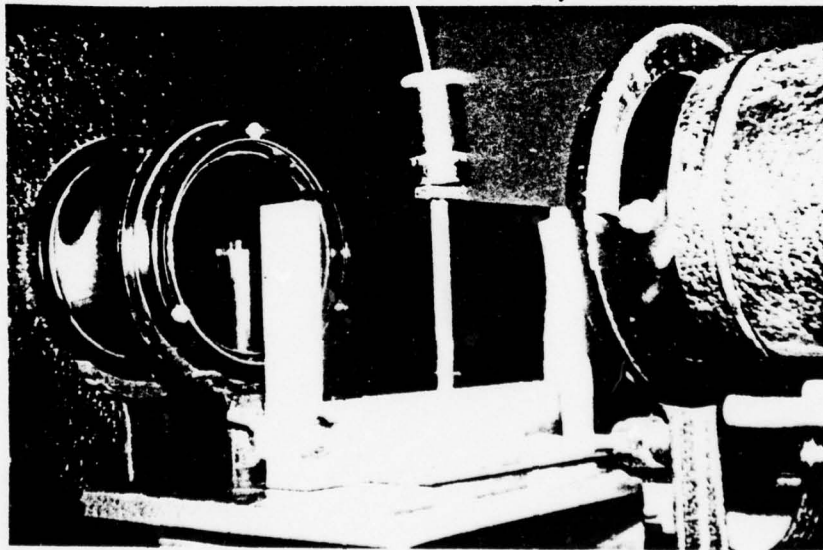


(b) Load platform and model with load applied

Fig. 3.16 Test apparatus employed in investigation



(c) Model frame and load platform



(d) Model frame with model and anchorage system

Fig. 3.16 (Continued)

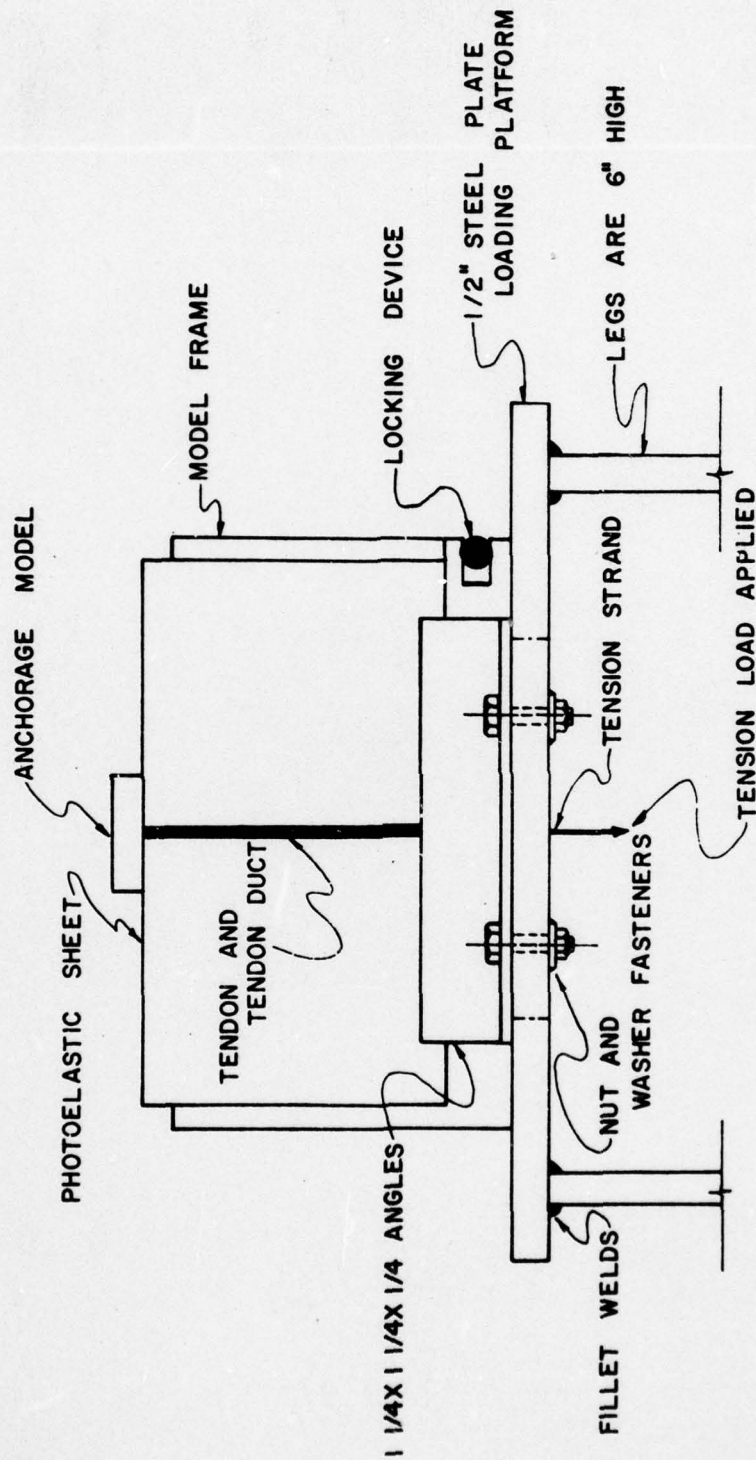


Fig. 3.17 Loading system elevation view

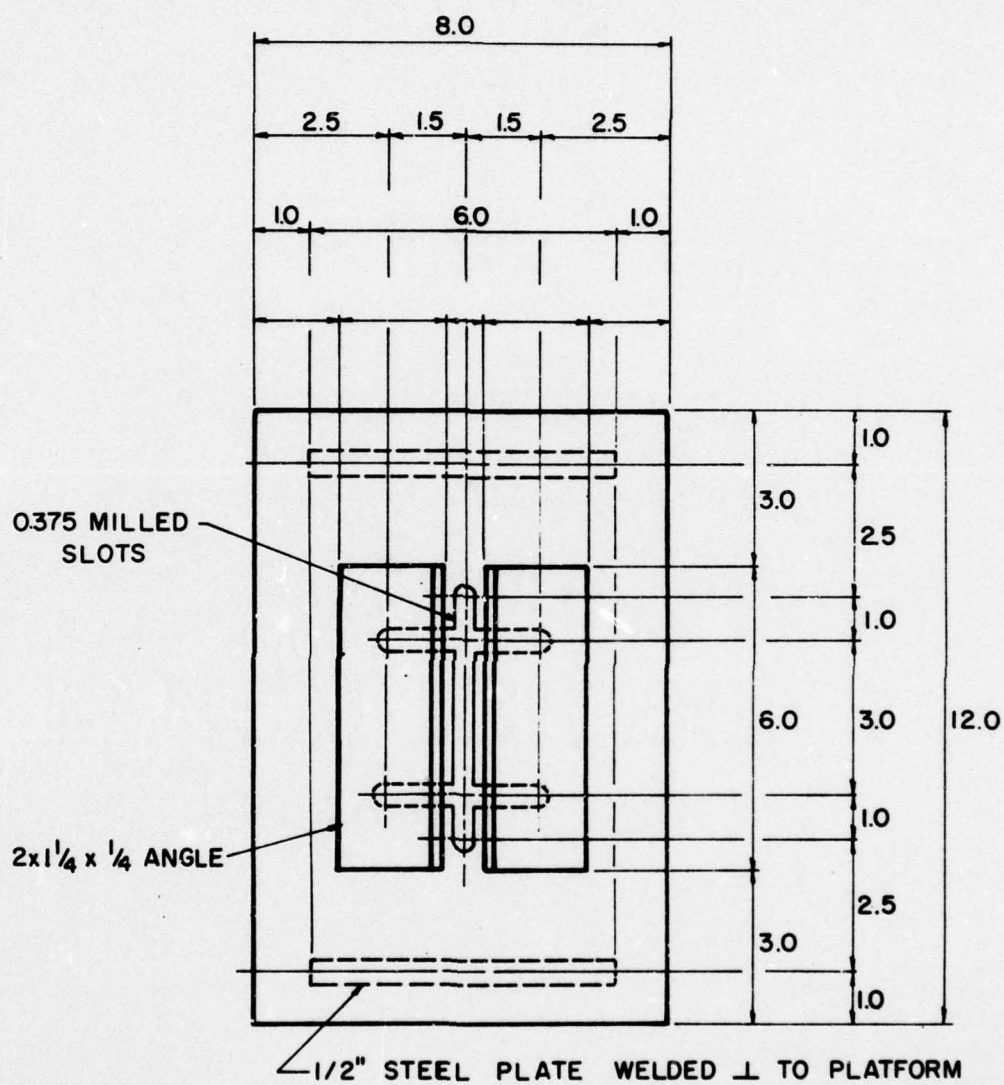


Fig. 3.18 Loading system plan view

3.3.2 Model Frame. A serious problem was introduced by the use of the photoelastic models discussed in Sec. 3.2, since they consisted of separate pieces. These pieces represented the correct two-dimensional projection of the plane passing through the tendon duct but did not behave as the real member would, since they were entirely independent of each other. There were substantial problems in aligning the separate pieces and in holding them in the same planes of action. This is an extremely important consideration for photoelasticity, where light rays passing through the model must be normal to the model and must enter the model along the same plane.

This problem was remedied by designing a model frame which held the separate photoelastic pieces in the same orientation and greatly eased the movement and adjustment of the composite model to ensure correct orientation for the tests. In effect, the model frame took the separate pieces of the model and combined them so that they acted as one member. The model frame, while providing rigidity to the system did not introduce stresses into the model except along the bottom of the frame. These would not affect the area being investigated around the anchorage. Great care was taken to ensure that horizontal forces were not introduced into the system by tightening the side wall (see Fig. 3.17) too tightly. Also, the separate pieces of each model were placed into the frame so that they were spaced apart by the proper distance to simulate the tendon duct. Once the pieces of a model had been properly aligned and spaced within the model frame, then the entire frame would be placed on the load platform and secured by the $1\text{-}1/4 \times 1\text{-}1/4 \times 1/4$ in. adjustable angles. The anchorage model and the tendon would then be placed into the system and the test conducted. The nature of the loading would reduce the pressure between the side wall and the model even further by tending to pull the model away from the frame wall and very little stress was introduced into the model by this contact. Figure 3.19 shows the photoelastic model frame.

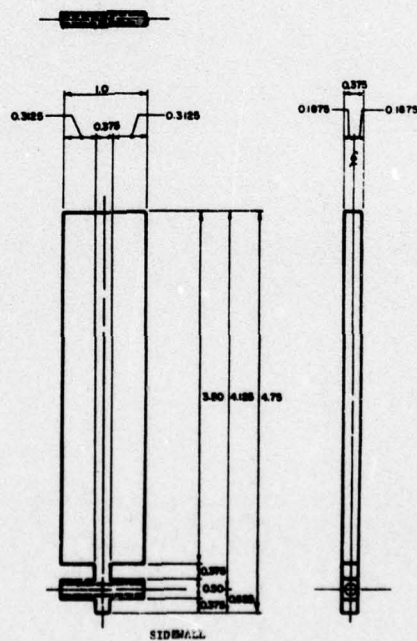
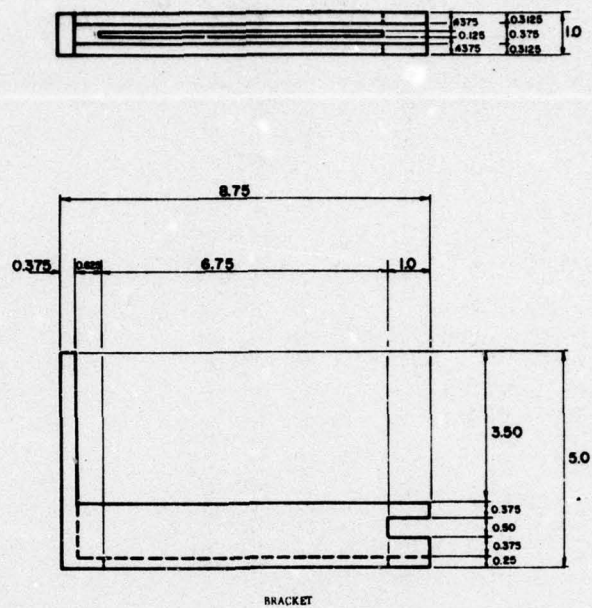


Fig. 3.19 Photoelastic model frame

3.4 Problems Encountered

3.4.1 Model Problems. The selection of the photoelastic model discussed in Sec. 3.2 created other problems which were not anticipated and for which there were no obvious solutions. One of these problems was the creation of residual stresses in the photoelastic material by the machining process. Some of the models required extensive machining to close tolerances. The selection of PSM-5 for the photoelastic material had been made taking into account its supposedly good machining characteristics. It was hoped that these characteristics would solve any residual stress problems. Unfortunately, the initial models constructed had extensive residual stresses and attempts to anneal these stresses proved unsuccessful. The annealing process is quite complicated and requires very sensitive equipment. The best solution to the problem of residual stresses was to avoid their introduction during the machining phase. This required tedious, very slow machining of the models and required several days for each model. However, as the machinist developed experience with the material, the residual stresses were greatly reduced and the problem was controlled. Also, the initial thickness selected for the photoelastic sheets was 0.375 in., and it was discovered that by reducing the thickness to 0.25 in. the residual stress created by machining was greatly reduced.

Another problem discovered during the testing phase was that extremely close tolerances were required between the photoelastic model and the anchor model to ensure smooth transfer of the load. Unfortunately, the tolerance required in certain cases could not be satisfactorily attained (see Sec. 4.3). The load, therefore, was not uniform in nature and in many cases became a series of concentrated loads. This affected the desired symmetry in the isochromatic and isocline diagrams. Also, the fact that the anchorage models were cast from lead created a rough surface which would not transfer stress uniformly to the much smoother photoelastic sheet. This

also led to isochromatic and isoclinic diagrams which were not as symmetrical as desired or which reflected concentrated loads instead of uniform loads. Various different methods were attempted to solve this problem, but it was a persistent consideration throughout the entire testing sequence. Section 4.3 discusses the attempts to correct the problem in greater detail. While it is regrettable that a completely smooth surface could not be created to ensure the uniform transfer of load, such an imperfect condition does reflect the actual situation found in the construction of post-tensioned members. The transfer of load between the anchorage system and the concrete member is probably far less than perfectly uniform, since there will be imperfections in the anchor steel as well as hard and soft spots in the surrounding concrete, depending on the location of hard aggregate and cement along the anchorage. The transfer of load reflected by the photoelastic model, therefore, while not being perfect may possibly reflect actual conditions where transfer of load between the post-tensioning anchorage system and the concrete member is also not perfect. This is a problem, however, in the comparison of test results when no two loading conditions are exactly the same. This situation complicated the analysis of test results.

The final model selected did not accurately reflect the tendon duct in the prototype. When the model was initially designed, the free boundary along the tendon duct was not considered a serious problem. Subsequent testing and comparison with analytical results showed this failure to reflect the restraint of the concrete stiffness and side cover in the prototype to the model tendon duct as a serious shortcoming of the model which lessened the ability to properly reflect the full behavior of some of the concrete prototypes. In spite of this boundary condition shortcoming, substantial useful information can be determined from the models.

3.4.2 Loading System Problems. There were several problems encountered with the loading system during the testing sequence

which deserve mentioning. The first of these was the need to design a more adjustable loading system so that the height of platform and its lateral location could be more easily adjusted when different areas of interest were discovered on one model or when different models were tested sequentially. The system was fairly inflexible and required too much time to adjust from one area to another. For any future work, modifications should be employed to the loading platform to allow for both vertical and horizontal movement without having to adjust the entire polariscope.

Another problem was the need to generate higher loads than were initially anticipated. The loading system worked excellently but there was a limit to the amount of load which could be applied. The gravity system should be enlarged so that larger loads could be applied to the tendons and in turn create a higher order of isochromatic fringes for more accurate interpretation. This would not be a complicated problem as all it would require would be enlarging the loading area and load receptacles so that greater loads could be employed. The present system would handle loads up to 100 lb/tendon. Any future system should be able to double that value.

An addition to the loading system which would have been of great value would have been the utilization of strain gages and monitoring equipment so that the value of strain and stress at various preselected locations on the photoelastic model would have been known. This added information would have greatly simplified the analysis of the values of stress at internal points by the "Shear Difference Method" (see Sec. 2.3). It would have provided valuable information for the analysis of each test specimen. It is highly recommended that any future work employ a series of strain gages located at key positions on the model.

CHAPTER 4

TEST RESULTS AND DISCUSSION

4.1 General Discussion of Interpretation of Results

4.1.1 Determination of Stress at Interior Points. The interpretation of photoelastic results is at best an inexact process. The theory surrounding the creation of isoclinic and isochromatic fringes is not difficult nor are the concepts of methods such as the "Shear Difference Method" for determining the state of stress at interior points in a photoelastic model hard to understand. However, when actually applying these theories, there are subtle considerations which can substantially affect the results and which are not readily apparent. The recording of data is an excellent example. In theory, isoclinic and isochromatic fringes are lines consisting of single points. In actuality, these fringes have discrete widths and are not a neat locus of points. There is an immediate problem in deciding the line of action for isochromatics or isoclinics. The best assumption is to assume the center of the fringe as the line. In the case of isochromatics, the error introduced by this assumption is very small, but in the case of isoclinics there can be a substantial problem. The dark outline which marks an isoclinic probably marks a range of parameters which may consist of several degrees, as opposed to one parameter or one degree reading. Data, therefore, must be carefully recorded and represents some subjective judgment. In this investigation, isochromatic fringes were recorded photographically, thus creating a permanent record which could be analyzed at a later time. The isoclinics, however, were recorded graphically by tracing the outline of each parameter as it was projected onto a screen. At the time this process was employed, it was felt it would be more than sufficient. However, when the

test data were later analyzed and attempts to use the "Shear Difference Method" were made, the data were found to lack sensitivity for the method to produce the desired accuracy. The isochromatic data also showed a lack of sensitivity. In most tests, a maximum of three clearly definable fringes was produced. Due to the size of the area which the analysis attempted to cover, this fringe count made it very difficult to determine the exact value of the fringe constant at any point not falling exactly on the fringe. Since a compensator of the Babinet or Babinet-Soleil variety was not employed during the testing procedure, the only method of determining the value of the fringe parameter was interpolation between existing fringes.¹³ This also added error to the calculations for determining the value of stress at interior points. The "Shear Difference Method" was discussed in detail in Sec. 2.3, including its sources of error. The method may produce sizable errors if the data are not sufficiently precise. The method is an approximation which gets more accurate as smaller intervals of integration are employed. Unfortunately, fairly large intervals of integration had to be maintained due to the relative insensitivity of recorded data for this series of tests. To augment the visual data, it would have been extremely helpful also to have employed a series of strain gages at various points of interest along the model to provide checks and input into the calculation of stress at interior points. Unfortunately, this concept was also not realized until after the testing had been completed. Thus, the calculations for the value of stress at interior points were subject to sizable errors, especially in the calculation of the transverse tensile stresses. These calculations will be discussed in more detail when each test is individually discussed. As has already been mentioned in Sec. 3.4, the difficulty in obtaining a uniform transfer of load between the anchor and the model also made it difficult to compare results, since no two loading conditions were exactly the same.

Since strain gages were not employed to determine a starting value for the calculation of stress at internal points, certain assumptions had to be made to provide a value from which to work. The initial value was located at a point where uniform compression appeared to exist according to isochromatic and isoclinic diagrams. The stress at this point was assumed to be equal to the load applied to that portion of the model divided by the cross-sectional area (P/A). For a model such as the one employed in Test #7, where the area of interest was symmetrically loaded, this assumption was good and the subsequent values of stress calculated from it should be fairly accurate. In Tests #1, #3, and #4, however, where the same assumption was made, it was not entirely correct. In Tests #1 and #3, the models are symmetrically loaded, but due to the boundary conditions of the duct, they actually consist of two eccentrically loaded pieces. The stress in the segments comprising each model would be influenced by the moment applied to the segment by the eccentric loading. The end conditions of the model would not allow tension to exist along the base, since the model was not fixed to the base, and this further affected the actual value of stress existing along the base. The assumption of a uniform compression existing with a value equal to P/A was overly approximate and ignored the stresses created by the eccentric load and boundary conditions. Test #4, while having a smaller model segment for analysis, had the same factors affecting the stresses created in the model. The values of stress calculated at interior points for these tests were affected by the error introduced by this assumption of the stress at the initial point. Longitudinal stresses calculated were probably low, since the stresses created by the moment would tend to increase the compressive stresses found under the load and decrease the compressive stress on the opposite side of the neutral axis of the section. The regions of uniform compression indicated by the photoelastic data probably did not extend across

the entire model, but the polariscope was not large enough to show where the region stopped. The actual calculation of the stress existing at this point is extremely difficult without additional information. For comparison purposes, however, as long as the same assumptions were made in each test and the boundary conditions of the models were similar, this error in the assumed value of the uniform compressive stress would not cause major problems. The tests could still be compared to each other and conclusions deduced. The values calculated would have an error, but the same error would exist in both tests, making comparisons possible.

4.1.2 Value of Test Results. The problems in determining the value of stress at interior points in the photoelastic models discussed in Sec. 4.1.1 did not invalidate all data. On the contrary, a great deal of direct information may be obtained from the data, as well as trends in stress distribution which give indications of possible trouble areas and can show areas of interest and regions in the anchorage zone which should merit special attention. Photoelasticity is never intended to produce exact or precise calculations, but rather is used to analyze complex problems and thus guide further studies. This is especially the case with two-dimensional photoelasticity. If the test results which follow are examined in this light, then they certainly offer valuable and usable information.

4.2 Test #1--Symmetric Loading with Single Flat Bearing Anchor

Test #1 was designed to examine the effects of the flat bearing anchor on a symmetrically loaded anchorage zone with a straight tendon duct. It was the first test in the series of tests and was intended to also provide a basis of comparison for successive tests. This particular loading condition had been examined by Christodoulides in a two-dimensional photoelastic investigation

neglecting the tendon duct and using a much smaller model.² A load of 84 lbs. was applied to the post-tensioning tendon of the model.

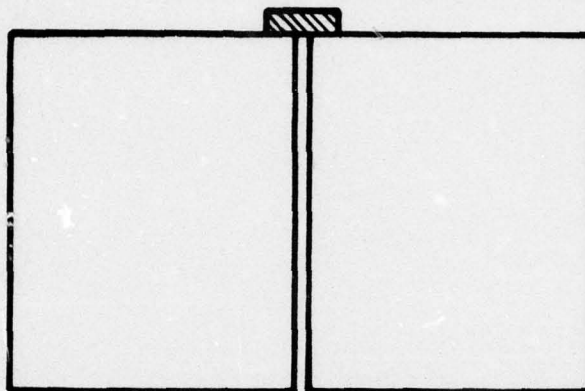


Fig. 4.1 Test #1--Symmetric loading with single flat bearing anchor

4.2.1 Observed Results. The isochromatic diagram for Test #1 is shown in Fig. 4.2 and the photograph of the actual isochromatics is shown in Fig. 4.3. The isochromatic fringe order denotes the use of a light field as is substantiated by the photograph. The grid employed for the calculations of the stress at internal points is shown in Fig. 4.2. The isochromatics reflect acceptable symmetry, but do show nonuniformity of load by differences in the shape of the diagrams on either side of the tendon duct. Note also the varying thickness of the isochromatic fringes and the relative distance between known values of fringe order. Sec. 4.1.1 outlined problems in determination of the value of the fringe order between isochromatic lines. Examination of point A on Fig. 4.2 indicates its isochromatic order (n) could range anywhere from $1/2$ to almost $1-1/2$. This determination would be greatly improved with use of some sort of compensator. The value used in

AD-A053 516

TEXAS UNIV AT AUSTIN

F/G 13/13

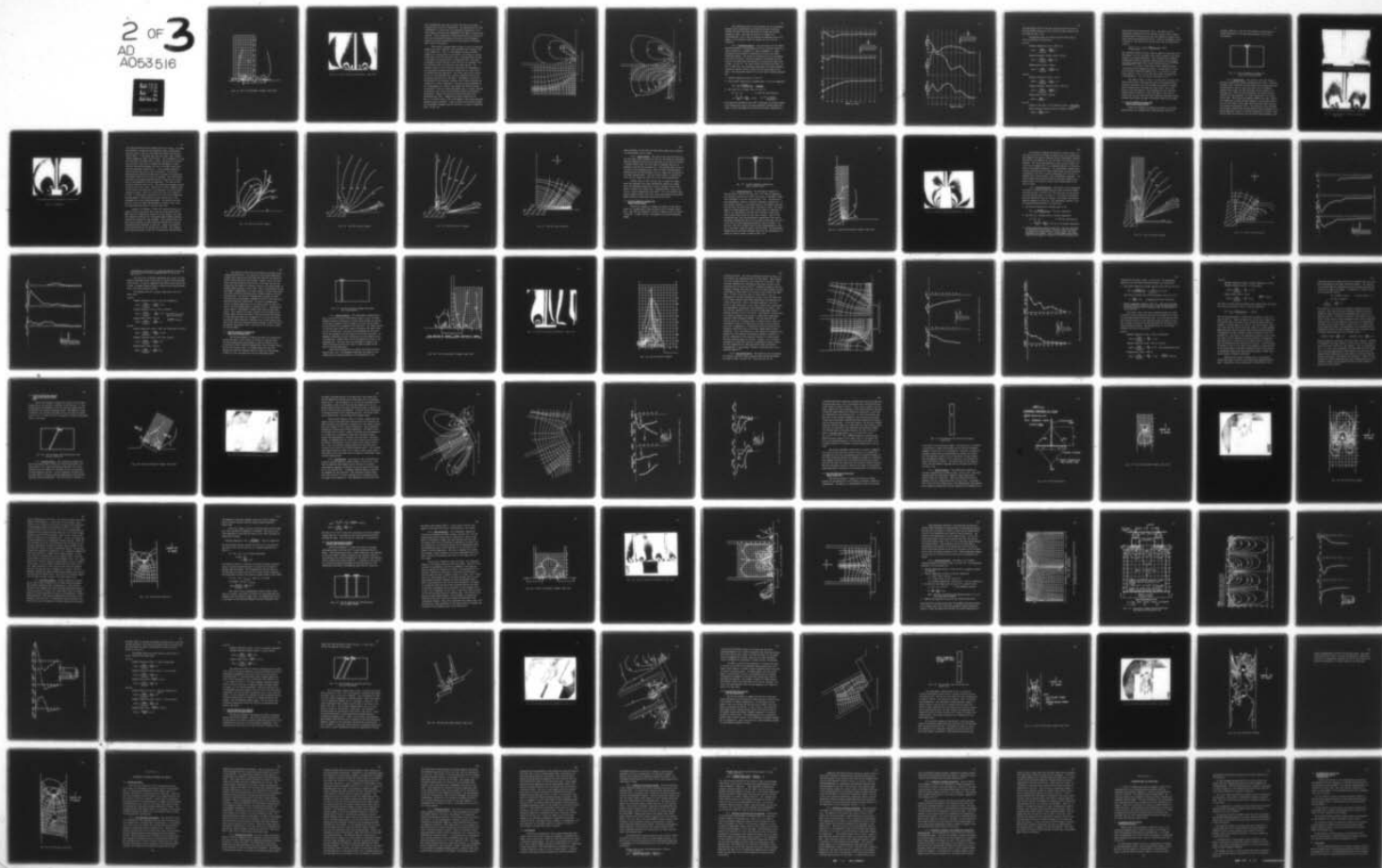
AN EXPLORATORY PHOTOELASTIC INVESTIGATION OF POST-TENSIONED CON--ETC(U)

AUG 77 S D VAUGHN

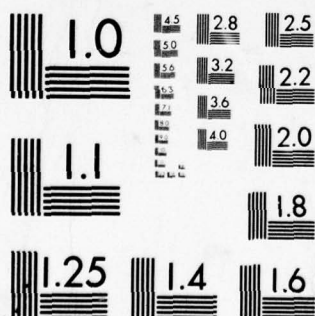
UNCLASSIFIED

. NL

2 OF 3
AD
A053 516



053516



MICROCOPY RESOLUTION TEST CHART
NATIONAL BUREAU OF STANDARDS-1963-A

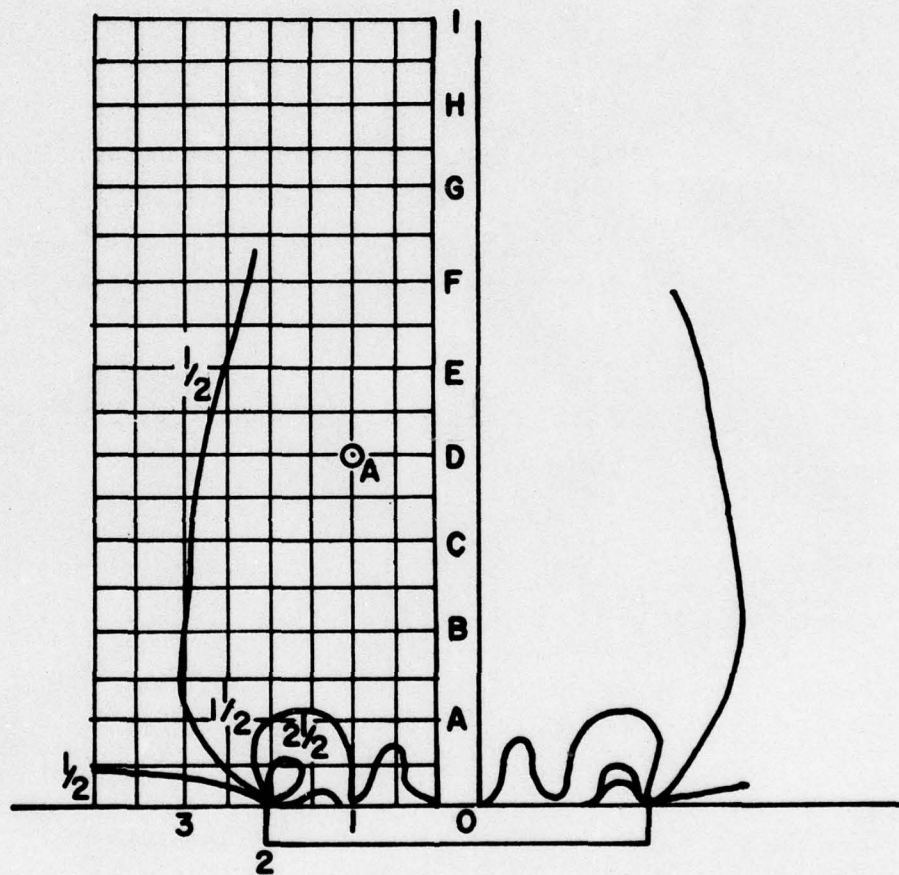


Fig. 4.2 Test #1--Isochromatic diagram, light field

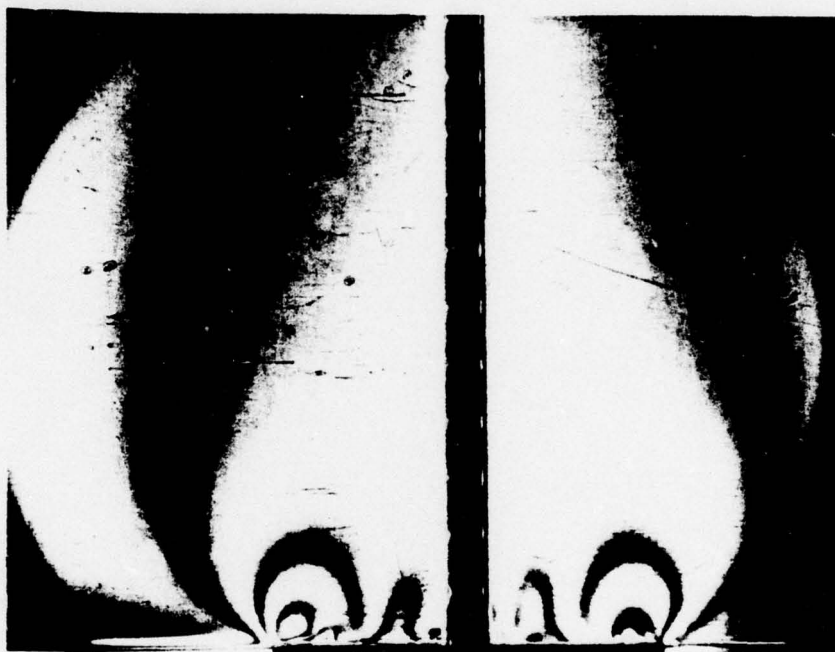


Fig. 4.3 Test #1 recorded isochromatics, light field

this investigation came from a tedious trial and error method working from a stress at a known point. By observing the $1/2$ order isochromatic, it can be seen to be gradually closing into a constant region which marks the beginning of the region of uniform compression. Since isochromatic fringes relate directly to the difference in the principal stresses at any point, the isochromatic diagram is an exact representation of the variation in principal shear stress in the model.

The isoclinic diagrams shown in Figs. 4.4 and 4.5 show good symmetry and, thus, indicate a fairly uniform load on either side of the tendon duct. Fig. 4.5 also appears to show a possible tendency for a large portion of the load to be acting as a concentrated load, since the isoclinics tend to converge toward the edge of the anchor as they would for a concentrated load. The exact convergence of these isoclinic lines could not be confirmed, since the isoclinics were not distinct at the anchor surface. The presence of the 0° or 90° isoclinic along with the convergence of the isochromatic diagram distinctly marked the area below level J as becoming uniform compression. The stress trajectories plotted in Fig. 4.4 are shown with the isoclinic parameters for the symmetrically opposite side of the model. The manner of the flow or distribution of the principal stresses can be clearly shown by the isostatics or stress trajectories. The work of Christodoulides in his investigation of a similar case showed data which had great correlation to Test #1 in shape and manner, but, of course, differed in intensity, due to the use of different geometric and material properties.² Figure 4.46 shows the stress trajectories from Christodoulides' work. Comparing the stress trajectories in Fig. 4.4 to those in Fig. 4.46 in the region of the anchor indicates generally good correlation. A good correlation also exists between the isochromatic diagrams from the two tests, as shown by comparing Figs. 4.2 and 4.47.

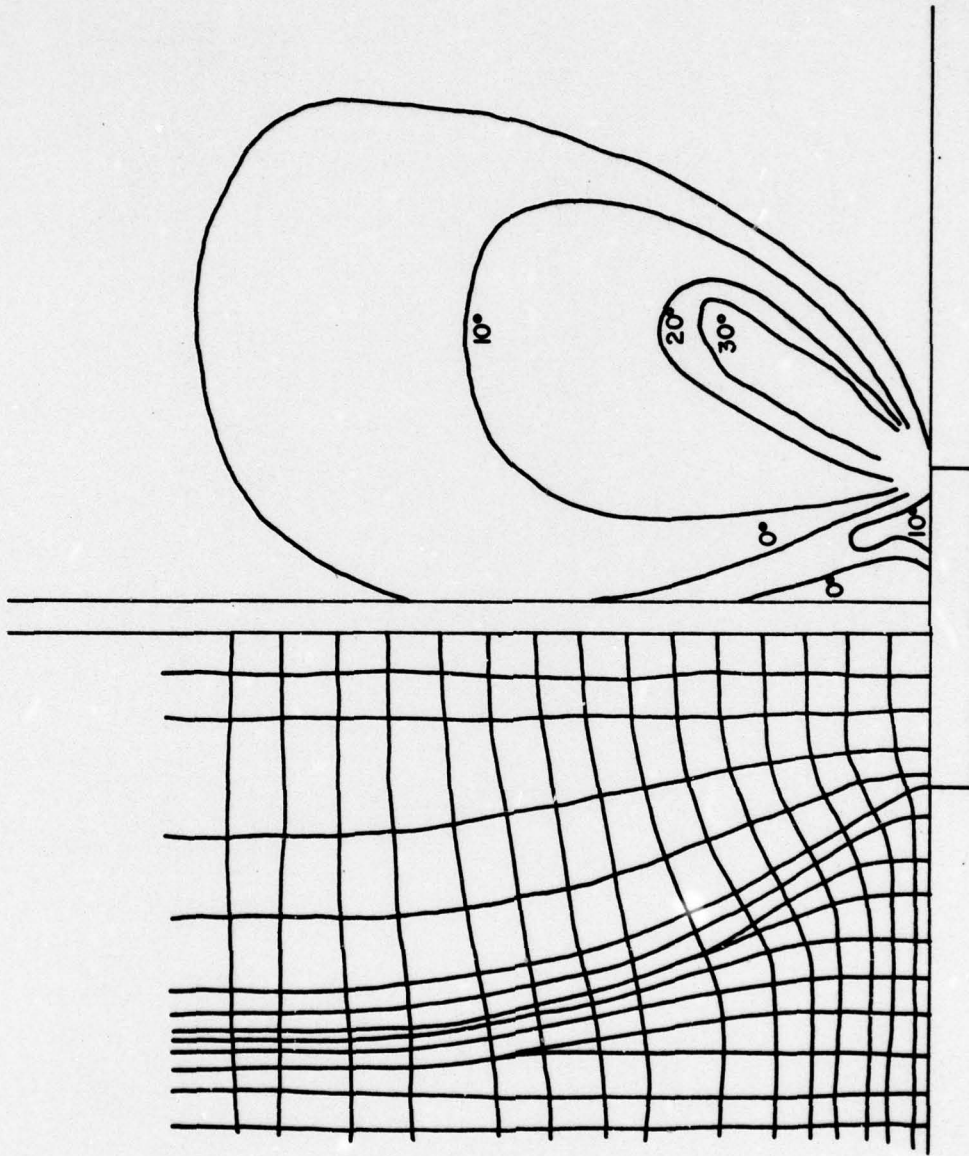


Fig. 4.4 Test #1 stress trajectory

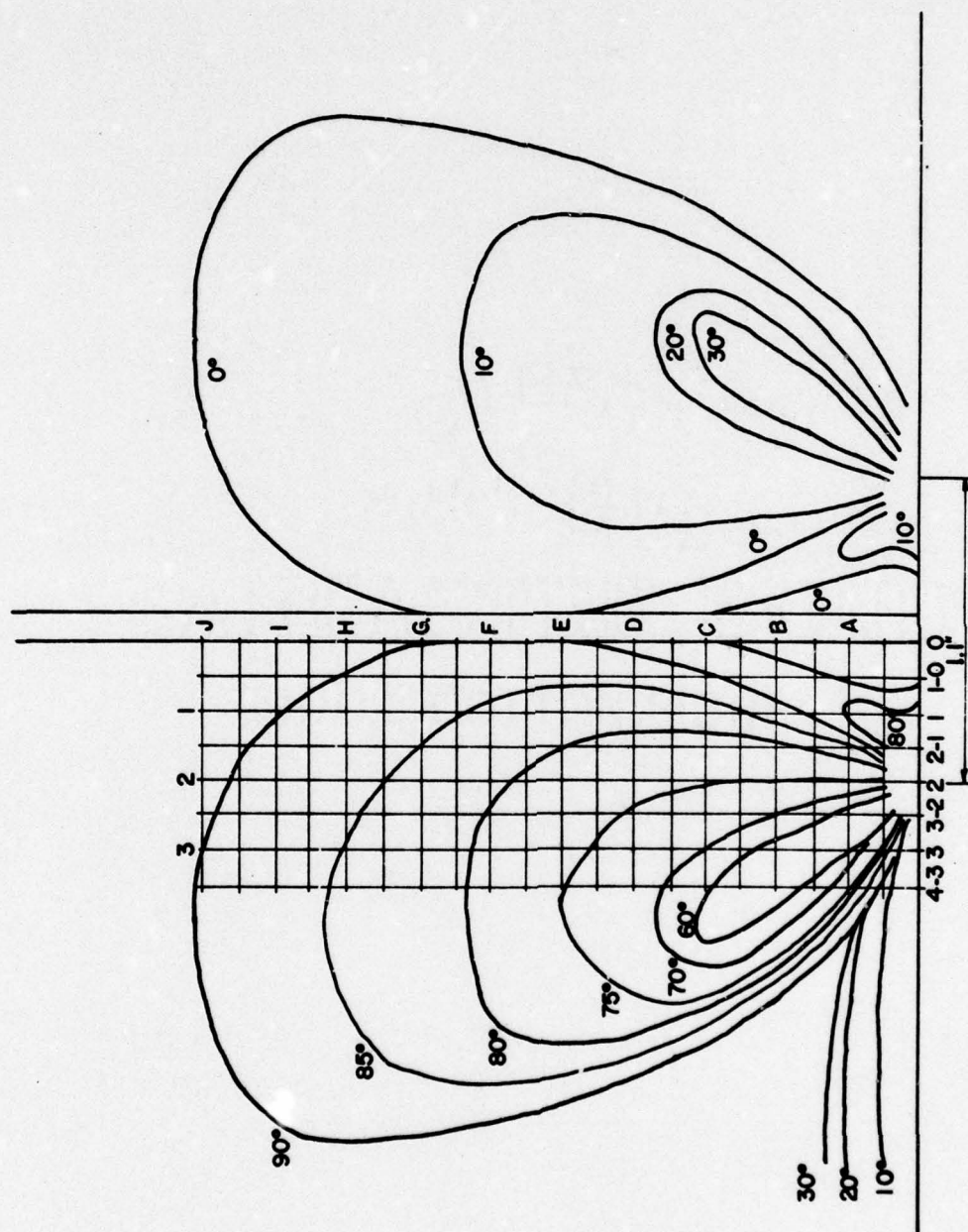


Fig. 4.5 Test #1 isoclinic diagram

The differences which do exist between the two isochromatic diagrams can be explained by the nonuniform surface conditions between the anchor and model which tend to disrupt the uniform transfer of load. Care must be taken not to compare the Christodoulides' test to Test #1 outside the immediate area of the anchor, as the boundary conditions between the two tests are different.

4.4.2 Calculated Results. The calculations for the "Shear Difference Method" of determining the stress at interior points are shown in Tables A4.1 through A4.7 found in Appendix A. These calculations are provided to demonstrate the use of the "Shear Difference Method". The tables of calculations for all succeeding tests will be omitted. The grids employed to determine the locations of the points where the values are calculated are shown both on Figs. 4.2 and 4.5. The final results are reflected in Figs. 4.6 and 4.7 which plot the calculated longitudinal and radial principal stresses at various levels of depth from the loaded edge of the model. The assumptions employed to use the "Shear Difference Method" are:

1. Uniform compression exists at level "J"
2. This uniform compression is assumed equal to 28.5 psi compression

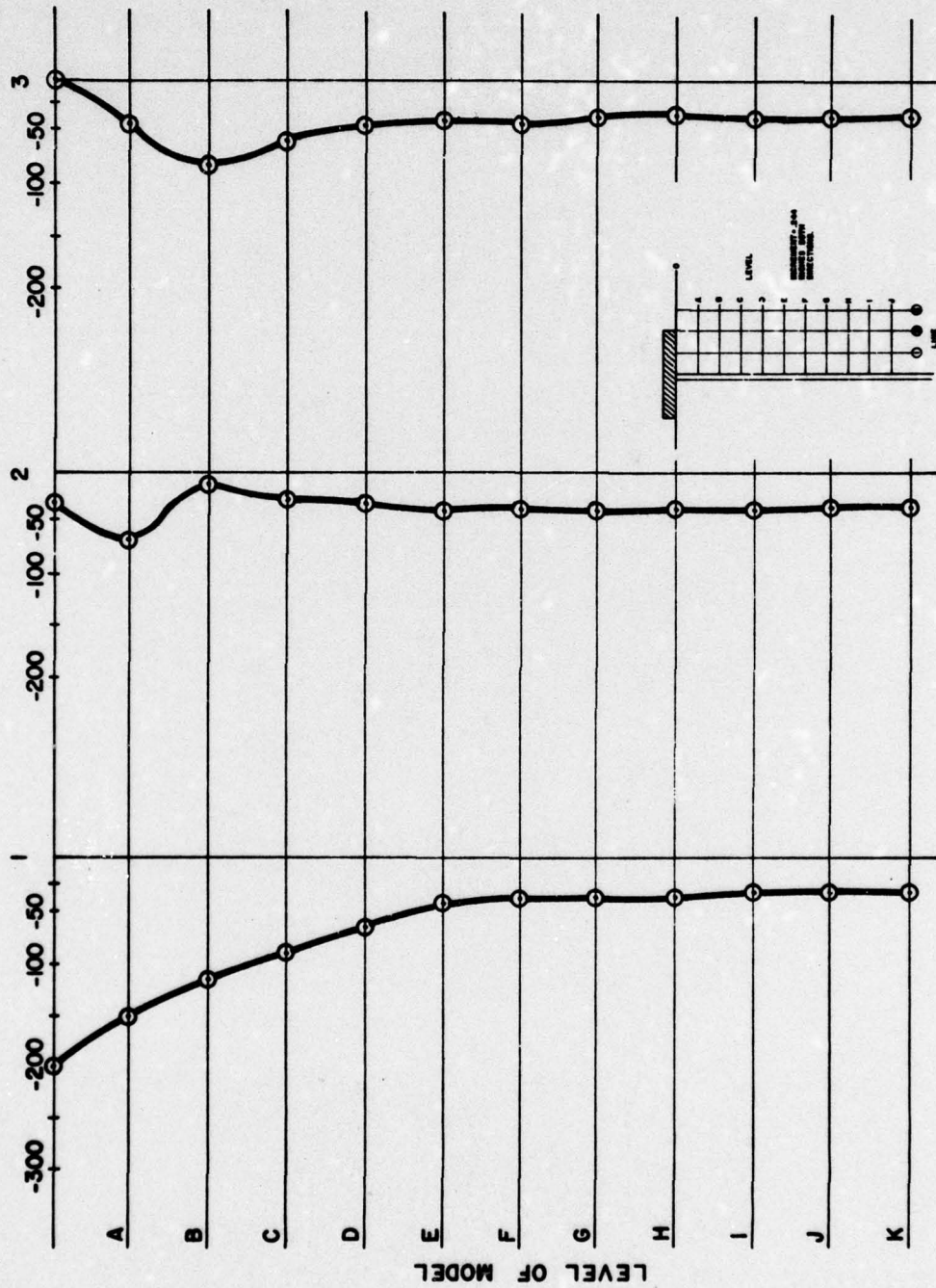
$$P/A = \frac{84 \text{ lbs.}}{(8 - 0.125)(0.375)} = \underline{\underline{28.5 \text{ psi}}}$$

3. The value for n (fringe order) at level "J"

$$nf = \sigma_1 - \sigma_2 \qquad f = 160 \text{ (for this material)}$$

$$n = \frac{\sigma_1 - \sigma_2}{160} = \frac{28.5}{160} = 0.178 \qquad \sigma_2 = 0 \text{ if uniform compression}$$

Trial and error procedures were used to determine the relative values of n (fringe order) and θ (isoclinic parameter) between known data lines, so that the method would produce the uniform compression at

Fig. 4.6 Test #1--Principal longitudinal stress Q

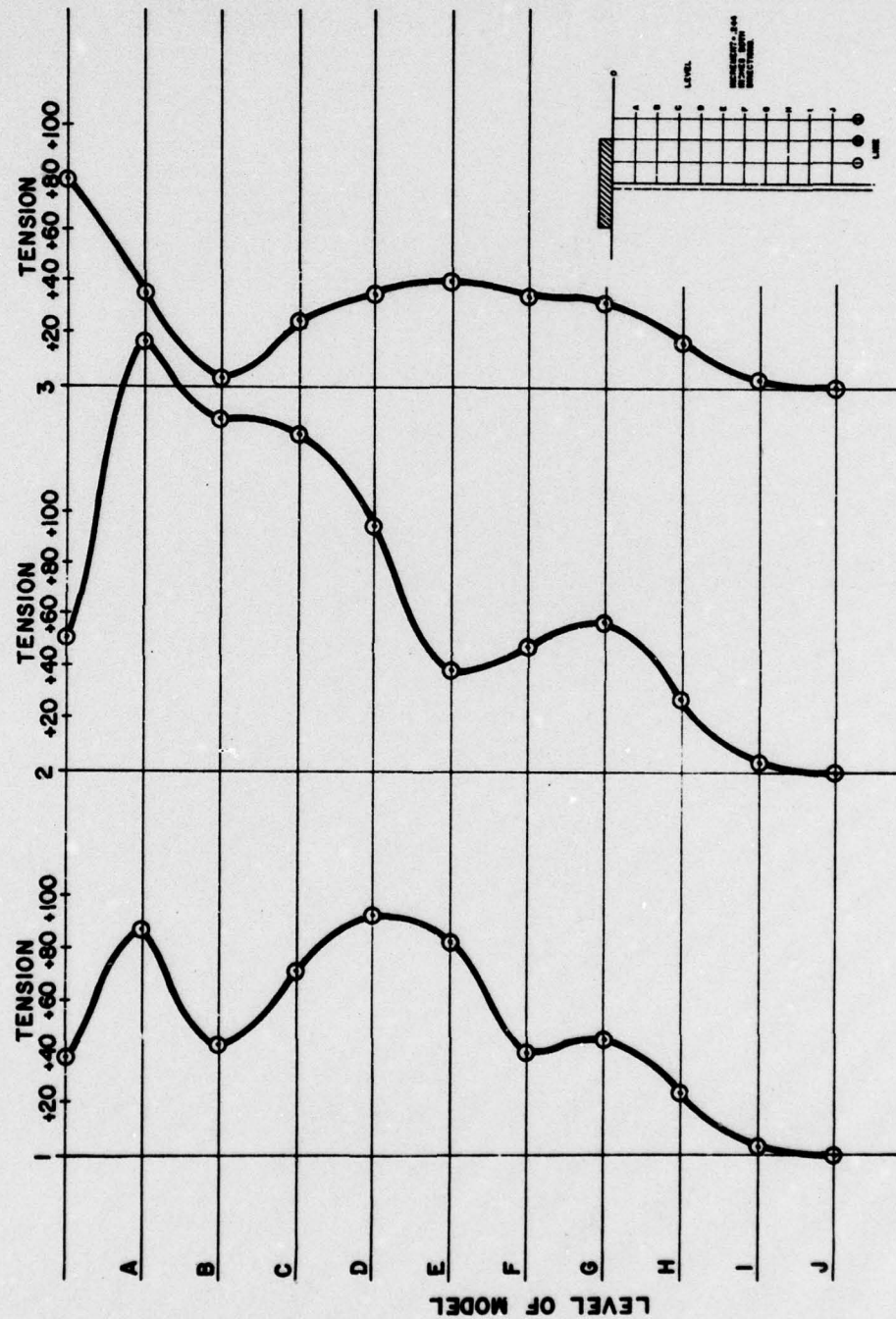


Fig. 4.7 Test #1--Principal transverse stress P

the known depth level "J" and when calculated from that point to the free surface would give a zero value for normal stress at the free edge (see Sec. 2.5).

The maximum values for stress along the three lines of action considered are shown below:

Line #1:

Maximum compressive stress = 200.4 psi

$$\text{Ratio} = \frac{\sigma_{\max}}{\sigma_{\text{uniform}}} = \frac{200.4}{28.45} \approx 7$$

Maximum transverse tensile stress = 90 psi

$$\text{Ratio} = \frac{\sigma_{\max}}{\sigma_{\text{uniform}}} = \frac{90}{23.45} \approx 3.2$$

Maximum shear stress = 160 psi

$$\text{Ratio} = \frac{\tau_{\max}}{\sigma_{\text{uniform}}} = \frac{160}{28.45} \approx 5.6$$

Line #2:

Maximum compressive stress = 72 psi

$$\text{Ratio} = \frac{\sigma_{\max}}{\sigma_{\text{uniform}}} = \frac{72}{28.45} \approx 2.5$$

Maximum transverse tensile stress = 168.4 psi

$$\text{Ratio} = \frac{\sigma_{\max}}{\sigma_{\text{uniform}}} = \frac{168.4}{28.45} \approx 6$$

Maximum shear stress = 200 psi

$$\text{Ratio} = \frac{200}{28.45} \approx 7$$

Line #3:

Stress at free edge = 5 psi (should be zero)-- respectable
correlation
Known transverse tensile stress at boundary = 80 psi

$$\text{Ratio} = \frac{80}{28.45} \approx 2.8$$

These values reflect appreciable error. The values for the compressive stresses are not too extreme, however, since a simple uniform stress calculation shows that the compressive stress at the anchor should be approximately 230 psi. There is reasonable correlation (230 vs. 200) with the calculated value from the photoelastic results:

$$\frac{P}{A_{\text{under anchor}}} = \frac{84}{(1.1 - 0.125)(0.375)} = 229.8$$

The transverse tensile stresses, however, appear to have great error. They appear to be far too large, with a more acceptable value being around 0.6 x uniform compression. This value has been confirmed through many different analytical methods and has received support from direct measurements from several different sources.^{2,8,11,18,19,22,23,24,25} An error in the value of the transverse tensile stress would not be unexpected, however. The discussion of error with the "Shear Difference Method" in Sec. 2.3 stated if σ_y was large relative to $(\sigma_1 - \sigma_2) \cos 2\theta$, then sizable error may exist in determining σ_x . This is exactly the present case.¹³

The value of Figs. 4.6 and 4.7 is that they do reflect the trend of the stress. They show the stress is not uniform under the anchor and reduces as the free edge of the anchor is reached. Since calculations at free edges are fairly exact, due to the nature of the isochromatics, the calculation for the transverse tensile stress at station 3 at the free edge is very close to correct and, as such, indicates large transverse spalling stresses developed just beyond the edge of the anchor along the free edge.

4.3 Test #2--Symmetric Loading with Single Inset Bearing Anchor

Test #2 was designed to examine the effects of the inset bearing anchor on a symmetrically loaded anchorage zone with a

straight tendon duct. The test was intended to provide data to analyze the effect of the inset bearing anchor on the stress distribution.

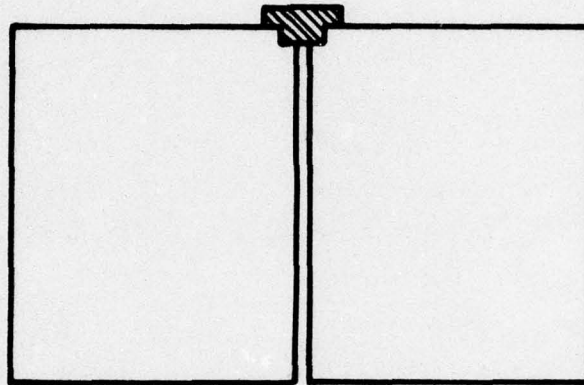
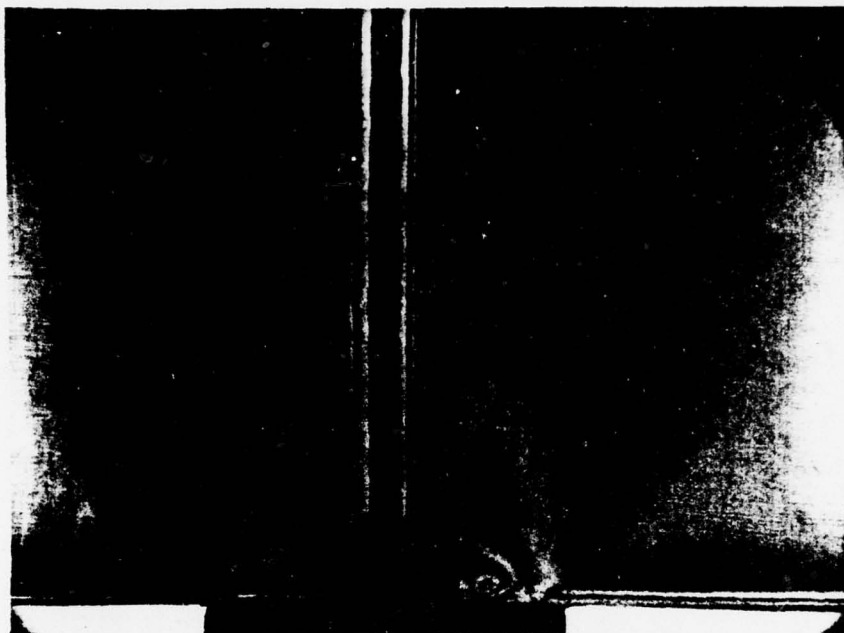


Fig. 4.8 Test #2--Symmetric loading with single inset bearing anchor

4.3.1 Observed Data. The testing of the inset bearing anchor was plagued with serious problems from the start. There were extremely close tolerances required between the anchorage model and the photoelastic model in order that they would fit properly together and transfer the load uniformly from the tendon to the anchorage zone. When the load was applied, the anchor would not transfer the load uniformly, but rather transferred it as concentrated loads. While there was apparent symmetry [see Fig. 4.9(a)], the loading was so biased by this tendency of concentrated loads to exist at the corners of the model where there was contact that the test became of questionable value. The problem was that the shape of the anchor required that the photoelastic sheet be machined to an almost impossible accuracy if uniform loading was to develop. Also, the fact that the anchor was cast from lead created problems, since

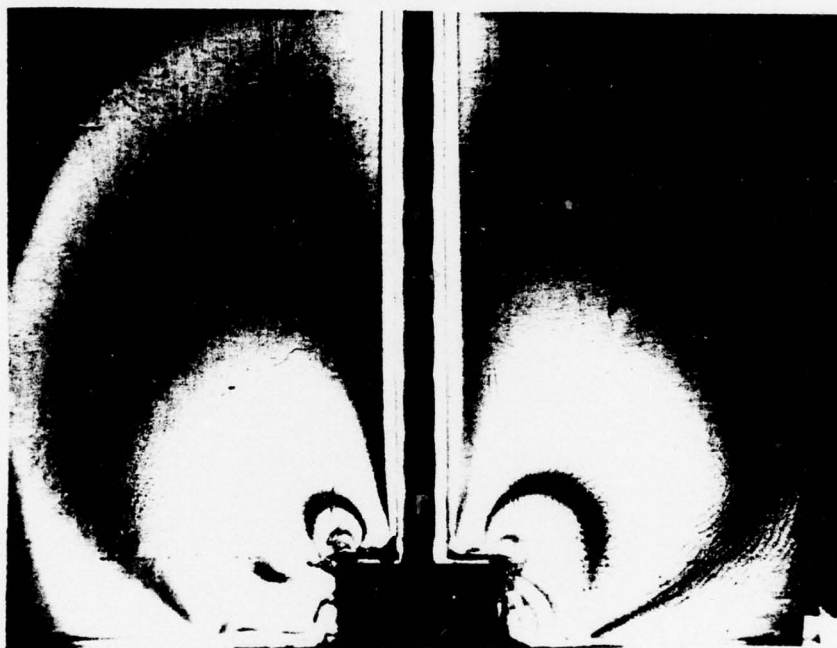


(a) Test #2 recorded isochromatics, light field



(b) Test #2A recorded isochromatics, light field

Fig. 4.9 Test Series #2 recorded isochromatics,
light field



(c) Test #2B recorded isochromatics, light field

Fig. 4.9 (Continued)

its actual dimensions varied slightly with each casting. To remedy this problem, a second test was conducted, where a photoelastic epoxy was used to create a bond between the anchor and the photoelastic sheet. It was hoped that this bond would make a smooth contact between the anchor and the model. The isochromatics for this test (Test #2A) are shown in Fig. 4.9(b), and while the left-hand upper portion of the model is showing the development of shear stresses from uniform loading, the rest of the model shows gross bias and completely unusable data. A third attempt was made to improve the bearing of the anchor on the model. A precision-machined brass anchorage was made which conformed to the existing photoelastic model slot as closely as possible. This brass anchorage model was extremely expensive and had a high level of conformance to the dimensions of the existing model. Test #2B was then conducted using the brass anchor. The isochromatic diagram is shown for this test in Fig. 4.9(c). While there is better symmetry than in Test #2A and the indication of the existence of partial uniform loading is present, these test results were also too irregular to be used. It was finally decided not to use Test #2 for comparison and development of conclusions for stress distribution in the anchorage zone of post-tensioned members. The decision was made also not to use the inset bearing anchor in further tests, since the same problem was likely to develop there also.

Figures 4.10 through 4.12 show the recorded isoclinic diagrams for each of the three tests using the inset bearing anchor. While there are similarities between all three diagrams, note that each diagram is different for the supposed same loading conditions (scales are different for each drawing). This indicates that each test did not generate the same loading conditions and the stress distributions were different in each case. Figure 4.13 shows the stress trajectories for the initial test, Test #2. This drawing does reflect the nature of the flow of stress since the isoclinics,

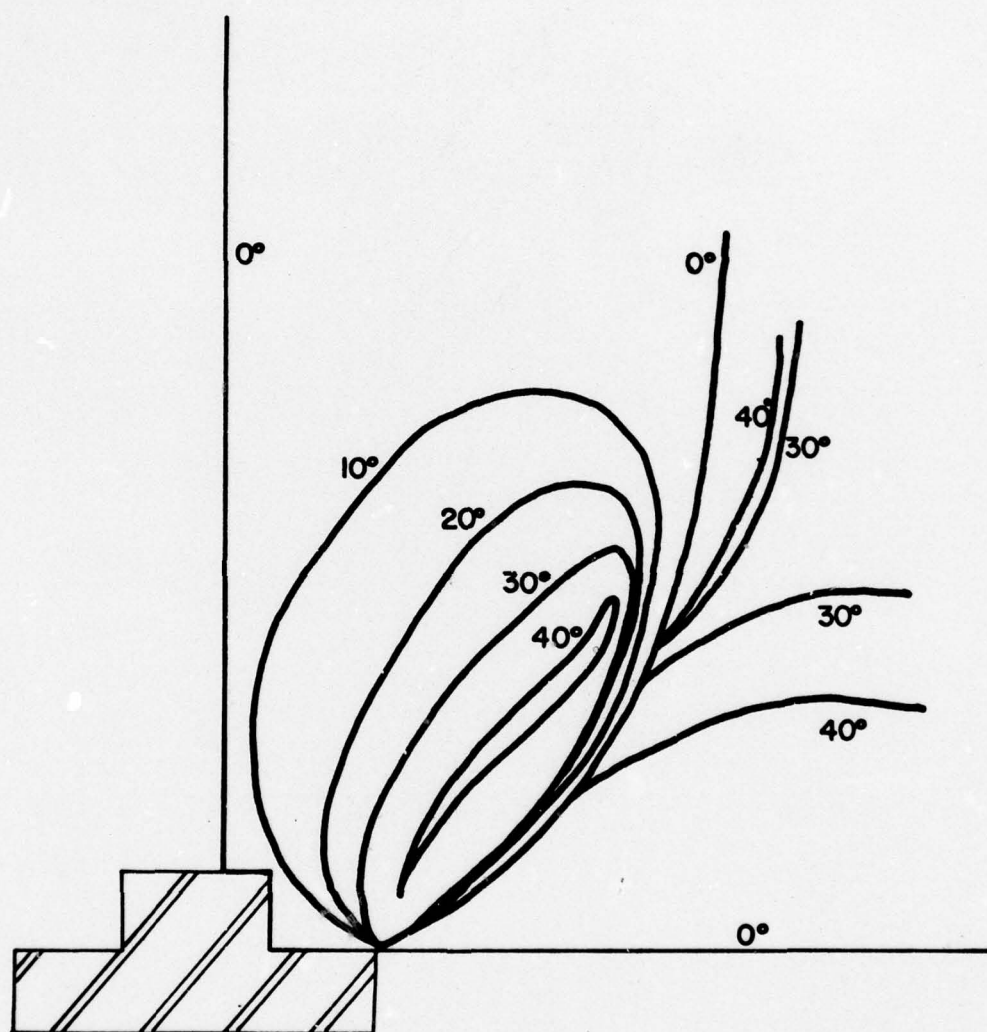


Fig. 4.10 Test #2 isoclinic diagram

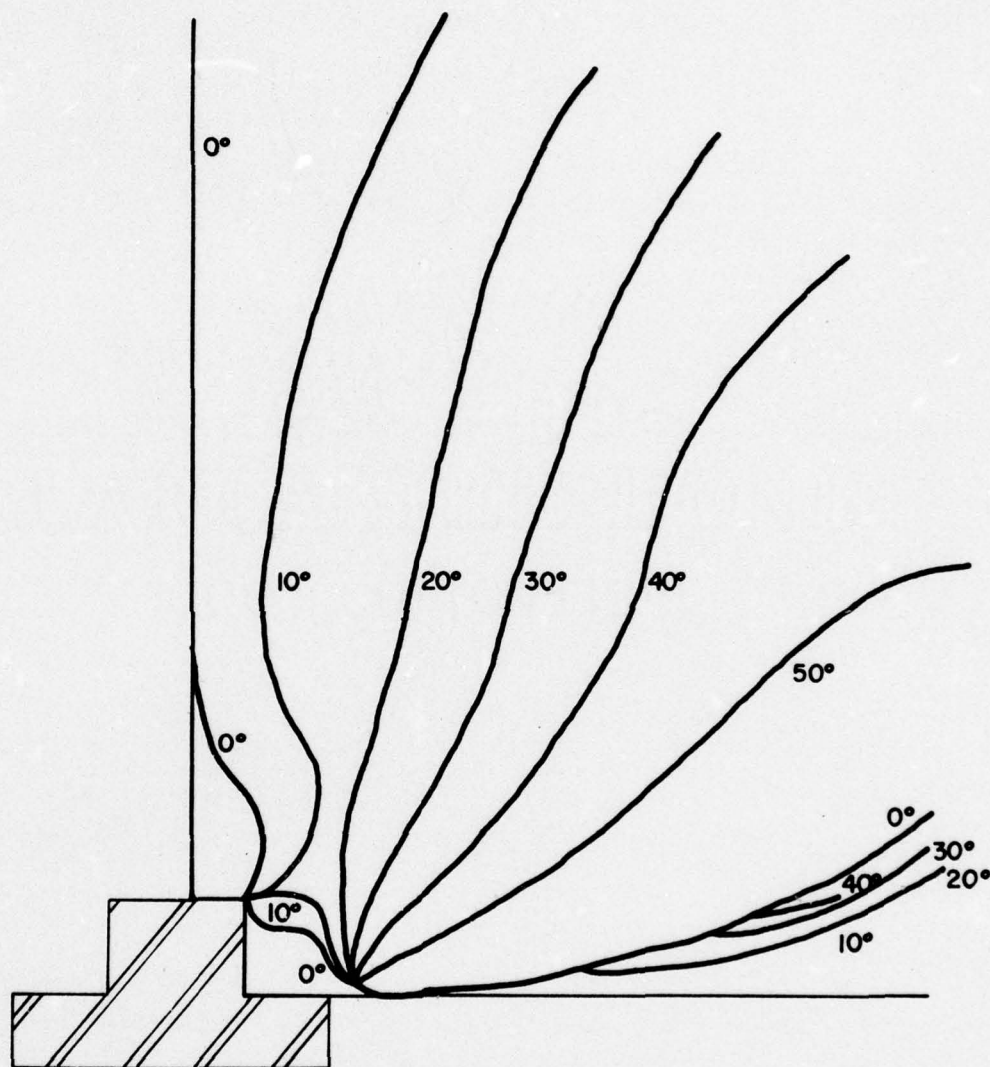


Fig. 4.11 Test #2A isoclinic diagram

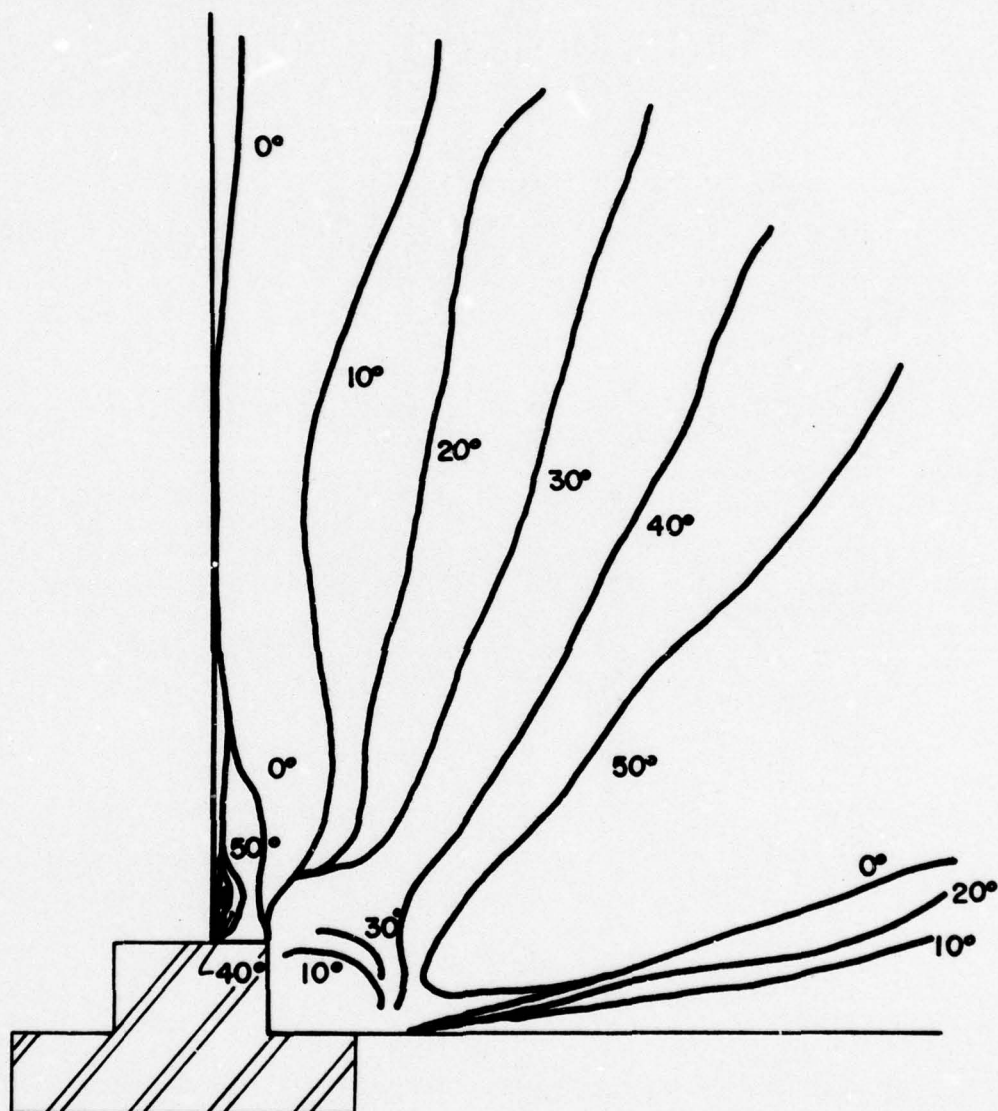


Fig. 4.12 Test #2B isoclinic diagram

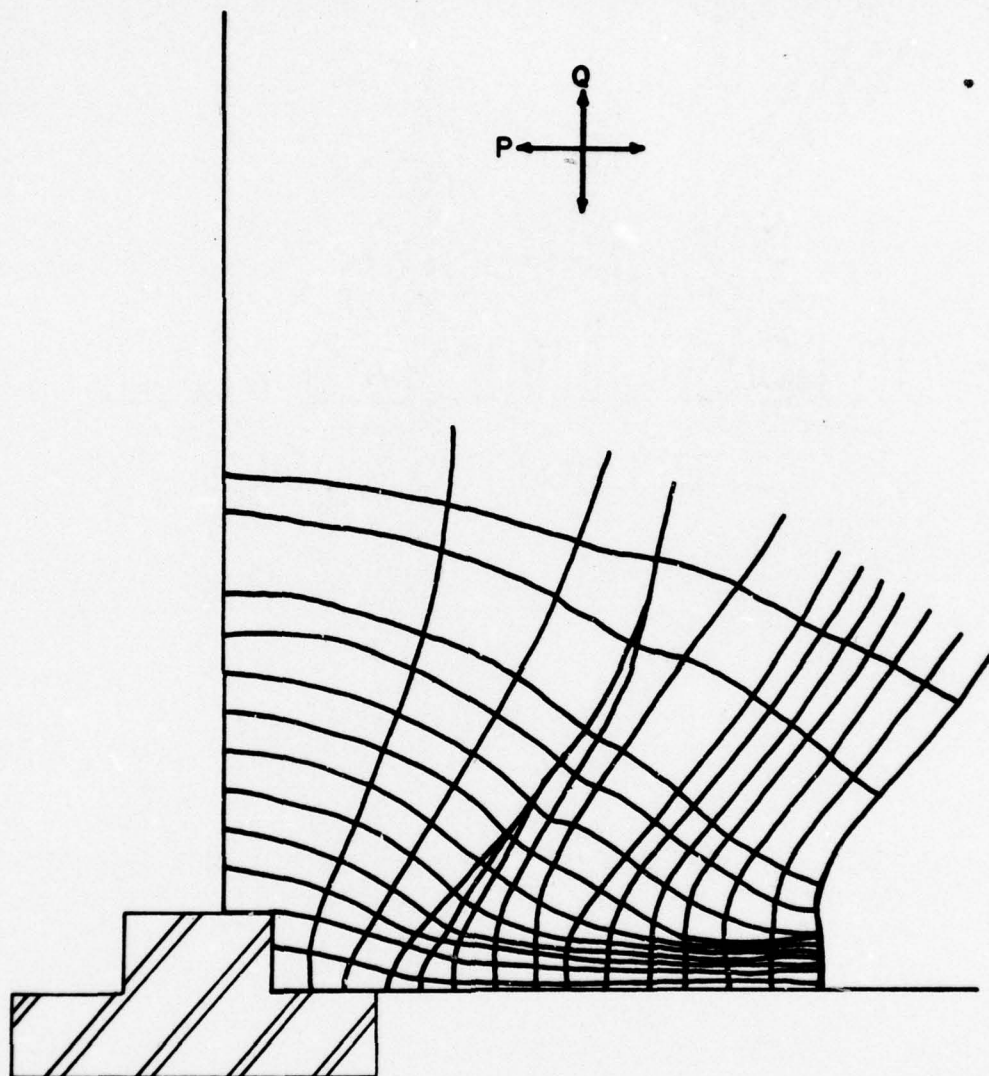


Fig. 4.13 Test #2 stress trajectory

while different, do all have the same general shape and so indicate the same general flow of stress.

4.3.2 Usable Results. The value of Test Series #2 lies in the fact that a major problem area with the test model was identified. When the anchorage required close tolerances in the model to provide a uniform contact area, the test model as designed could not be machined to provide the necessary fit. This problem would not be as critical in the remaining tests, since the other anchorage models, especially the flat bearing model, did not require the tolerances of the inset bearing anchor. Even the conical anchor is tapered and, thus, did not require the exact fit of the inset bearing anchor.

Another value of this test was that it showed how complicated the anchorage zone stress distribution becomes in a member where the anchorage system does not have a uniform surface along which to transfer the tendon load. Reexamining Figs. 4.9(a), (b), and (c), clearly demonstrates that point. It is very doubtful that perfect surface contact will exist in any post-tensioned prestressed member between the anchorage system and the end block.

4.4 Test #3--Symmetric Loading with Single Conical Anchor

Test #3 was designed to examine the effects of the conical anchor on a symmetrically loaded end block with a straight tendon duct. The test was intended to provide a comparison for the results of Test #1. A load of 85 lbs. was applied to the post-tensioning tendon.

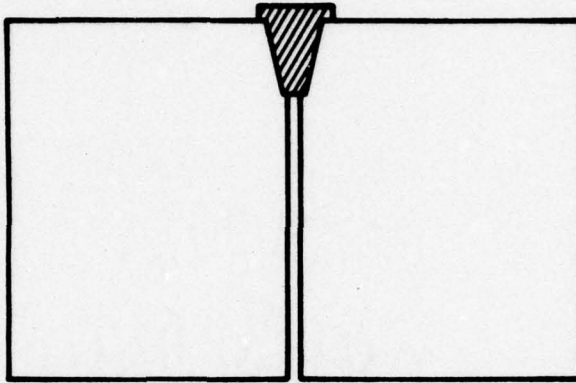


Fig. 4.14 Test #3--Symmetric loading with single conical anchor

4.4.1 Observed Results. The isochromatic diagram for Test #3 showed a bias to the right side. The load was apparently not the same on both sides as there is one more isochromatic fringe order developed on the left side (see Fig. 4.15). The pattern of the isochromatics, however, indicates a generally uniform load. It was decided, therefore, to go ahead with the test analysis and work with the left side which would give conservative values. The large number of fringes generated by the conical anchor in comparison to Test #1 for approximately the same load indicates a much larger shear stress being created by this type of anchor. There is the possibility that load concentrations are appearing at the ends of the anchor bearing directly on the free edge of the model, and very little load is being transferred along the inclined surface. In any case, there are extremely high stresses being generated at the top of the anchor along the edge of the end block. The isochromatic diagram with its grid and reference points for the determination of stress at interior points is shown in Fig. 4.15.

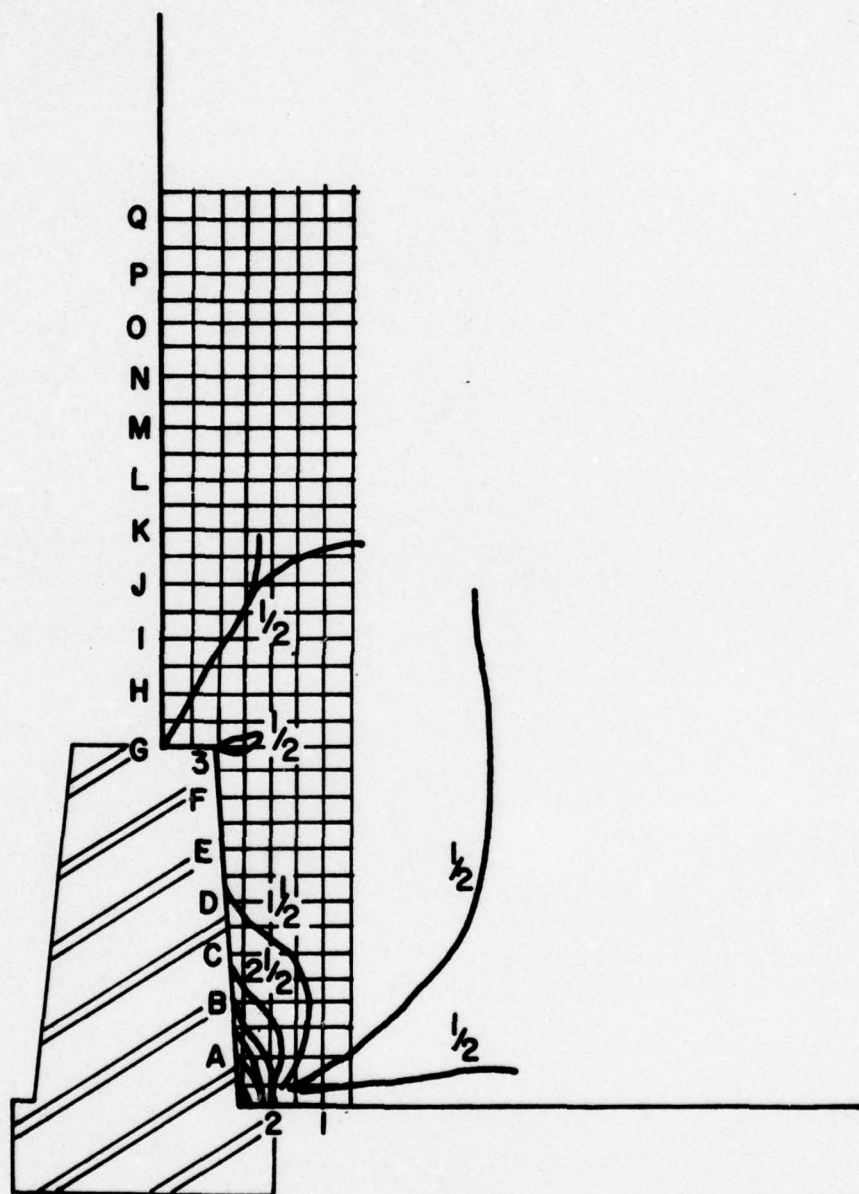


Fig. 4.15 Test #3--Isochromatic diagram, light field

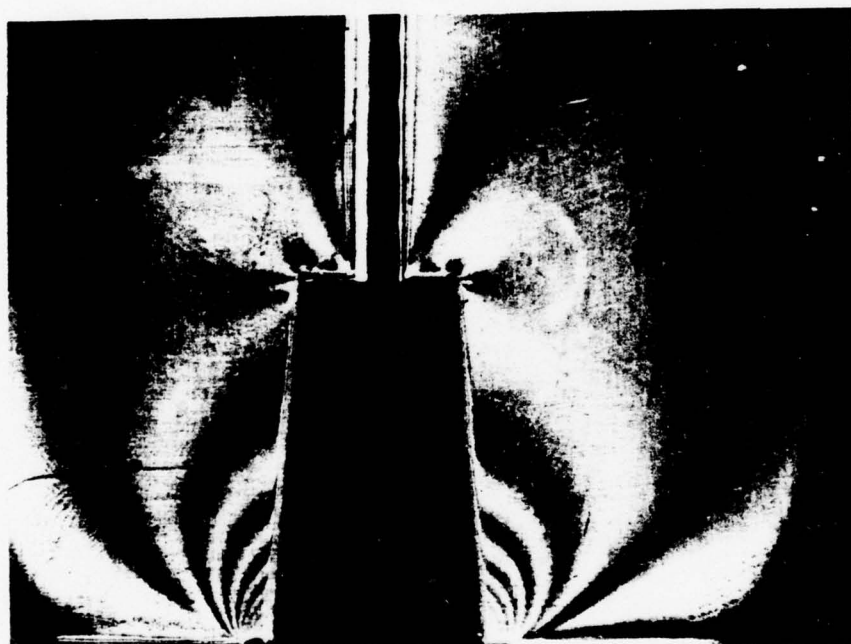


Fig. 4.16 Test #3 recorded isochromatics, light field

The isoclinic diagram with the grid is shown in Fig. 4.17. Only the left half of the model is shown, since the isoclinics had good symmetry (as would be expected from the isochromatic diagram) and only the calculations for the left half of the model were to be analyzed. The one problem indicated is that the zero degree isoclinic is not complete and it is extremely difficult to locate the start of the uniform compression. The isochromatic diagram shows a definite area where the 1/2 order fringes merge and this indicates an approach to an area of uniform compression, but the lack of a complete zero isoclinic makes visual establishment impossible. The stress trajectories calculated from the isoclinic parameters are shown in Fig. 4.18 and give a good visual representation of the flow of stress.

4.4.2 Calculated Results. The results of the calculations for stress at interior points using the "Shear Difference Method" are shown in Figs. 4.19 and 4.20. The grids used for the calculations are shown in Figs. 4.15 and 4.17. The actual calculations have been omitted but they are similar to the sample calculations shown in Appendix A for Test #1. The assumptions employed to use the "Shear Difference Method" for Test #3 are:

1. The uniform compression is assumed equal to P/A

$$P/A = \frac{85 \text{ lbs.}}{(8 - 0.125)(0.375)} = 28.8 \text{ psi compression}$$

2. The value of n (fringe order) at uniform compression

$$nf = \sigma_1 - \sigma_2 \quad f = 160 \text{ (for this material)}$$

$$n = \frac{\sigma_1 - \sigma_2}{160} = \frac{28.8}{160} \approx 0.18 \quad \sigma_2 = 0 \text{ if uniform compression}$$

3. Uniform compression begins at level "S". This was calculated by starting at the free edge of the model where the stresses are known and working down line 1 until a value ≈ 28.8 psi compression was reached. Due to the percentage error experienced with the degree of accuracy of the data obtained by the

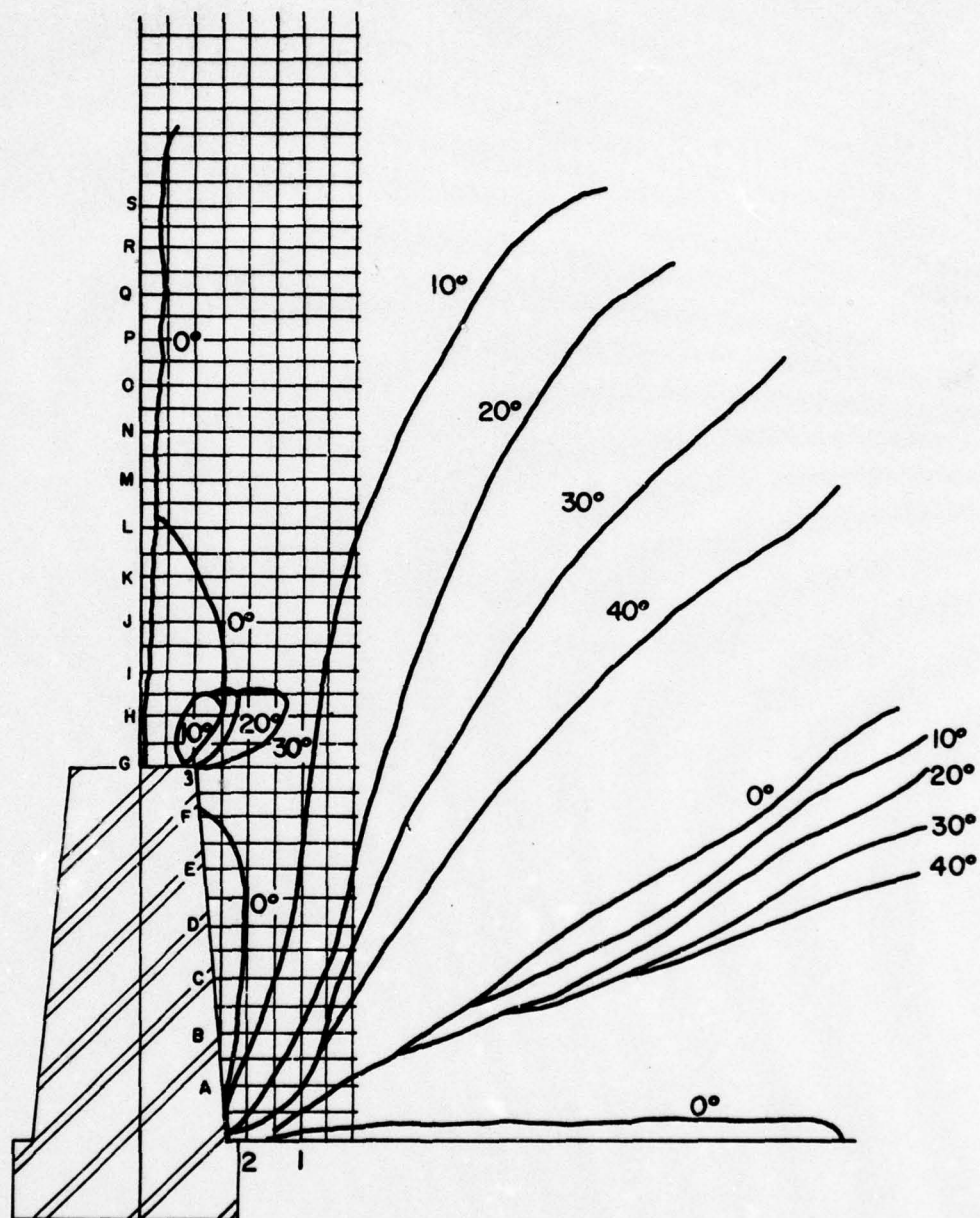


Fig. 4.17 Test #3 isoclinic diagram

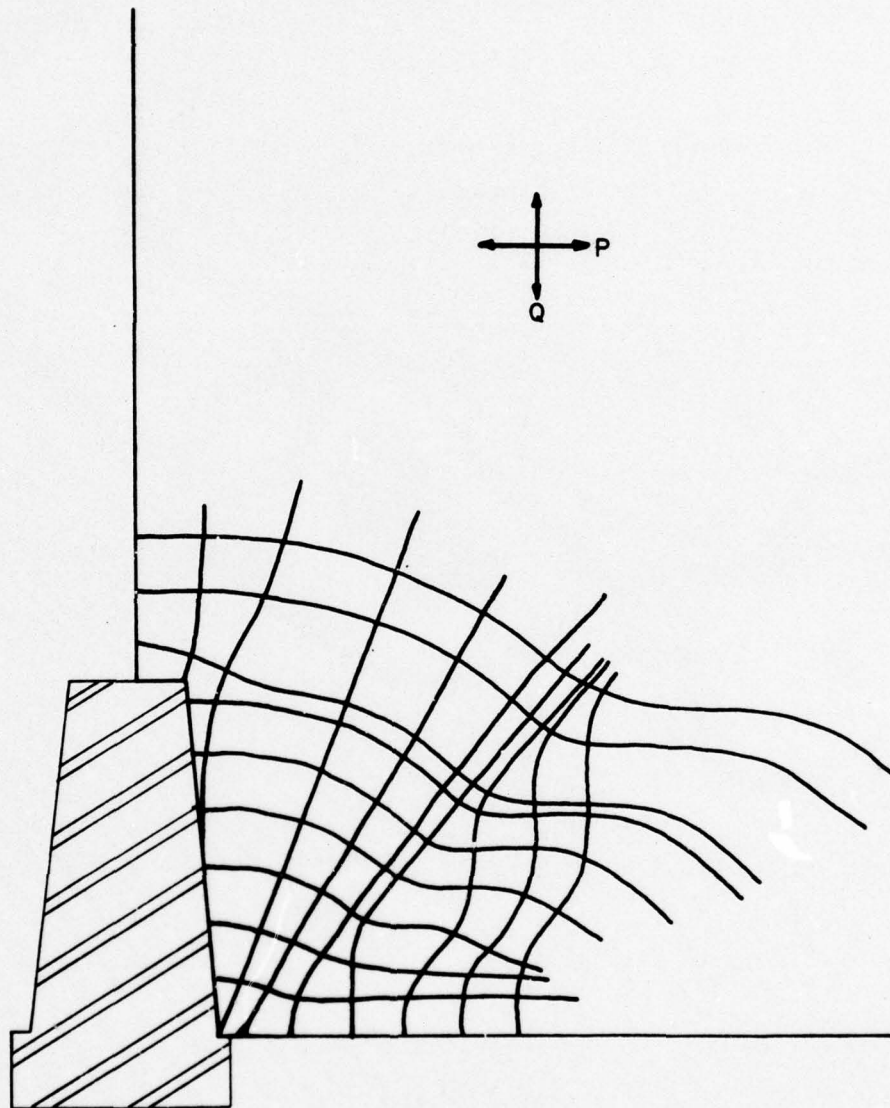


Fig. 4.18 Test #3 stress trajectory

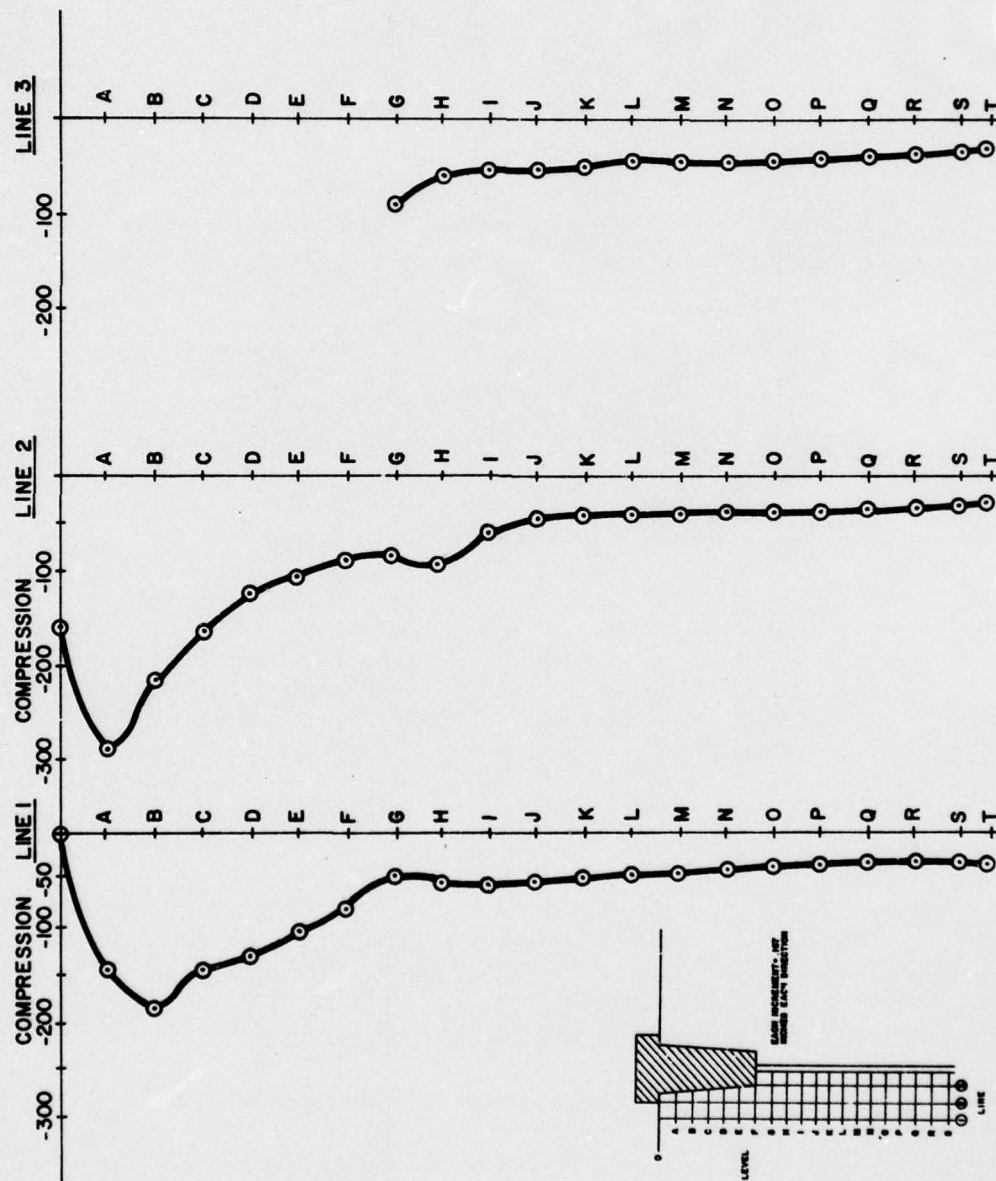


Fig. 4.19--Principal longitudinal stress Q

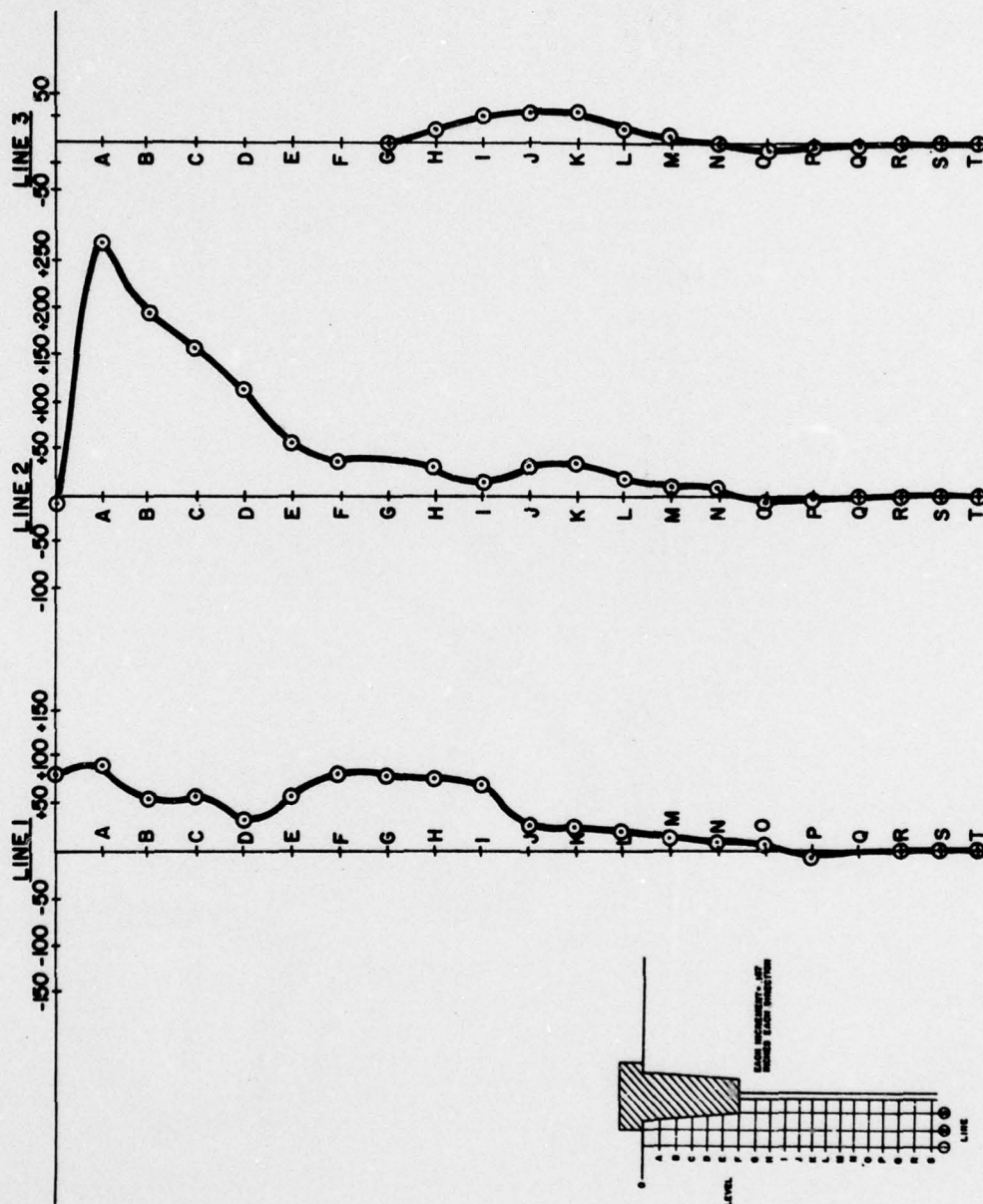


Fig. 4.20 Test #3--Principal transverse stress P

investigation, this level is a rough approximation at best and an actual level of uniform compression may not exist (see Sec. 4.1.1).

Once the level of uniform compression was located, the same method as employed in Test #1 was used to calculate stresses along lines 2 and 3. It must be emphasized that these results should only be used to examine trends as there are large errors associated with them, as has been discussed earlier.

The maximum values for stresses along lines 2 and 3 are shown below:

Line #1:

Maximum compressive stress = 187.2 psi compression

$$\text{Ratio} = \frac{\sigma_{\max}}{\sigma_{\text{uniform}}} = \frac{187.2}{28.8} \approx 6.5$$

Maximum transverse stress = 80 psi (tension)

$$\text{Ratio} = \frac{\sigma_{\max}}{\sigma_{\text{uniform}}} = \frac{80}{28.8} \approx 2.8 \quad (\text{calculated at a free edge, so reliable})$$

Maximum shear stress = 120 psi

$$\text{Ratio} = \frac{\tau_{\max}}{\sigma_{\text{uniform}}} = \frac{120}{28.8} \approx 4 \quad \frac{1.5(160)}{2} = 120 \text{ psi}$$

Line #2:

Maximum compressive stress = 289.5 psi compression at level B

$$\text{Ratio} = \frac{\sigma_{\max}}{\sigma_{\text{uniform}}} = \frac{289.5}{28.8} \approx 10.05$$

Maximum transverse stress = 270.5 psi (tension)

$$\text{Ratio} = \frac{\sigma_{\max}}{\sigma_{\text{uniform}}} = \frac{270.5}{28.8} \approx 9.4$$

Maximum shear stress = 520 psi

$$\text{Ratio} = \frac{\tau_{\max}}{\sigma_{\text{uniform}}} = \frac{520}{28.8} \approx 18$$

The values for line 3 are not included as they have no real comparison with Test #1. The values for the stresses shown above probably have large errors associated with them and the transverse tensile stress values are far too high. However, the errors with these calculations and with Test #1 are of the same type and comparing both sets there is an obvious trend for the conical anchor to develop larger stresses in every case. This is substantiated by the isochromatic diagram which is a direct measure of shear stress where the conical anchor has developed twice as many fringes as the flat bearing anchor. The ratios of maximum shear stresses are taken directly from the isochromatic diagram and there is much less error associated with their calculation. The ratio of maximum shear stress to uniform compression for the conical anchor is about 18 and for the flat bearing anchor is between 6 and 7. This gives the conical anchor a development of almost three times as much shear stress. This tendency for larger stresses to be developed by the conical anchor has been indicated in the field, where flat bearing or inset bearing anchors were designed for a structure and tested successfully under laboratory conditions, but conical anchors were used in the field and cracking problems developed in the structure.⁵ Any further study should take a close look at the stresses created by conical anchors.

4.5 Test #4--Eccentric Loading with Single Flat Bearing Anchor

Test #4 was designed to examine the effects of eccentricity of the end anchor on the creation of stresses in the end block. The flat bearing anchor was employed so that the effects of the eccentricity could be analyzed independently of any stresses created by the type of anchor used. A straight tendon duct was also employed, so that duct geometry would not enter into the problem. A load of 76 lbs. was applied to the post-tensioning tendon.

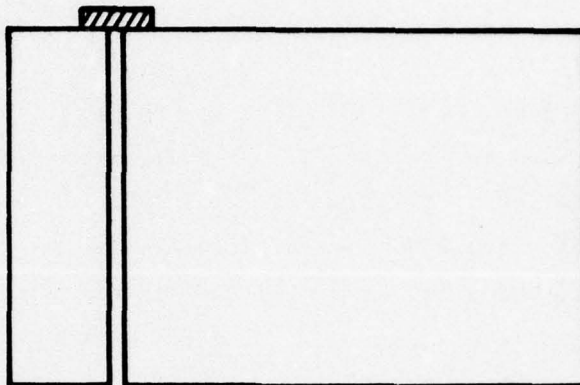


Fig. 4.21 Test #4--Eccentric loading with single flat bearing anchor

4.5.1 Observed Results. The isochromatic diagram shown in Fig. 4.22 and the recorded isochromatics shown in Fig. 4.23 show a markedly different distribution of shear stress between the portion of the model bounded by the free edges (left side) and the larger portion formed by the remainder of the end block. The larger portion of the model gives almost the classic distribution for shear stress due to a uniform load. The other portion demonstrates the effect due to the presence of the free edge in the vertical direction. An immediate observation is that eccentricity and the presence of the free edge have a marked effect on the distribution of stress in the anchorage zone. Note also that the isochromatic fringes on the smaller end block portion do not give a visual location for the start of uniform compression.

The isoclinic diagram for the smaller end block portion is shown in Fig. 4.24. The parameters show that the region is very complicated with large variations in the orientation of the

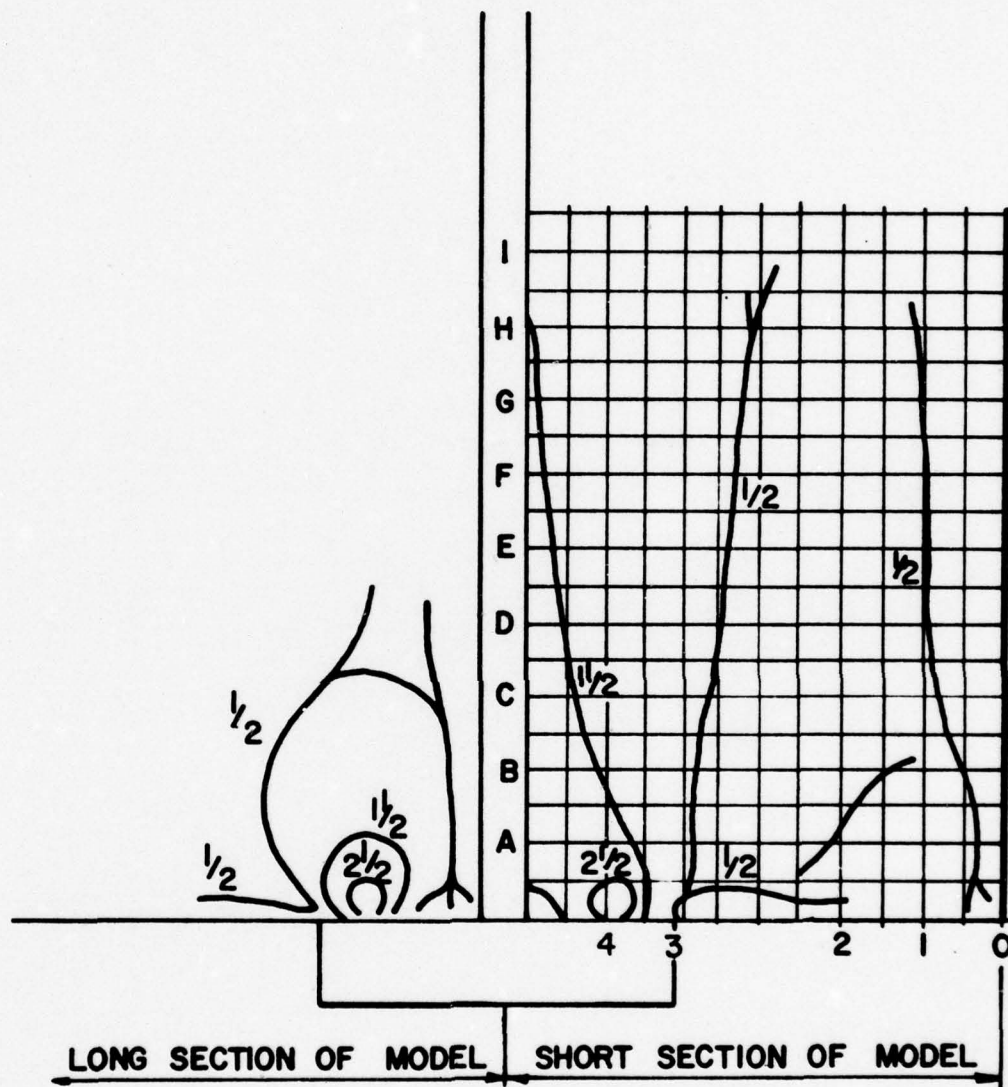


Fig. 4.22 Test #4 isochromatic diagram, light field

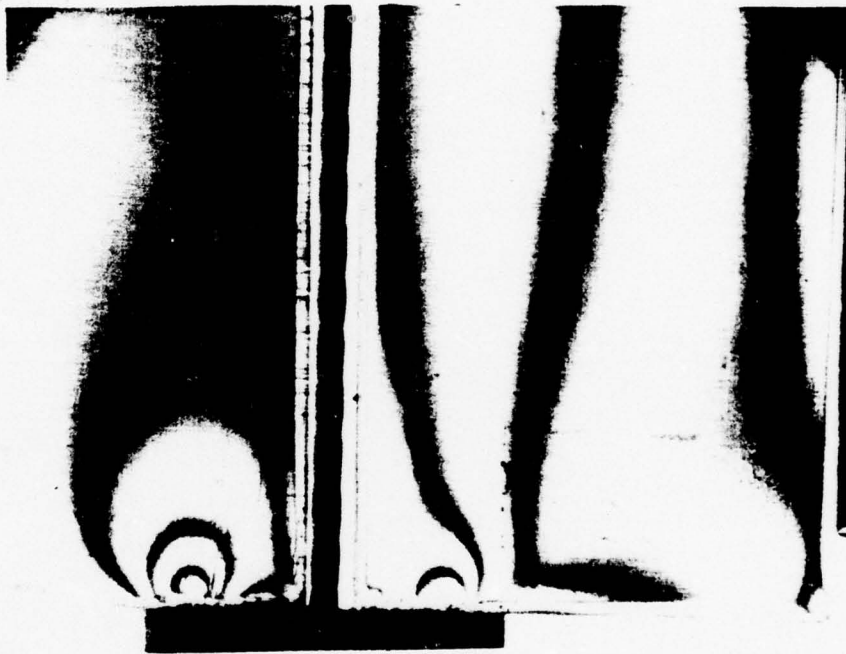


Fig. 4.23 Test #4 recorded isochromatics, light field

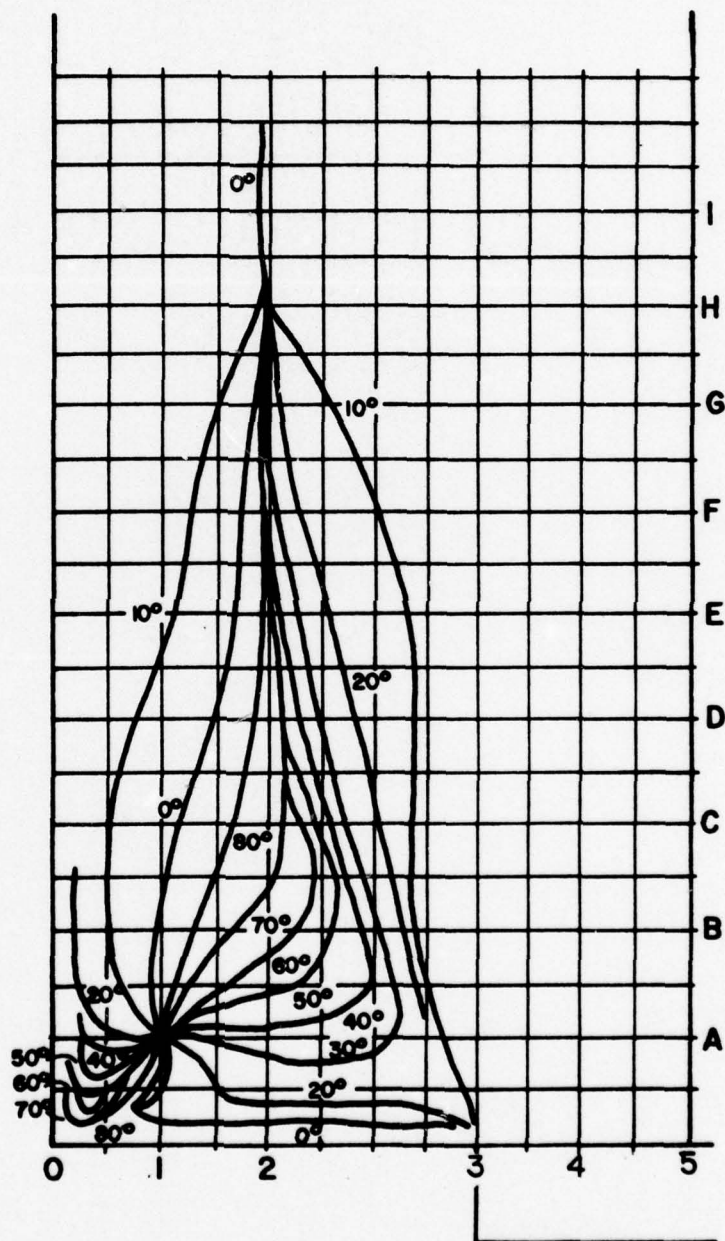


Fig. 4.24 Test #4 isoclinic diagram

principal stresses. The stress trajectories plotted in Fig. 4.25 also reflect the complicated nature of this region. There appears to be an isotropic point ($\sigma_1 = \sigma_2$) along line 1 at level A. The isoclinic parameters all intersect at that point and this is the indication for an isotropic point.⁶ Looking once again at the isochromatic diagram, this same point lies in an area between 1/2 order isochromatics, which means it could have a zero fringe order magnitude. If this is the case, then, at that point $\sigma_1 = \sigma_2 = 0$. Examining the recorded isochromatics of Fig. 4.23, this region has a very light intensity which would substantiate the presence of no stress at that point. This is extremely important, for if the stress at that point goes to zero, then it would mark a point where the longitudinal stresses went from compression to tension. This was the first instance of the creation of longitudinal tensile spalling stresses in any of the tests. Unfortunately, the data were not sensitive enough in this region to confirm this supposition using the "Shear Difference Method". The data would not give accurate values for n (fringe order) at various points, since all isochromatic lines in the region have the same order and without some sort of compensator to interpolate correctly between the isochromatics there was no way of correctly reading these critical parameters. Also, the isoclinics in this region are extremely close together and they compound the problem by making it difficult to get the orientation of the principal stresses at critical points with the necessary degree of accuracy. However, it is certainly reasonable to assume the creation of longitudinal tensile stresses and this supposition has been supported by other photoelastic investigations of the stresses created in anchorage zones of post-tensioned members.^{2,4}

4.5.2 Calculated Results. The results of the calculations for stress at interior points using the "Shear Difference Method" are shown in Figs. 4.26 and 4.27. The grids used for the

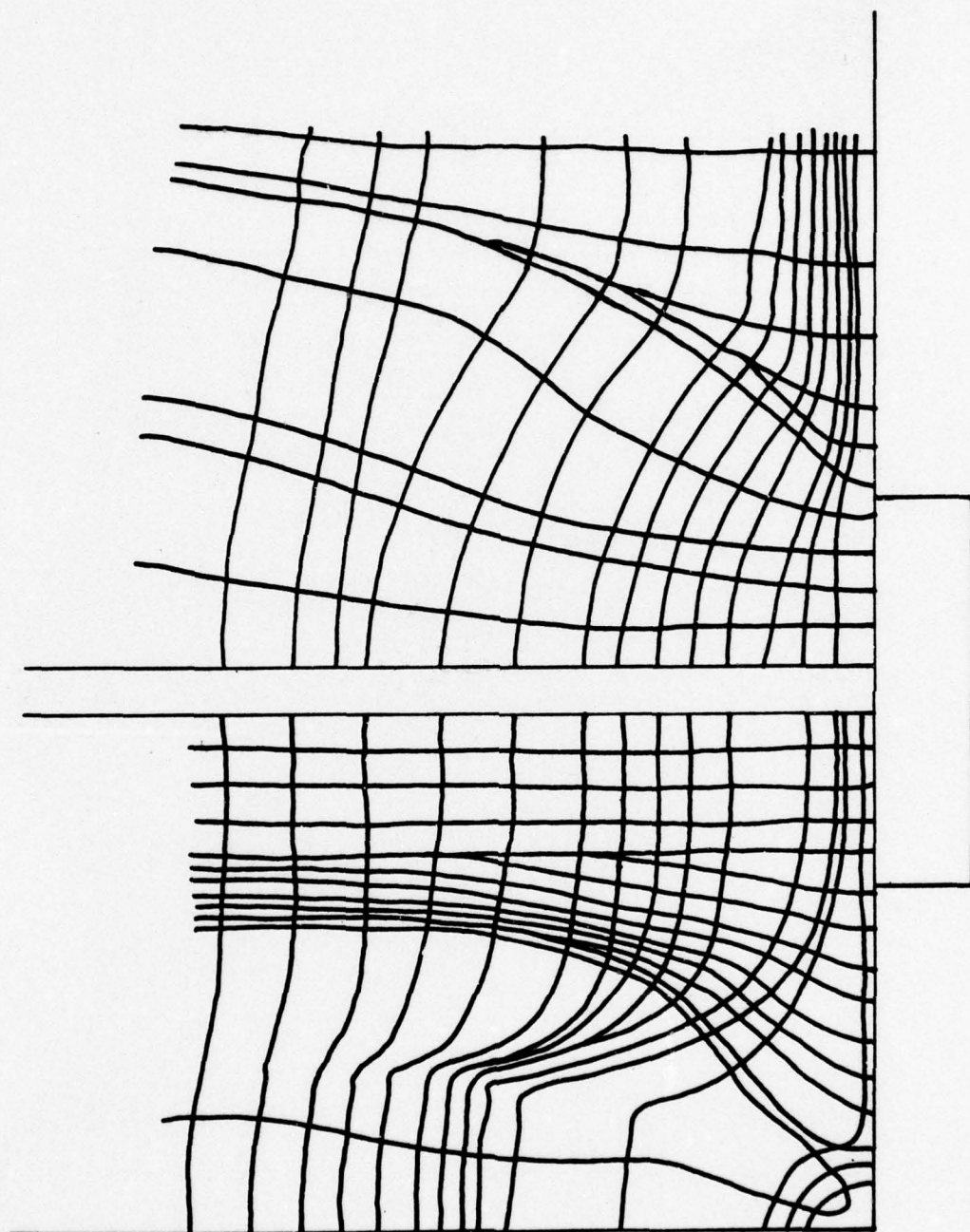


Fig. 4.25 Test #4 stress trajectory

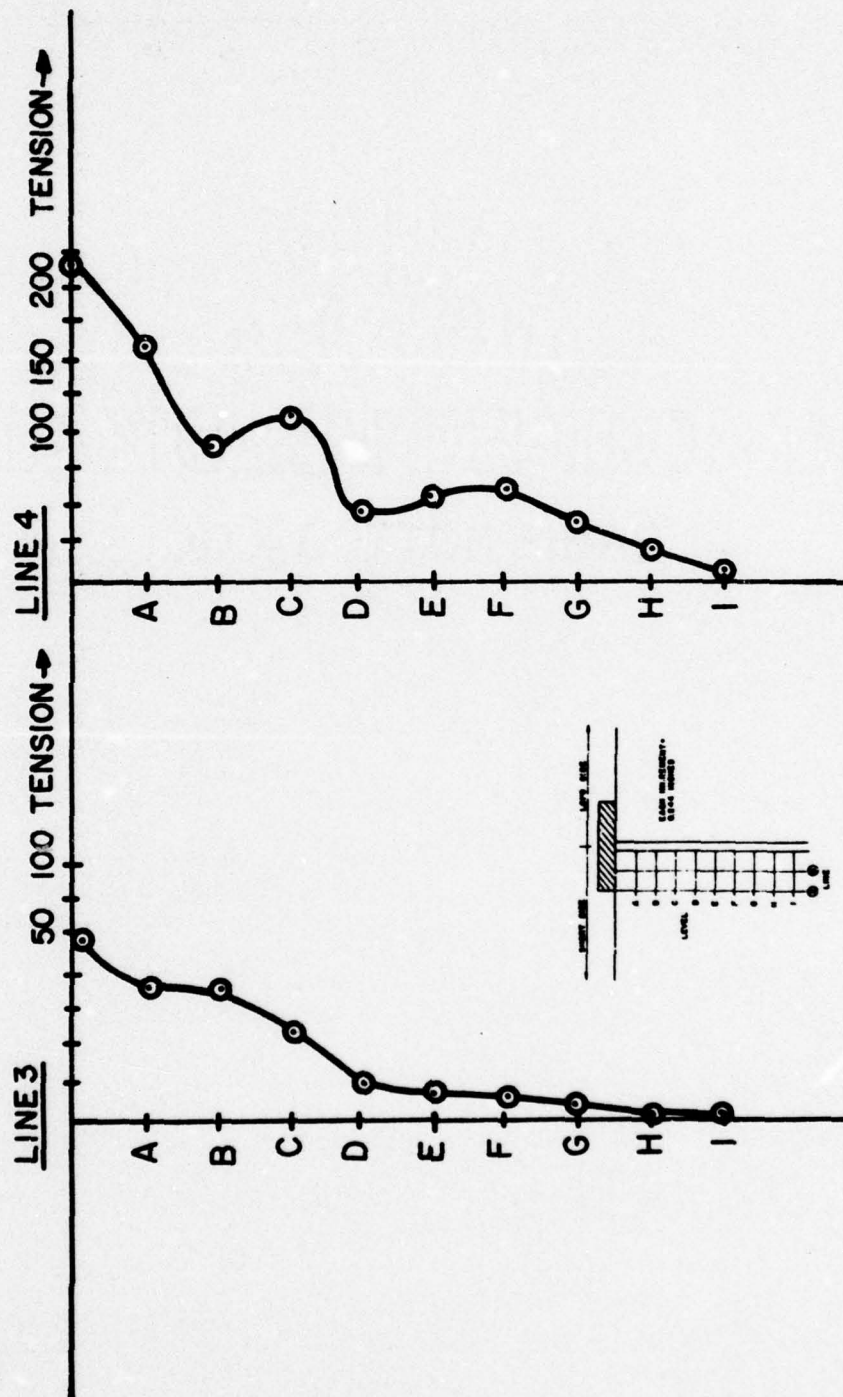


Fig. 4.27 Test #4--Principal transverse stress P

calculations are shown on Figs. 4.22 and 4.24. The assumptions employed to use the "Shear Difference Method" are listed below:

1. The uniform compression assumed applied by the load was 70.5 psi

$$P/A = \frac{(76/2)}{(1.4375)(0.375)} = \frac{38}{0.539 \text{ in.}^2} = 70.5 \text{ psi}$$

This value correlated well with the apparent value for $n = 0.5$

$$n = \frac{70.5}{160} \approx 0.44 \quad \text{so, } \underline{0.44 \text{ vs. } 0.5} \text{ (good correlation)}$$

2. Uniform compression exists at level "I". This value was taken from the isoclinic diagram and was a rough estimate marked by the intersection of the 10° parameters and the continuation of the 0° isoclinic.

Only lines 3 and 4 were used to generate values for stress at interior points, because the data were too insensitive to calculate with any accuracy beyond that point. As in all previous tests, the calculated values for the transverse tensile stresses are subject to large error due to the data available and the nature of the "Shear Difference Method". The maximum values for the stresses along the two lines is shown below:

Line #4:

Maximum compressive stress = 185 psi compression

$$\text{Ratio} = \frac{\sigma_{\text{max}}}{\sigma_{\text{uniform}}} = \frac{185}{70} \approx 2.64$$

Maximum transverse stress = 215 psi (tension)

$$\text{Ratio} = \frac{\sigma_{\text{max}}}{\sigma_{\text{uniform}}} = \frac{215}{70} \approx 3.05 \text{ (very questionable value)}$$

Maximum shear stress = 200 psi

$$\text{Ratio} = \frac{\tau_{\text{max}}}{\sigma_{\text{uniform}}} = \frac{200}{70} \approx 2.85 \quad \frac{2\frac{1}{2}(160)}{2} = 200 \text{ psi}$$

Line #3:

Maximum compressive stress = uniform compression = 80 psi

Maximum transverse stress = 51 psi tension

$$\text{Ratio} = \frac{\sigma_{\max}}{\sigma_{\text{uniform}}} = \frac{51}{70} \approx 0.73$$

Maximum shear stress = 20 psi

$$\text{Ratio} = \frac{\tau_{\max}}{\sigma_{\text{uniform}}} = \frac{20}{70} \approx 0.28 \quad \frac{\frac{1}{2}(80)}{2} = 20 \text{ psi}$$

Note that if uniform load distribution were assumed under the anchor, the stress there would be equal to 208 psi compression.

$$P/A = \frac{76}{(1.1 - 0.125)(0.375)} = 208 \text{ psi}$$

The calculated photoelastic stress under the anchor at line 4 was equal to 185 psi. These two numbers are fairly close, however, the distribution under the anchor is not uniform and should vary to a minimum at the free edge of the anchor. This would require, therefore, that interior stresses under the anchor go to values somewhat higher than what would be present under uniform loading conditions. The compressive stress, therefore, under the anchor at line 4 is probably low. The value of the compressive stresses at line 3 under the anchor are also probably low as the intervals of integration were large and at a point just to the right of line 3 in the free edge the compressive stress would have to be zero. The stress under the anchor at line 3 is not zero, but the method of calculation due to the insensitivity of the data limiting the size of the interval of integration simply could not be accurate enough to handle those abrupt changes in boundary conditions.

Comparing the eccentric loading case to the concentric loading case found in Test #1, some interesting comparisons may be drawn. Limiting all stress calculations to those found on free

edges which may be determined directly from observed data will avoid errors introduced by the "Shear Difference Method". The eccentric case produced apparent longitudinal tensile stresses along the near vertical free edge of the member. The magnitude of these stresses can be calculated directly.

$$\sigma_1 = 1/2(160) = 80 \text{ psi} \quad (\text{at free edge } \sigma_2 = 0)$$

$$\sigma_1 = 80 \text{ psi tension}$$

$$\frac{\sigma_1}{\sigma_{\text{uniform}}} = \frac{80}{70.5} = 1.1$$

The concentric case produced no measurable longitudinal tensile stresses. Both cases did produce transverse tensile stress just beyond the anchors along the free horizontal edge, which can be measured directly. It should be noted that the eccentric case produced a larger region of these transverse tensile stresses than the concentric case, but the magnitude of the stress was approximately the same with both areas having a fringe order of $1/2$, which indicates transverse tensile stress magnitudes of approximately 80 psi. Comparing the ratios of these stresses with their respective values of uniform compression gives the following results:

$$\text{Eccentric ratio} = \frac{80}{70.5} \approx 1.1 \quad \text{Concentric ratio} = \frac{80}{28.5} \approx 2.8$$

Before drawing any conclusions from these ratios, however, it should be remembered the fringe constant " $1/2$ " was not at the free edge in either case and it may vary at the boundary. Also, as discussed in Sec. 4.1.1, there was considerable error associated with the assumption of uniform compression for these models, and since they are geometrically different great caution should be used when relating uniform compression ratios between the two models. In Test #1, the existence of uniform compression was never substantiated by the isochromatic diagram, but was assumed from the isoclinic diagram to make calculations possible.

4.6 Test #5--Single Flat Bearing Anchor with Inclined Tendon Duct

Test #5 was designed to examine the effects of an inclined tendon duct on the creation of stresses in the end block. A flat bearing anchor was employed so that the stresses created would not be affected by an internal anchorage system. The geometric considerations for the end block and tendon duct are discussed in detail in Sec. 3.2.6. A load of 100 lbs. was applied to the post-tensioning tendon of the model.

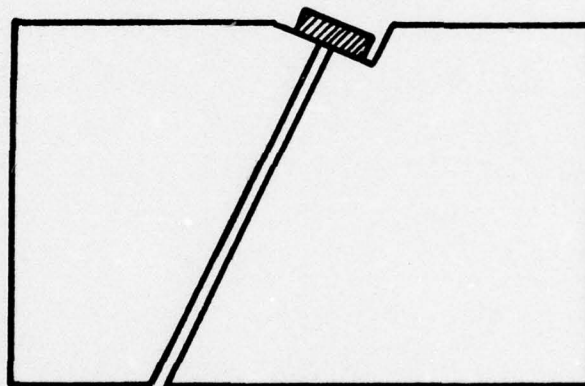


Fig. 4.28 Test #5--Single flat bearing anchor with inclined tendon duct

4.6.1 Observed Results. The isochromatic diagram from Test #5 is shown in Fig. 4.29 and the recorded isochromatics are shown in Fig. 4.30. These isochromatics show that, due to the inclination of the tendon duct, the model has two very different portions bounded by the duct. The duct separates the model into two areas which are totally different geometrically, and thus have different stress distributions. Since the tendon is inclined to

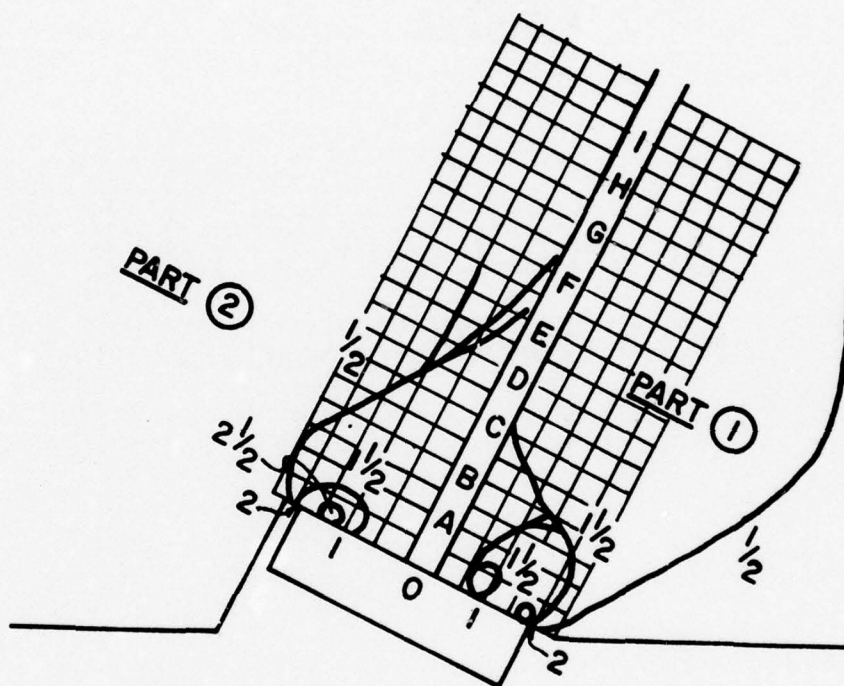


Fig. 4.29 Test #5 isochromatic diagram, light field

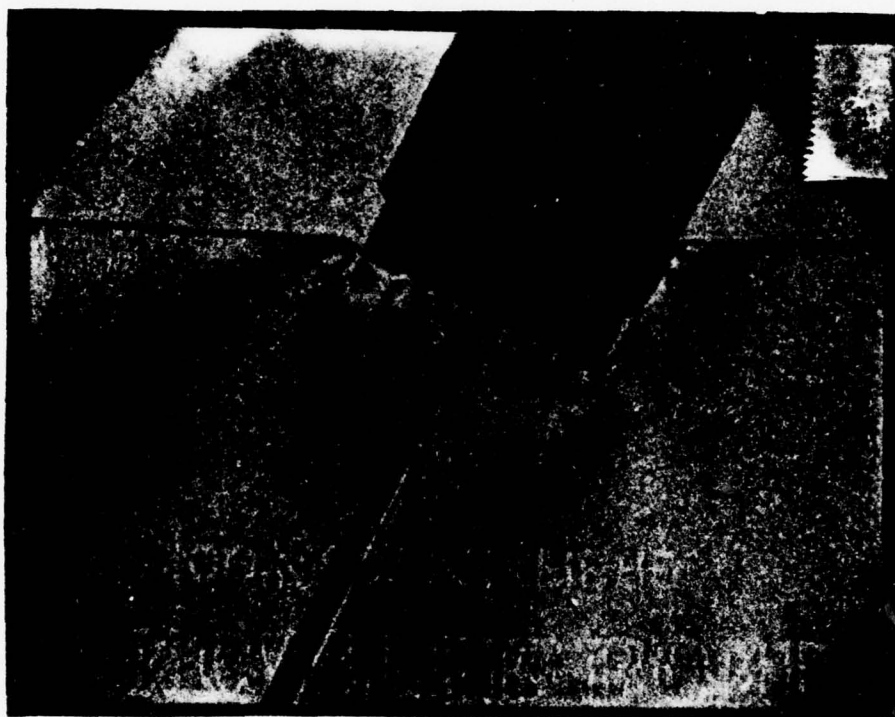


Fig. 4.30 Test #5 recorded isochromatics, light field

the right, the right portion of the model has a much larger base and the compressive stresses have a much larger area to eventually spread out to. Just the opposite is true for the left-hand portion of the model as well as the fact that the tendon duct acts as a boundary which orients the stress distribution along it and will not allow a vertical stress distribution. A vertical stress orientation is entirely possible in the right-hand portion. The stress trajectories shown in Fig. 4.32 also show this boundary effect.

The isoclinic diagram in Fig. 4.31 shows a region where the larger portion of the model (note both isoclinic and isostatic diagrams reversed from isochromatic diagram) has a zero degree isoclinic and, thus, appears to be in uniform compression. The isochromatic diagram also confirms this uniform compression. The small portion of the model does not show a region of apparent uniform compression. It is quite safe to assume the tendon duct inclination greatly affects the distribution of stresses within the model. The model, however, as designed does not reflect any stresses being created in the model by the pressure of the inclined tendon against the duct wall. Also, the isoclinic diagram indicates an isotropic point located at the corner of the notch holding the anchor. The recorded isochromatics show the corner to be a point of zero stress, and so above this point in the model there are apparent longitudinal tensile stresses being created.

4.6.2 Recorded Data. The results of the calculations for stress at interior points are shown in Figs. 4.33 and 4.34. Note that the model has been broken up into two parts for analysis reflecting the geometric differences in the two parts of the model due to the inclined duct. A slightly different method of solution was employed for this situation. The transverse stresses along level "E" (see Fig. 4.31) were computed first by working from the free edge of the tendon duct. The longitudinal stresses were then

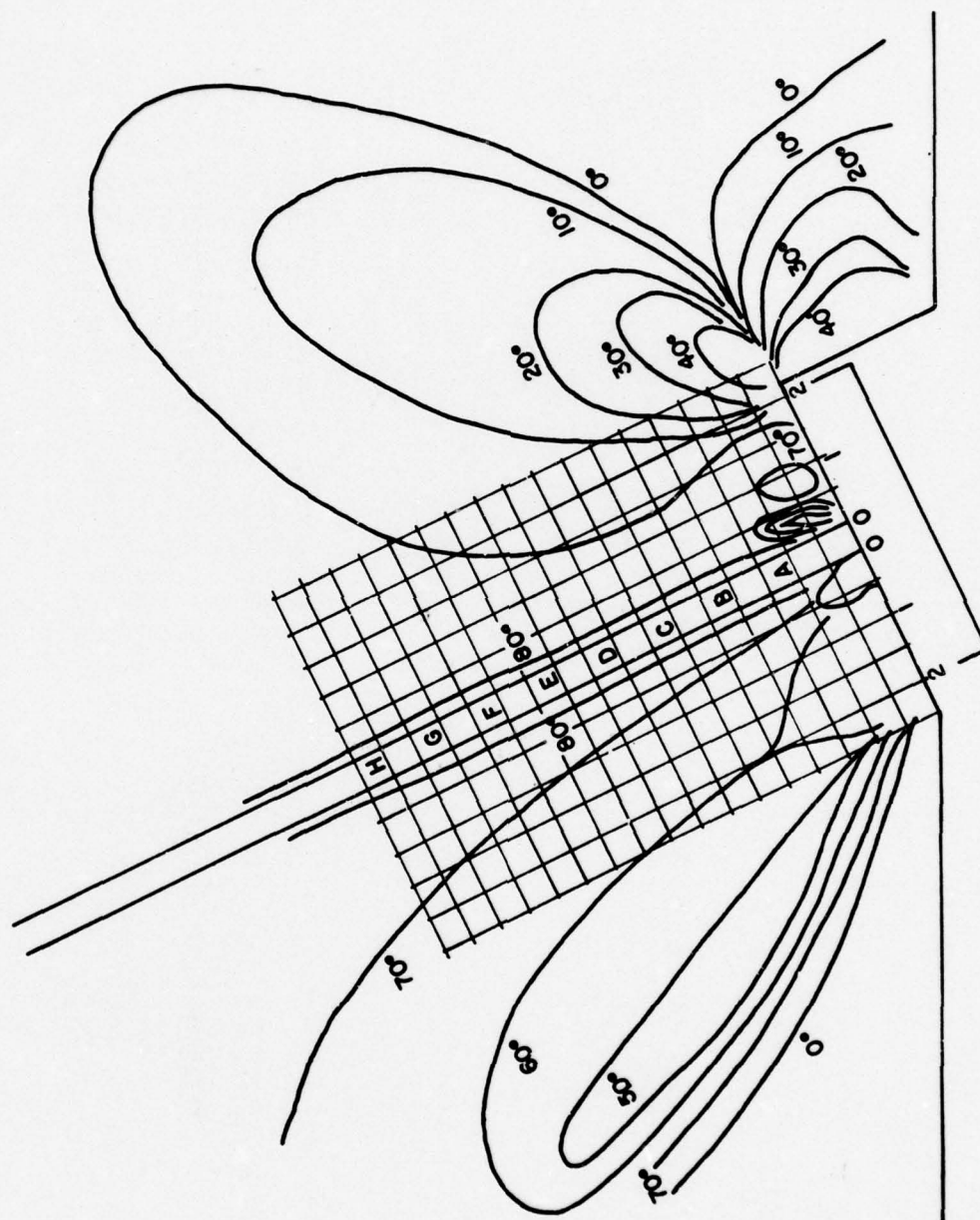


Fig. 4.31 Test #5 isoclinic diagram

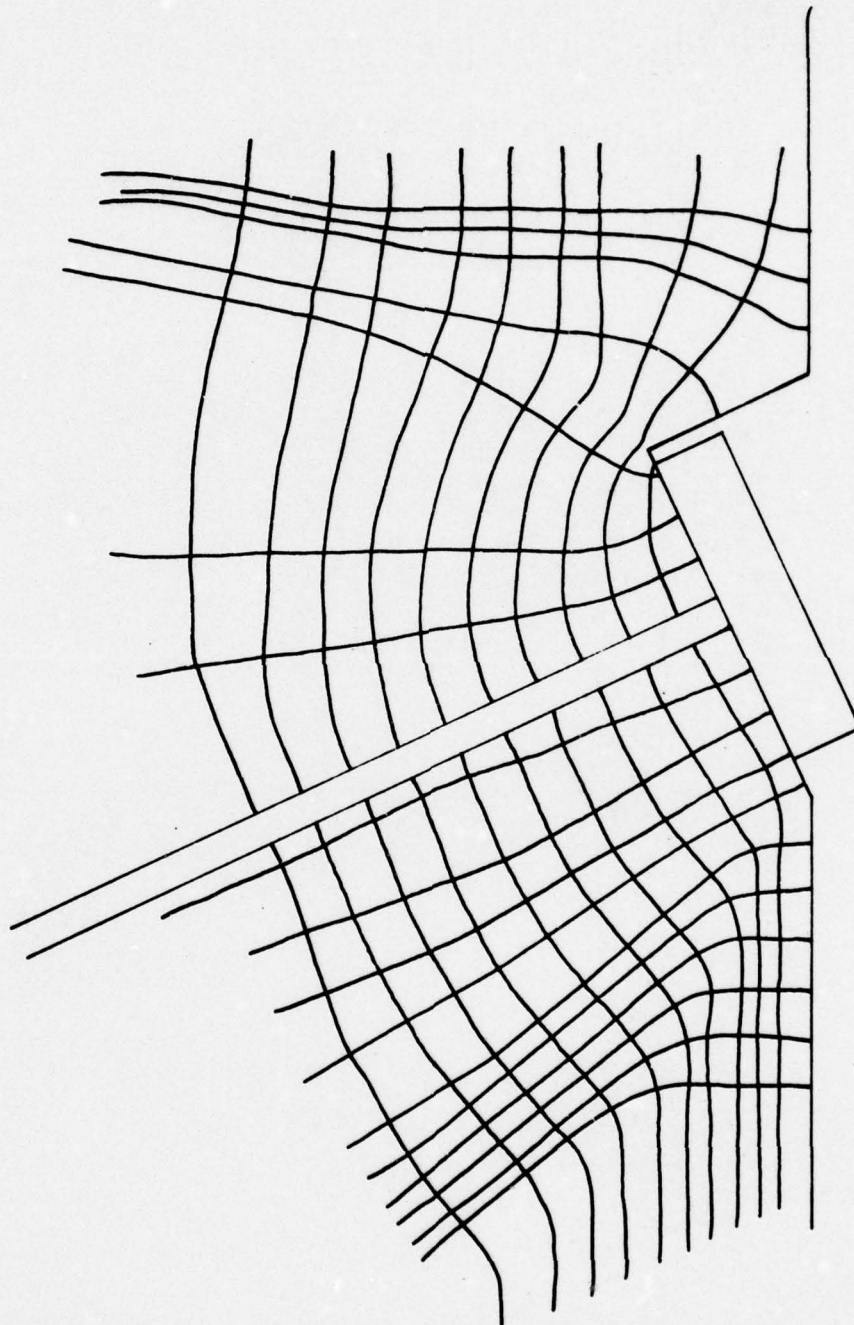


Fig. 4.32 Test #5 stress trajectory

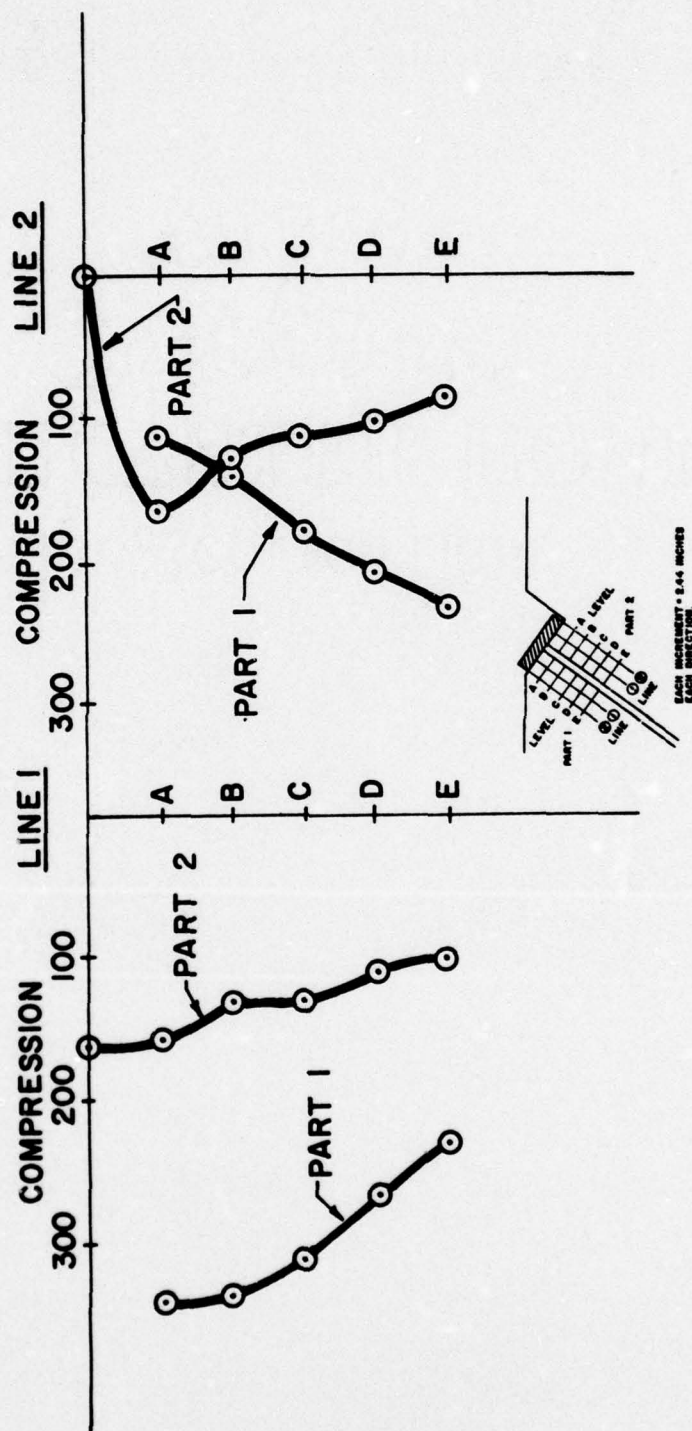


Fig. 4.33 Test #5--Principal longitudinal stress Q

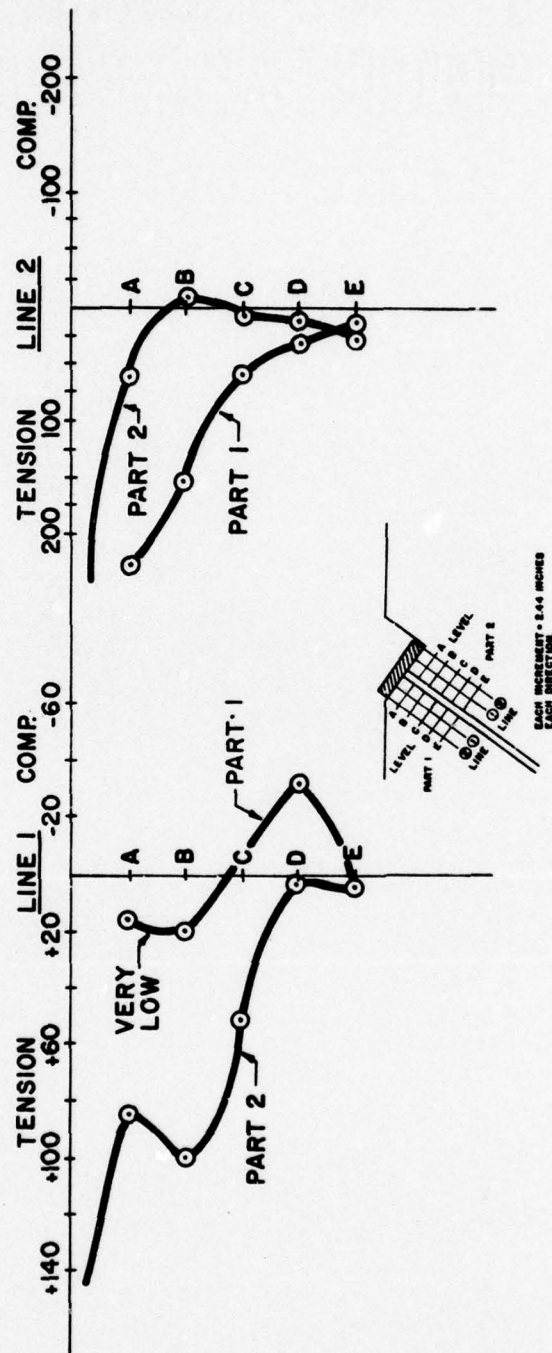


Fig. 4.34 Test #5--Principal transverse stress P

calculated from these transverse stresses along level E and then the stresses along lines 1 and 2 on both parts were calculated from the known values of stress at level E. Great care was taken to use the proper angle θ for the calculations in the "Shear Difference Method", θ being the angle between the orientation along which τ_{xy} acts and the orientation of the principal axes. In all previous tests this was equal to the isoclinic parameter, since the grid was oriented along x and y axes which coincided with the horizontal and vertical axes of the polariscope. In Test #5, however, the grid was oriented along the inclined tendon duct, which mean that the isoclinic parameter had to be adjusted by the difference in orientation between the reference axis of the polariscope and the axis of the grid, which is the axis along which τ_{xy} acts in this case (see Sec. 2.3).^{6,9,12,13,14} This different method of calculation was employed because symmetry is no longer valid for this model and, due to the varying dimensions of the two parts with depth, it is extremely difficult to determine a uniform compression at any one level.

The author recommends a great deal of caution in comparing the results of this test with previous tests, as the methods for recording data for this investigation were not sensitive enough for the "Shear Difference Method" and changing the method of calculation could change calculated values of stress at the same point using data from the same test (especially the transverse tensile stresses). What the calculated results do show are the trends of distribution along lines which run parallel to the orientation of the tendon duct.

4.7 Test #6--Web Cross Section with Single Tendon Duct

Test #6 was designed to examine the effects of tendon pressure on the tendon duct in an inclined or parabolic tendon duct configuration. The model is a representation of the cross section

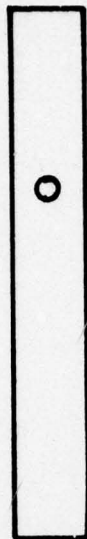


Fig. 4.35 Test #6--Web cross section with single tendon duct

of the web of a post-tensioned member. The tendon duct is centered in the web and a tendon runs through the duct and has a downward component of force due to its inclination. The model is loaded by running a seven-strand post-tensioning wire through the drilled hole and applying a tensile force to the strand in such a manner that the downward component of force applied to the model may be easily calculated by statics. The tensile load on the tendon was 50 lbs. and the downward component felt by the model was 39 lbs. (see Fig. 4.36).

4.7.1 Observed Results. The isochromatic diagram and recorded isochromatics are shown in Figs. 4.37 and 4.38. Both these diagrams show the isochromatic fringes as being symmetrically located around the tendon duct. They also indicate the load is tending to act as a concentrated load, or point load. An examination of the isoclinic diagram (Fig. 4.39) substantiates this apparent point loading by showing the isoclinic parameters all merging at the

$$\sqrt{5^2 + 4^2} = 6.4 \text{ in.}$$

DOWNWARD COMPONENT OF FORCE

$$\frac{5}{6.4}(25) = 19.5 \text{ lbs (each side)}$$

TOTAL DOWNWARD FORCE =

$$2(19.5 \text{ lb.}) = \underline{\underline{39 \text{ lbs.}}}$$

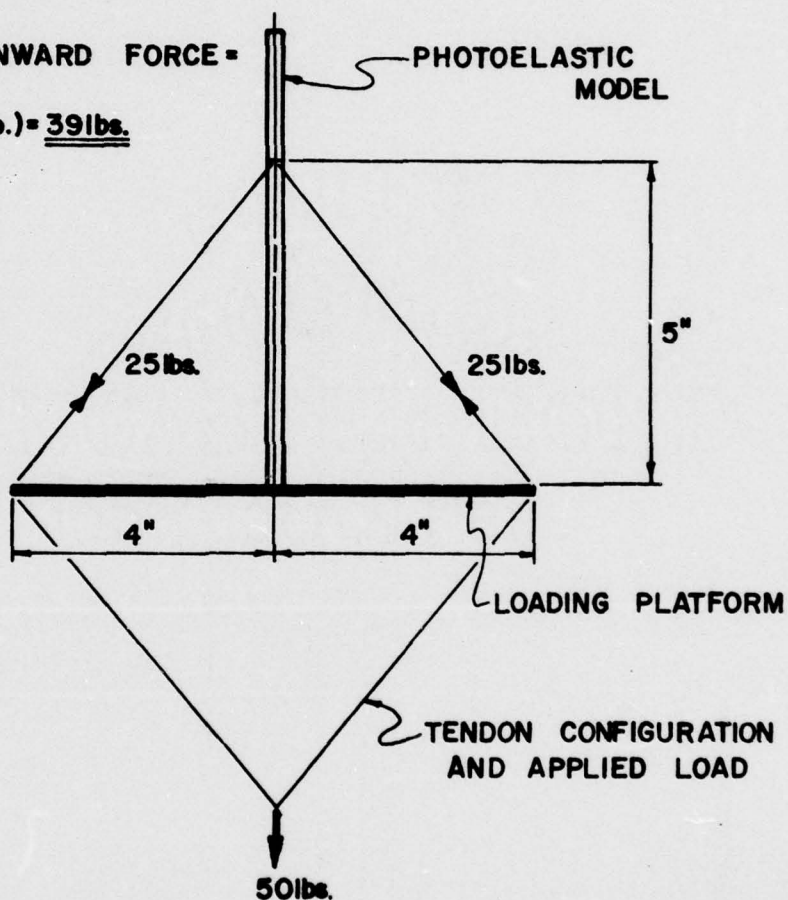


Fig. 4.36 Test #6 loading plan

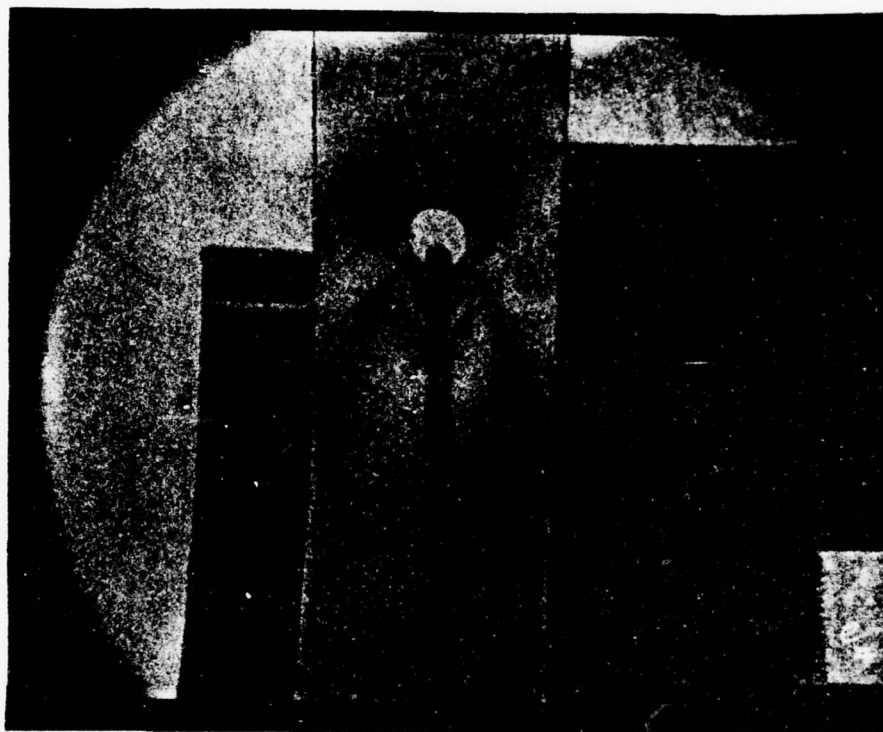


Fig. 4.38 Test #6 recorded isochromatics, light field

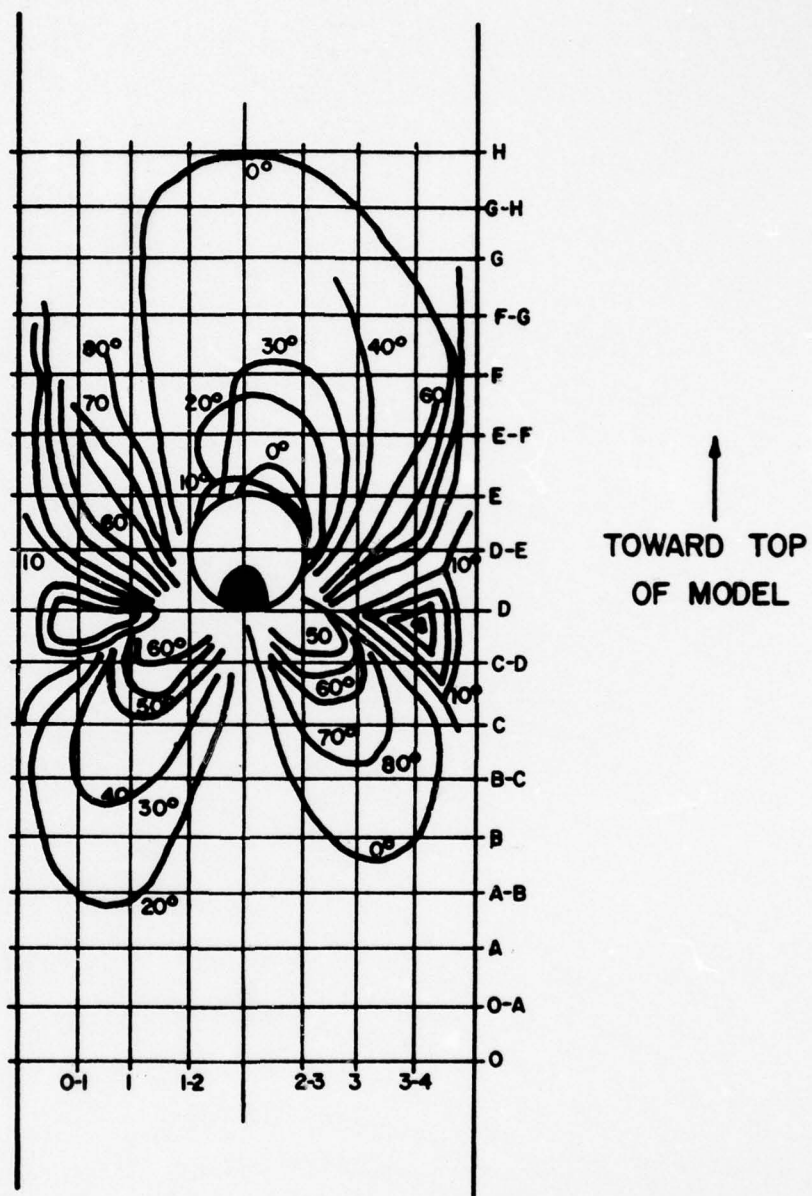


Fig. 4.39 Test #6 isoclinic diagram

point of application of the load. The isoclinic diagram also shows another interesting fact. Along level "D" in the model, there appears to be a region of zero stress, as shown by the orientation of the merging isoclinics indicating the location of isotropic points on either side of the load. This fact is substantiated by examining the isochromatic diagram which has two $1/2$ order fringes merging at line "D" and indicating a level of zero stress by symmetry on either side of the applied load. In fact, the entire duct is being subjected to circumferential tensile stresses. Below the duct and under the point of application of the load there are compressive longitudinal stresses and within a short distance of the applied load a region of uniform compression exists. The isoclinic diagram also indicates a loading bias. For a completely symmetrical load, there should be a symmetrical isoclinic diagram. In this case, there is an obvious bias to the loading, which is even more clearly shown in the stress trajectory diagram in Fig. 4.40. There should be an isoclinic parameter running along the axis of symmetry of the model. The zero degree isoclinic has been biased by the load, which apparently is not totally vertical and the parameter does not run along the axis of symmetry as it should. The isochromatic diagram also shows extremely large maximum shear stresses directly under the applied load. This also is an excellent indication of large principal stresses in the same general area.

4.7.2 Calculated Results. The data produced for Test #6 did not lend itself to analysis by the "Shear Difference Method". The isoclinic parameters were extremely hard to trace and were extremely close together which made interpolating between them difficult and subject to large error, since small errors in tracing resulted in large differences in value for the parameters. Regions became congested. This made determining the correct location of parameters very difficult. The biased load also presented a problem, since an axis of symmetry of the model existed, but the exact

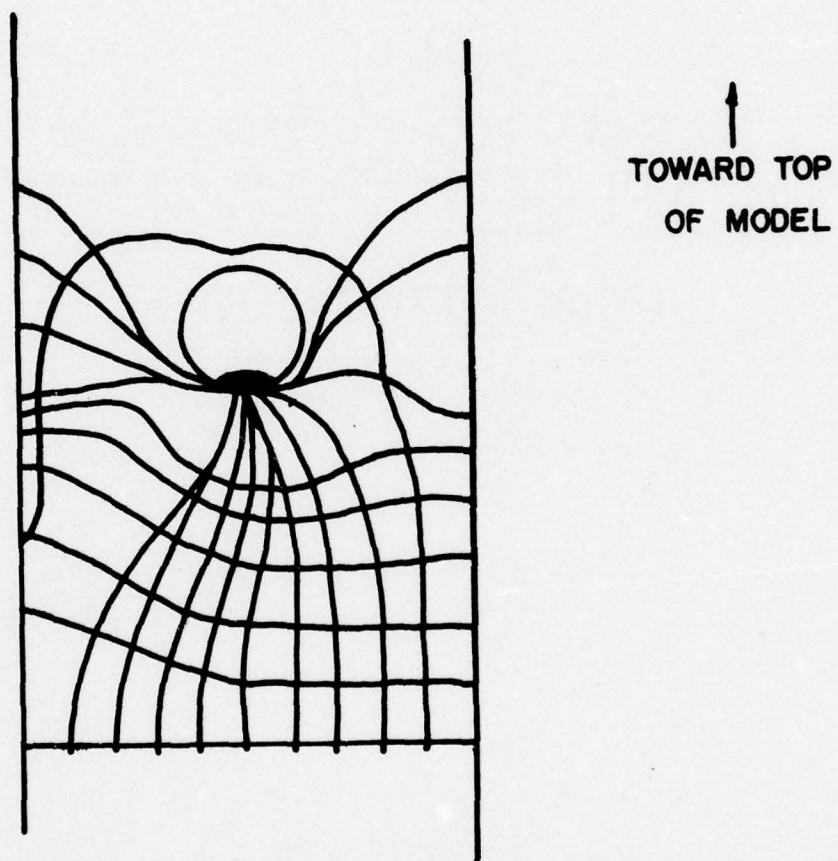


Fig. 4.40 Test #6 stress trajectory

relationship of the shear stresses across that axis of symmetry was not obvious from the isoclinic diagram, which indicated a biased load.

There are, however, several calculations which could be made and, thus, determine the magnitude of stresses. The value of uniform compression in the model was equal to P/A , since the model was symmetrically loaded.

$$\text{Uniform compression} = P/A = \frac{39 \text{ lbs.}}{(1'')(0.25'')} = 156 \text{ psi compression}$$

The photoelastic material constant for the 0.25 in. thick material was equal to 240, so the value for n at uniform compression was equal to:

$$nf = (\sigma_1 - \sigma_2) = \sigma_1 \text{ at uniform compression}$$

$$n(240) = 156$$

$$n = \frac{156}{240} = 0.65$$

The indicated value for n from the isochromatic diagram's apparent region of uniform compression was 0.5, so there was correlation between these two values. The circumferential tensile stress at the free edge of the duct at level D-E is also directly computable and should give an idea of the relative tensile stress in that region.

$$nf = (\sigma_1 - \sigma_2) = \sigma_{\text{circum}}, \text{ since at a free edge}$$

$$(1/2)(240) = 120 \text{ psi} = \sigma_{\text{circum}}$$

$$\text{Ratio } \frac{\sigma_{\text{circum}}}{\sigma_{\text{uniform}}} = \frac{120}{156} \approx 0.77$$

This value of the circumferential tensile stress at that point is reliable, since there is little error associated with the reading of the isochromatic fringe order. The maximum shear stress in the model is also directly measured from the isochromatic data.

$$\tau_{\max} = \frac{\sigma_1 - \sigma_2}{2} = \frac{nf}{2} = \frac{4.5(240)}{2} = 540 \text{ psi}$$

$$\text{Ratio} = \frac{\tau_{\max}}{\sigma_{\text{uniform}}} = \frac{540}{156} \approx 3.5$$

The value of 4.5 for n in the last calculation is the last readable fringe order due to the tendon at that point obscuring vision and blocking the light. This calculation, therefore, is conservative.

4.8 Test #7--Multiple Flat Bearing Anchors with Straight Tendons

Test #7 was designed to examine the effects of multiple anchorage systems on the end block of a post-tensioned concrete member. Flat bearing anchors and straight tendon ducts were employed so that the effects of other variables on the stresses created in the anchorage zone could be minimized and the effects of the multiple anchors could be more clearly observed. A variation of this particular situation has been investigated by Christodoulides in a two-dimensional photoelastic investigation neglecting the tendon duct

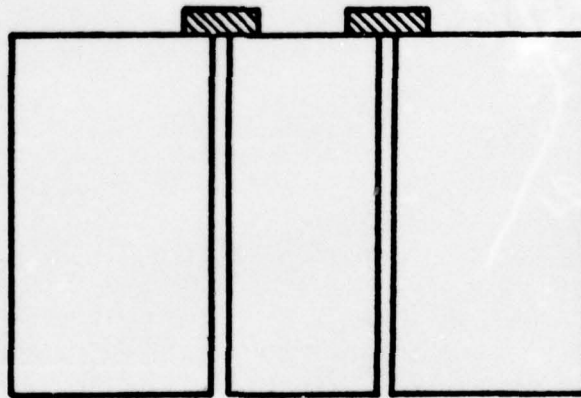


Fig. 4.41 Test #7--Multiple flat bearing anchors with straight tendons

and using a much smaller model.² A total load of 130 lbs. was applied to the model with 65 lbs. being applied to each tendon.

4.8.1 Observed Results. The isochromatic diagram and recorded isochromatics are shown in Figs. 4.42 and 4.43. For the region being studied between the two tendon ducts, there is symmetry of isochromatic fringes with some variation directly under the anchors which can be attributed to differences in surface contact between the two lead anchor models and the photoelastic sheet. The isochromatics give a good indication of the location of the region of uniform compression. The axis of symmetry of the model runs through a region between two $1/2$ order isochromatics and presents a problem in determining the value of the fringe order in this region.

The isoclinic diagram for this test (Fig. 4.44) shows good symmetry, with slight variations under each anchor. There is a zero isoclinic corresponding to the axis of symmetry of the model as would be expected for symmetrical loading. Christodoulides,^{2,4} in his work, indicated the existence of a non-zero isotropic point located along this axis of symmetry (Point I-1 on Fig. 4.46). While there is a region along line 3 on the model between levels A and B which became extremely congested and could have possibly been a point of intersection for all the isoclinic parameters, the method of tracing the broad isoclinics when recording them did not allow for positive confirmation of the existence of this isotropic point. If Fig. 4.44 is examined, the fact that it may exist cannot be ruled out and the isotropic point may certainly exist. The isoclinic diagram also shows strong evidence of the existence of uniform compression at level "G", which is certainly substantiated by the isochromatic diagram. The stress trajectories are shown in Fig. 4.45 and they give a good indication of the rapid creation of uniform compression by the confining action of the tendon ducts.

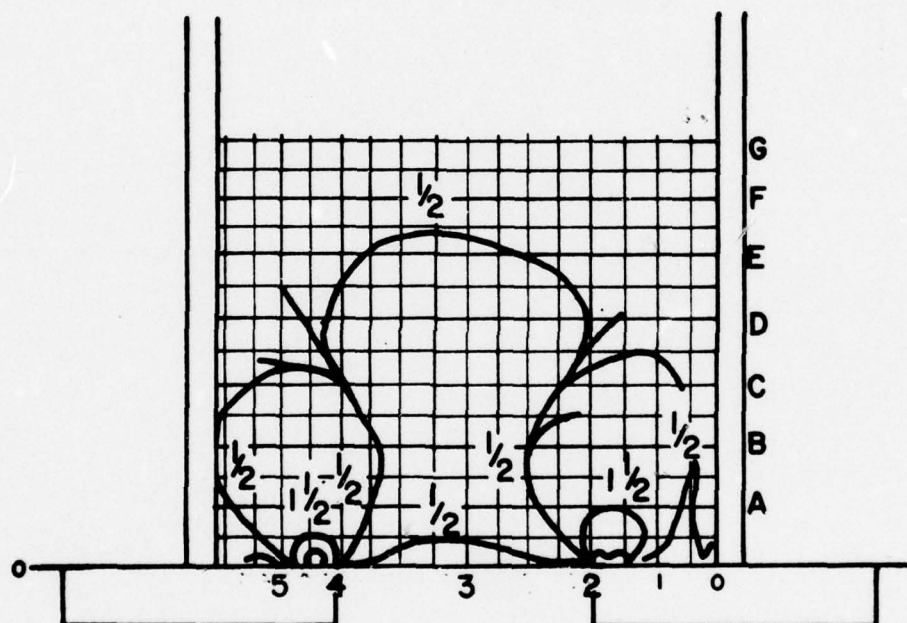


Fig. 4.42 Test #7 isochromatic diagram, light field

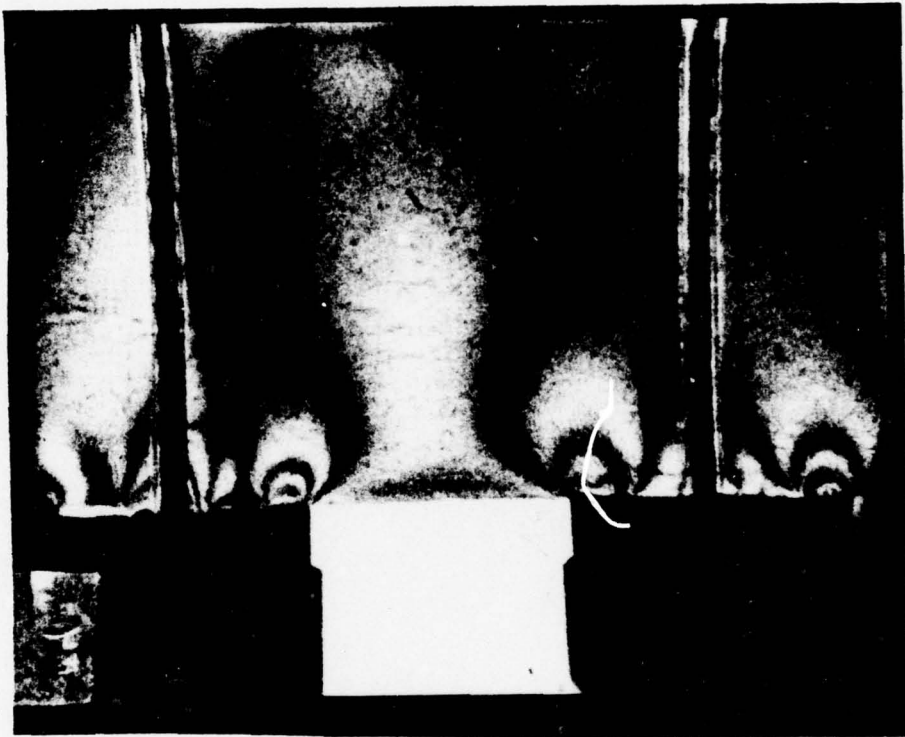


Fig. 4.43 Test #7 recorded isochromatics, light field

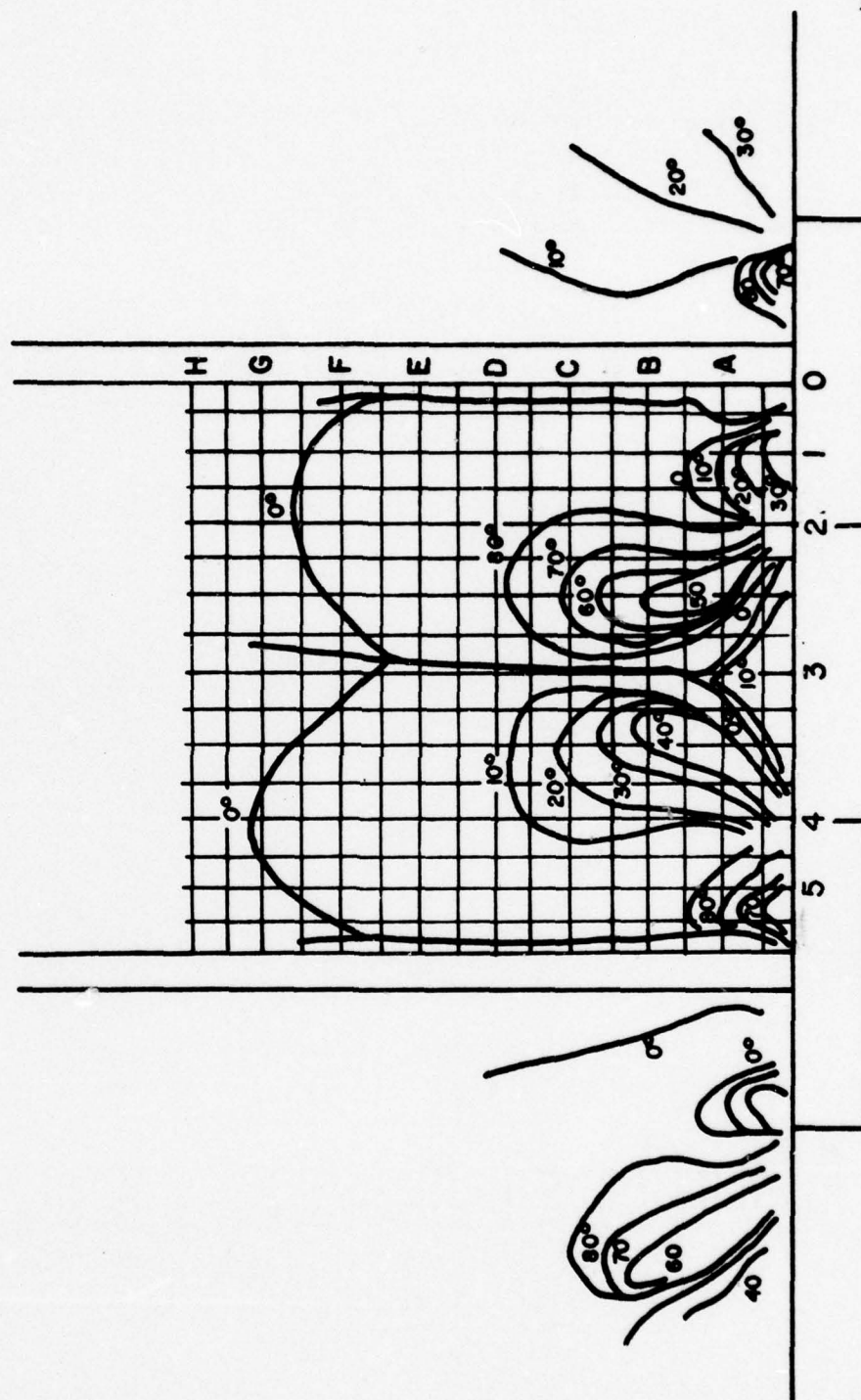


Fig. 4.44 Test #7 isoclinic diagram

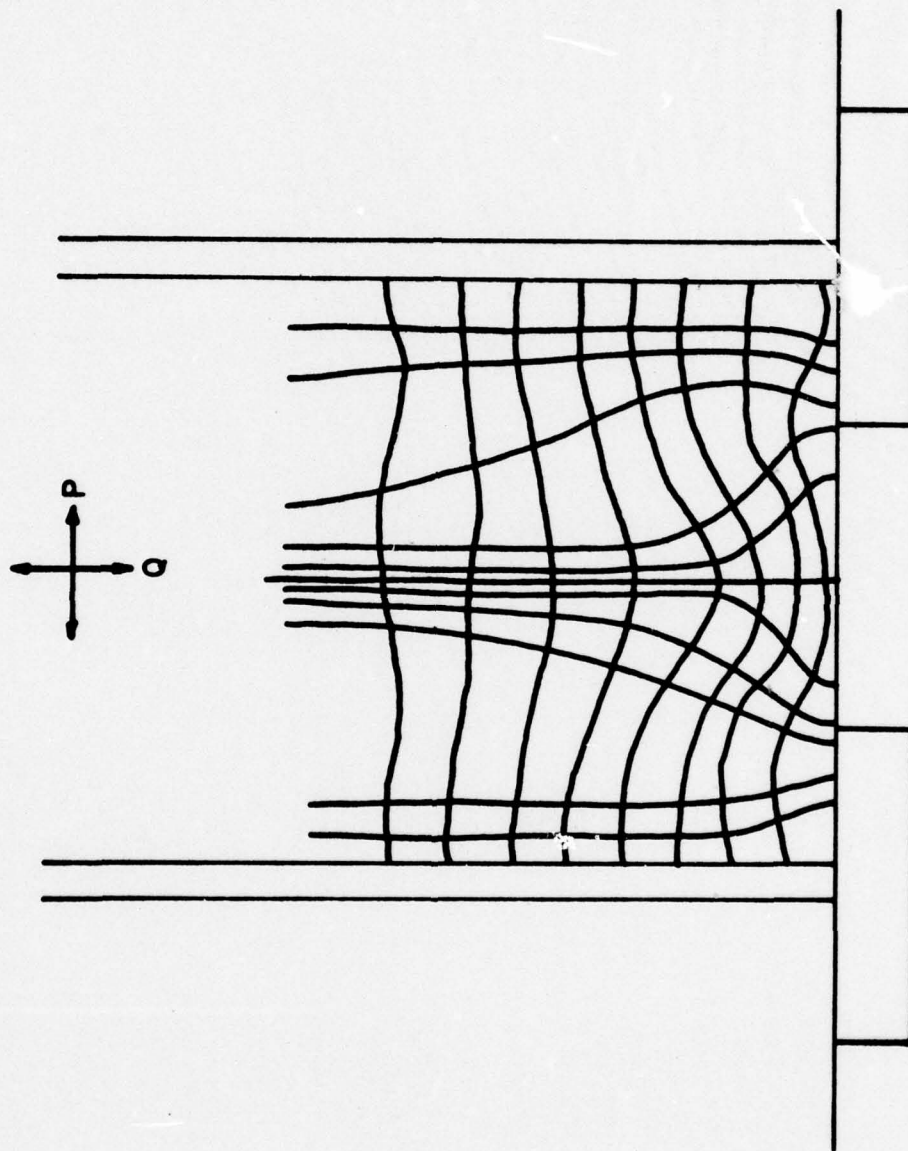


Fig. 4.45 Test #7 stress trajectory

Christodoulides conducted a two-dimensional photoelastic analysis which examined the region between two bearing-type anchors. His test was very similar to Test #7, except that he neglected the effects of the tendon duct and loaded his model externally. The results of the photoelastic test are shown in Figs. 4.46 to 4.48. These results show a very good correlation with the test results for Test #7 shown in Figs. 4.42 to 4.45 for the same regions between the bearing anchors. The differences in the two tests may be attributed to the presence of the tendon duct in Test #7 and the surface conditions between the anchor and the model in Test #7 which do not allow for uniform transfer of load. These differences between the two tests are not major and the two tests do substantiate one another.

4.8.2 Calculated Results. The results of the "Shear Difference Method" are shown in Figs. 4.49 and 4.50. The assumptions employed to use the method are:

1. Uniform compression exists at level "G" due to symmetry in model and loading
2. Uniform compression is equal to 125 psi compression

$$P = 65/2 + 65/2 = 65 \text{ lbs.}$$

$$A = 2.075 \times 0.25 = 0.25 = 0.519 \text{ in.}^2$$

$$\sigma_1 = \text{uniform compression} = 65/0.519 \text{ in.}^2 = 125 \text{ psi compression}$$
3. The value of the fringe order at level "G" is equal to 0.52

$$\sigma_1 - \sigma_2 \text{ at } G = 125 \text{ psi} \quad f = 240 \text{ (material constant)}$$

$$n = \frac{125}{f} = \frac{125}{240} = 0.52$$

Note: Excellent correlation with observed value of $n = 0.50$ from isochromatic diagram.

4. Symmetry was employed to solve for the stresses along line 3

Trial and error procedures were used to determine the relative values of n (fringe order) and θ (isoclinic parameter) between known data points, so that the method would produce the uniform compression at

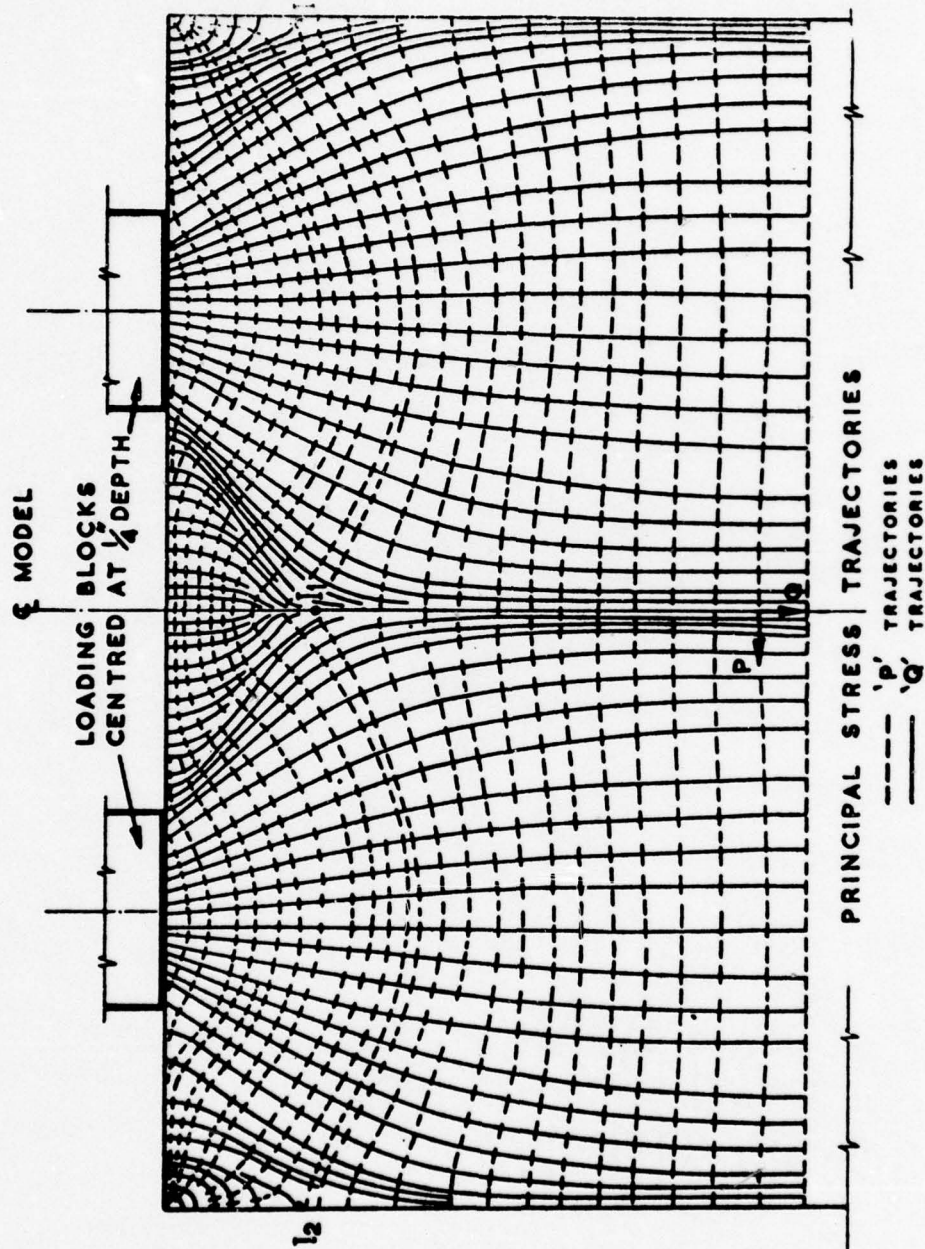


Fig. 4.46 Principal stress trajectories from Christodoulides' two-dimensional photoelastic test

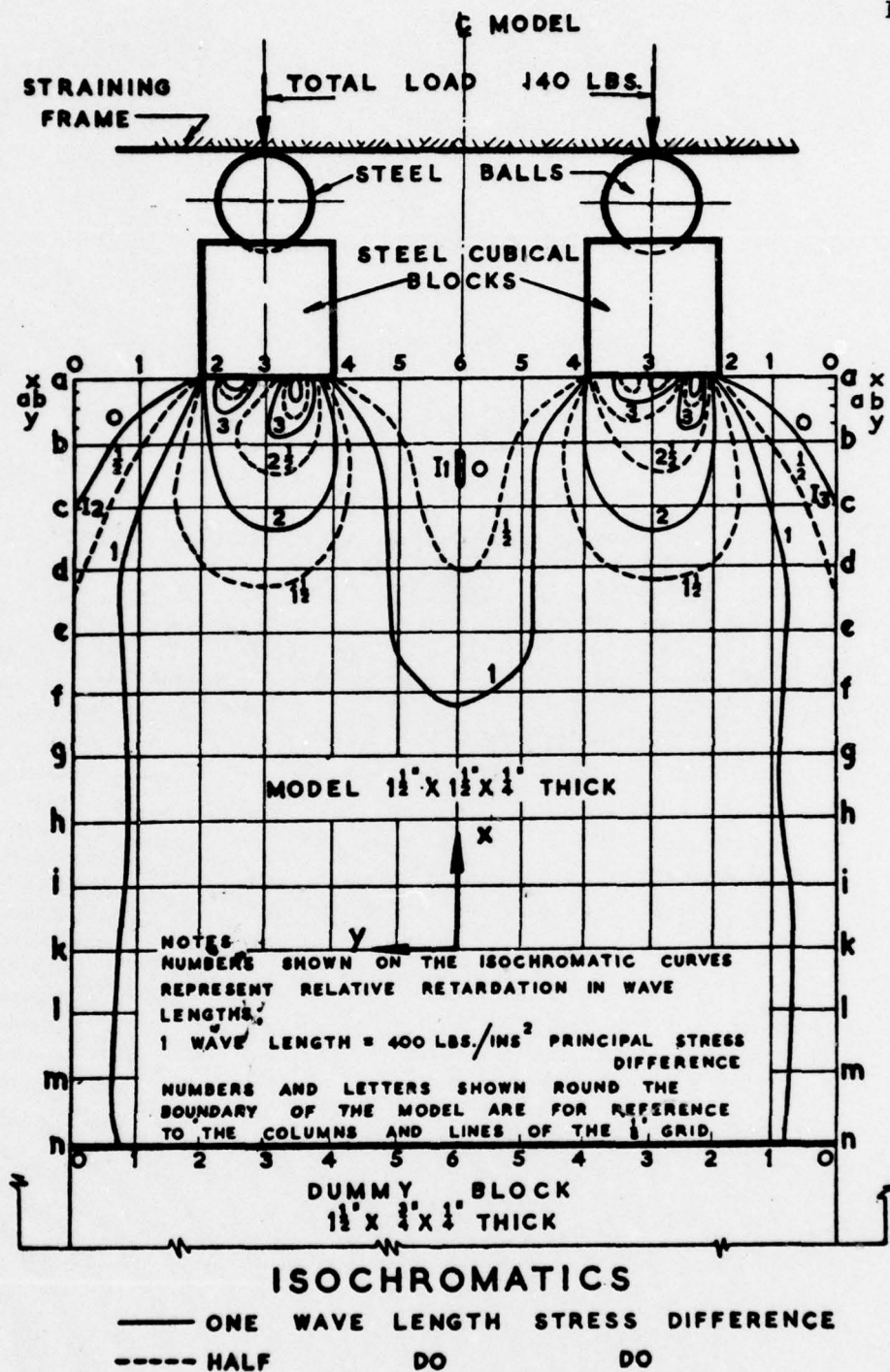


Fig. 4.47 Isochromatic fringes from Christodoulides' two-dimensional photoelastic test

NOTES
 NUMBERS ON ISOCLINICS DENOTE THE ANGLE IN DEGREES OF THE PRINCIPAL DIRECTIONS TO THE VERTICAL AND HORIZONTAL FACES OF THE MODEL WHICH ARE TAKEN AS AXES OF REFERENCE.

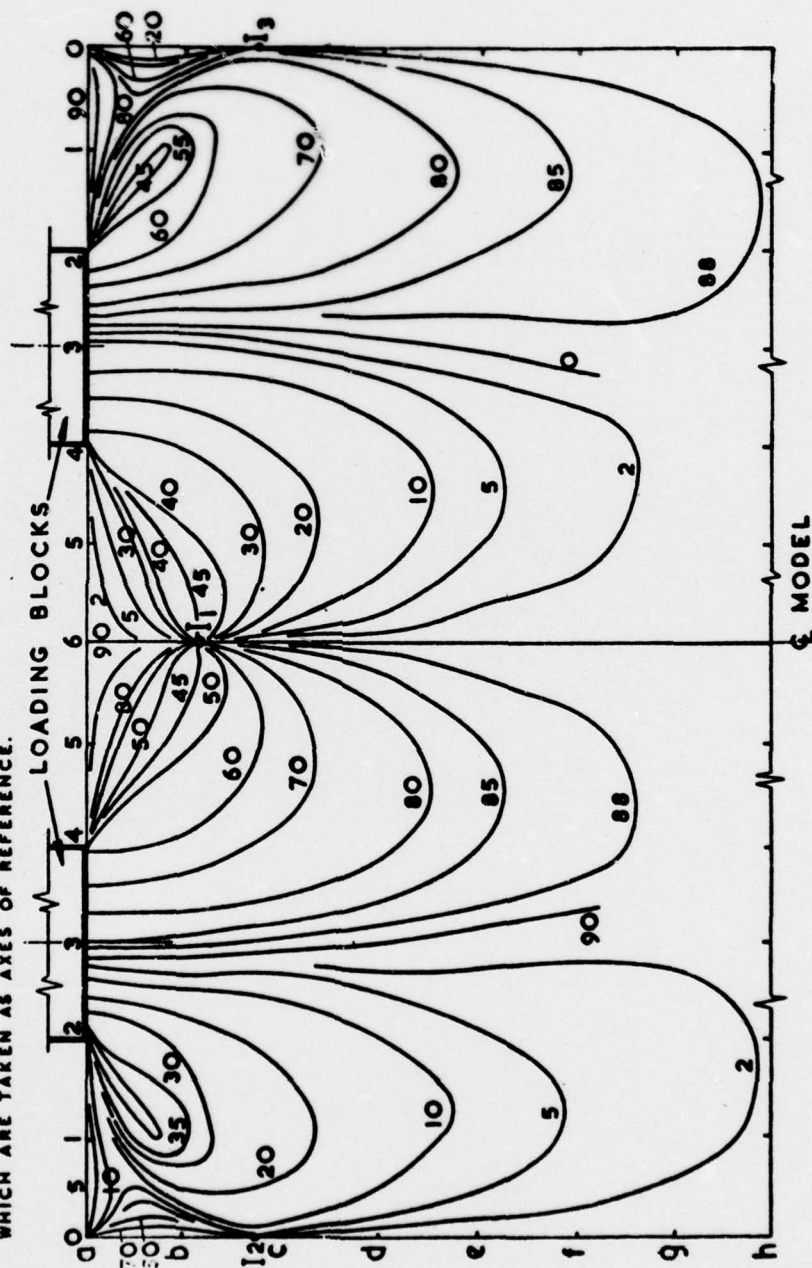


Fig. 4.48 Isoclinic diagram from Christodoulides' two-dimensional photoelastic test

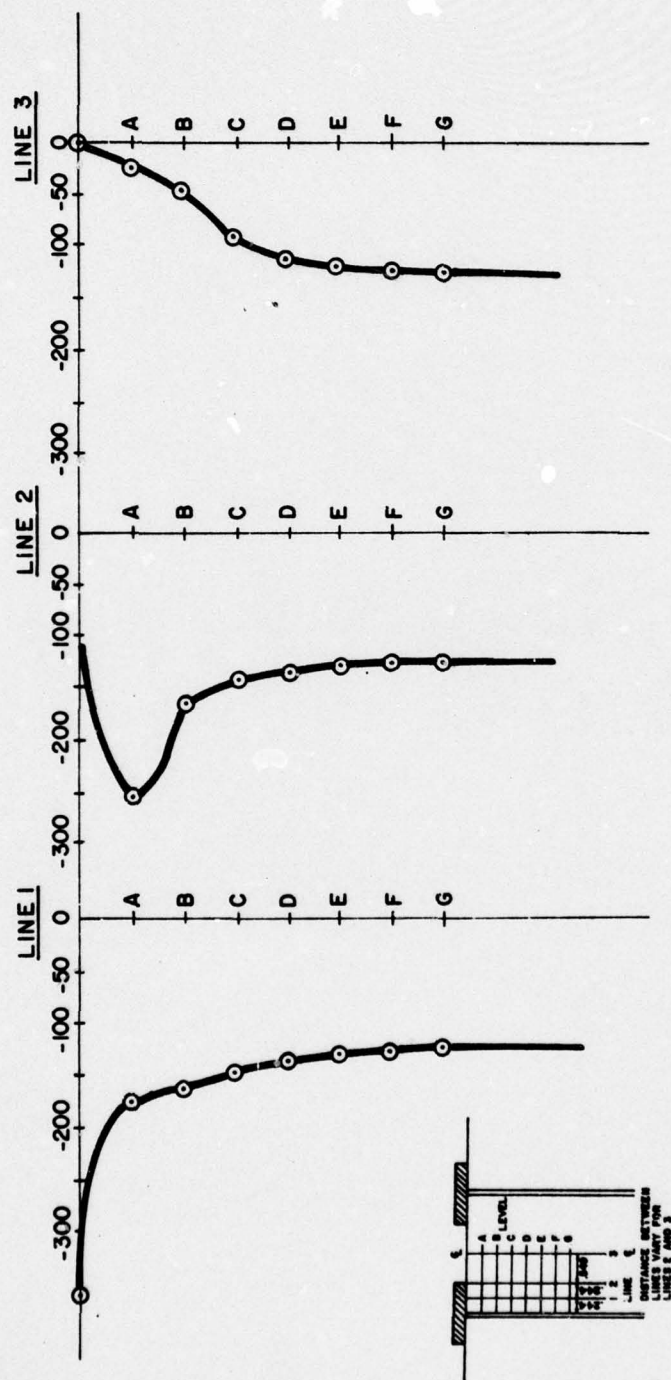


Fig. 4.49 Test #7--Principal longitudinal stress Q

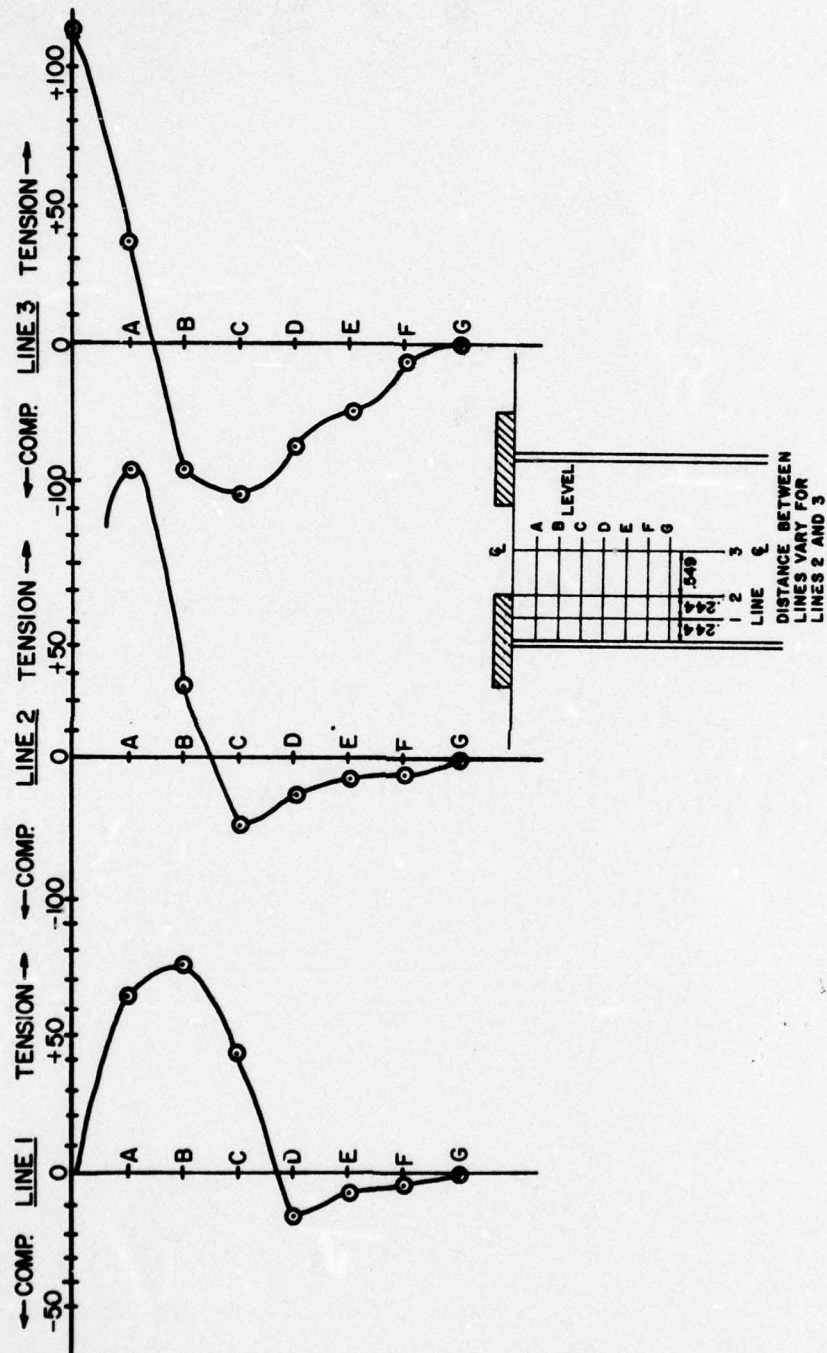


Fig. 4.50 Test #7--Principal transverse stress P

the known depth "G" and when calculated from that point to the free surface would give a zero value for normal stress at the free edge. The same sources of error as discussed in previous tests are present in this test.

The maximum values for stress along the three lines of action considered are shown below:

Line #1:

Maximum compressive stress = 363 psi compression

$$\text{Ratio} = \frac{\sigma_{\max}}{\sigma_{\text{uniform}}} = \frac{363}{125} \approx 2.9$$

Maximum transverse tensile stress = 74 psi tension

$$\text{Ratio} = \frac{\sigma_{\max}}{\sigma_{\text{uniform}}} = \frac{74}{125} \approx 0.6$$

Maximum shear stress = $\frac{1}{2}(240) = 60$ psi

$$\text{Ratio} = \frac{\tau_{\max}}{\sigma_{\text{uniform}}} = \frac{60}{125} \approx 0.5$$

Line #2:

Maximum compressive stress = 254 psi compression at Level A

$$\text{Ratio} = \frac{\sigma_{\max}}{\sigma_{\text{uniform}}} = \frac{254}{125} \approx 2.0$$

Maximum transverse tensile stress = 105 psi tension

$$\text{Ratio} = \frac{\sigma_{\max}}{\sigma_{\text{uniform}}} = \frac{105}{125} \approx 0.84$$

Maximum shear stress = $\frac{1}{2}(240) = 180$ psi

$$\text{Ratio} = \frac{180 \text{ psi}}{125} \approx 1.44$$

Line #3:

Maximum compressive stress = 125 psi at uniform compression

Maximum transverse tensile stress = 120 psi tension

$$\text{Ratio} = \frac{\sigma_{\text{max}}}{\sigma_{\text{uniform}}} = \frac{120}{125} \approx 0.96$$

$$\text{Maximum shear stress} = \frac{\frac{1}{2}(240)}{2} = 60 \text{ psi}$$

$$\text{Ratio} = \frac{\tau_{\text{max}}}{\sigma_{\text{uniform}}} = \frac{60}{125} \approx 0.5$$

The values and ratios for this test showed the best correlation of any of the tests conducted to previous analytical and direct measurement investigations and were fairly close to the work of Christodoulides.^{2,4} Christodoulides found a maximum compression ratio on his equivalent of line 2 of Test #7 to be 750/373 \approx 2.0 vs. 2.0 found for Test #7. He found a maximum transverse tension stress to exist on the axis of symmetry between the models which was equal to \approx 0.6 uniform compression. While the value for the corresponding transverse tensile stress in Test #7 was 0.96 uniform compression, this was the best correlation of any of the tests conducted. It also verified the existence of large transverse tensile spalling stresses which are created in a region between the two anchors. The distributions shown in Figs. 4.39 and 4.40 do give reasonable descriptions of how the stresses are distributed over depth in the model.

4.9 Test #8--Multiple Flat Bearing Anchors with Inclined Tendons

Test #8 was designed to investigate the effect of multiple anchors with inclined tendons. The test was limited in nature as no calculations for stress at interior points were done and the sole intention of the test was to provide general information. Flat bearing anchors were used for the test and the inclination of the

tendon ducts was the same as used in Test #5. A total load of 65 lbs. was applied to each tendon.

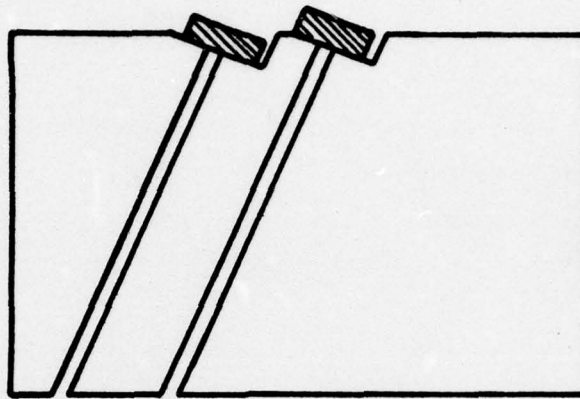


Fig. 4.51 Test #8--Multiple flat bearing anchors with inclined tendons

The isochromatic diagram shown in Fig. 4.52 gives very little data from which to work. Due to the geometric conditions and notched end block, there is very little symmetry. The isochromatics do indicate that uniform compression is reached rapidly. There also appears to be an interaction between the two anchorages, as there is a $1/2$ order isochromatic which extends from the edge of one anchor to the edge of the other. The isoclinic diagram shown in Fig. 4.54 does little to assist in the analysis of this area. The isoclinics observed during the testing were close together and obscure. There was extreme difficulty in observing them and determining their starting and stopping points. There is an isoclinic zero parameter which aligns itself with the axis of symmetry of the model indicating symmetric loading at the point where the parameter runs along the axis of symmetry. Above that point, however, an extremely complicated area exists in which longitudinal tension and compression are being

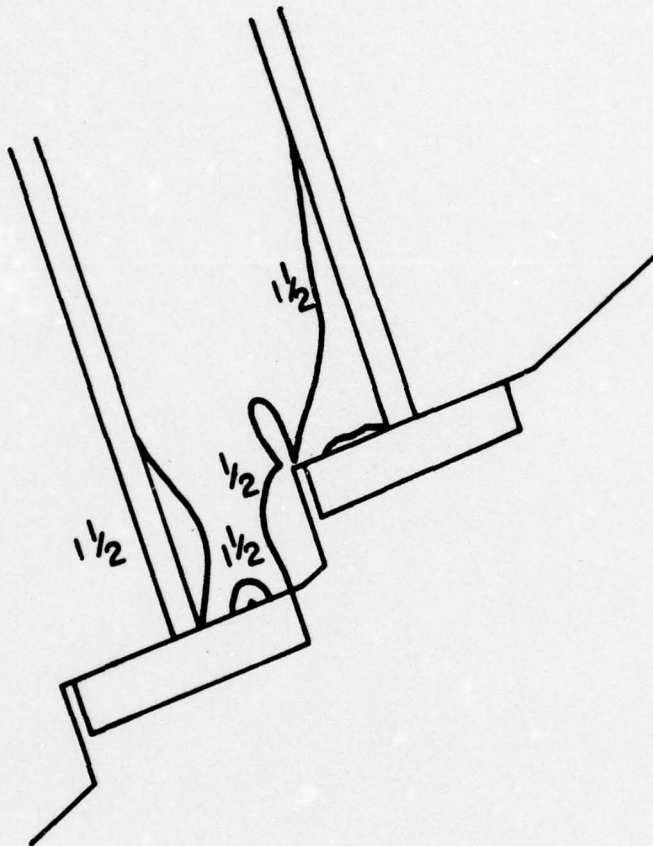


Fig. 4.52 Test #8 isochromatic diagram, light field

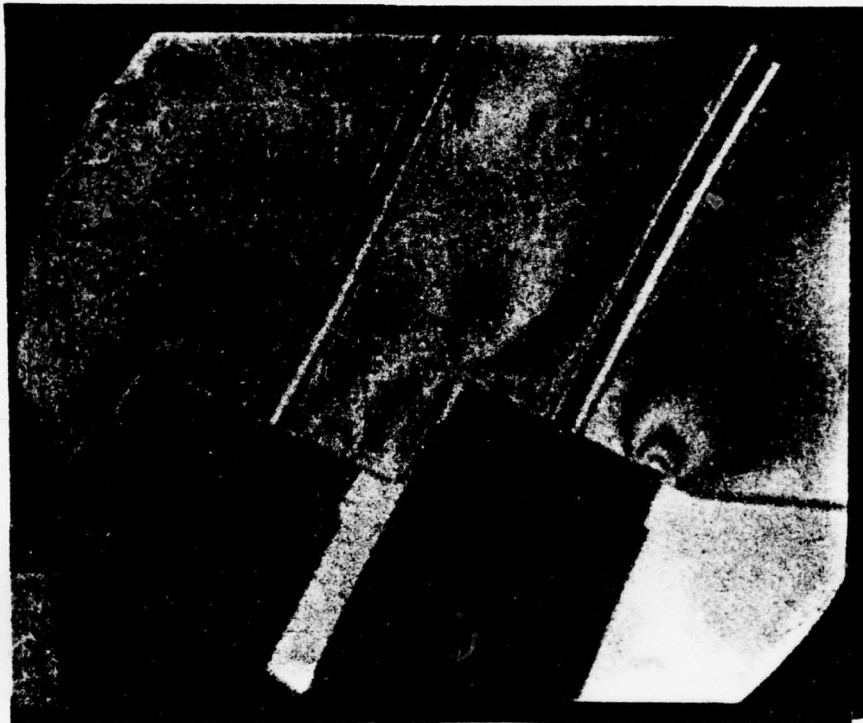


Fig. 4.53 Test #8 recorded isochromatics, light field

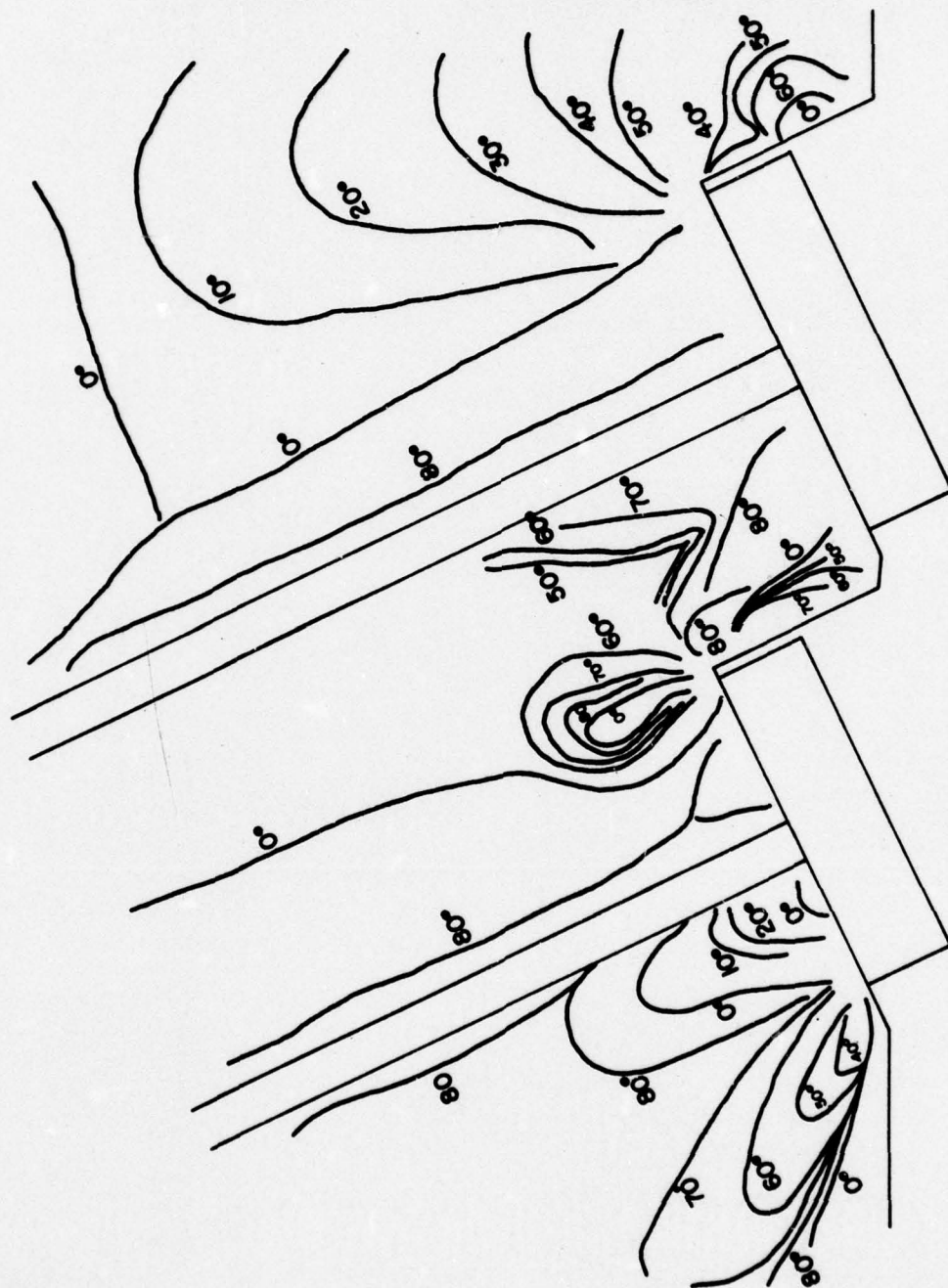


Fig. 4.54 Test #8 isoclinic diagram

created by the different anchors in the same area and their interrelationship is not readily obtainable from visual observation. The stress trajectories in Fig. 4.55 show the effect of the tendon ducts in orienting the stresses along the free edge orientation despite their natural inclination to assume vertical orientations.

To conduct a detailed investigation of a complex area such as the one in Test #8, the investigator should employ every technique at his disposal to provide as much information about the state of stress at interior points. He should employ a grid of strain gages to provide data as well as investigating areas of interest through photo enlargement so that much more precise data could be generated and analyzed. Any attempt to employ the "Shear Difference Method" without these additional aids would be extremely difficult and would generate errors of such magnitude as to make the effort of little value.

4.10 Test #9--Web Cross Section with Two Tendon Ducts

Test #9 was designed to augment Test #6 and provide additional information on the effects of tendon pressure on tendon ducts with inclined or draped configurations. An additional duct was added to the cross section and both ducts were loaded in the same manner as discussed in Test #6. A load of 60 lbs. was applied to each tendon but the loading system did not lend itself to the use of multiple tendons and unequal downward components of load were provided to the two ducts. The investigation was not intended to generate exact values, however, so the existence of unequal loadings was not significant. Also, there was not a large difference between the two downward components of load.

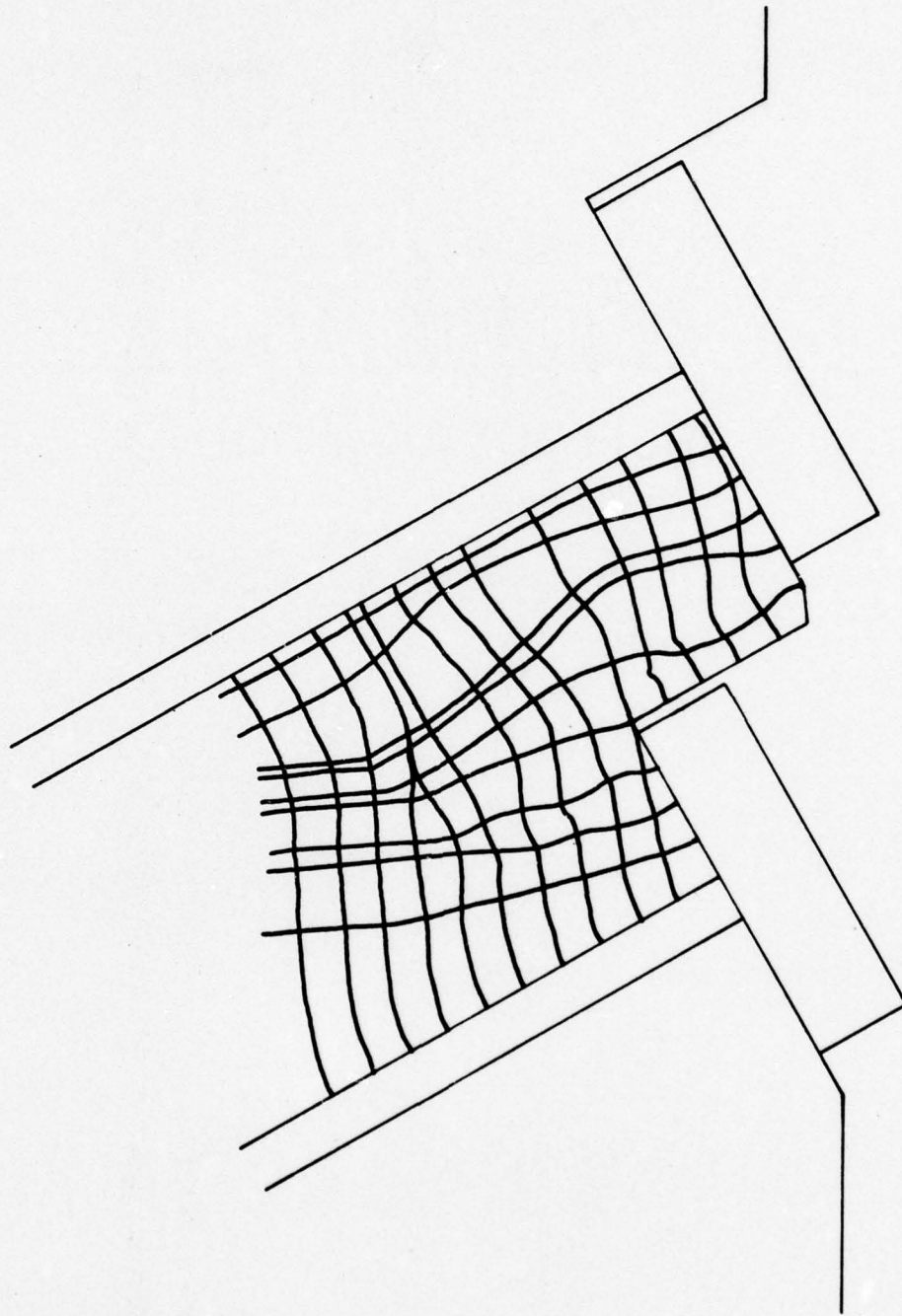


Fig. 4.55 Test #8 stress trajectory

NOTE: DIAMETER
OF DRILLED HOLE
IS 0.25"

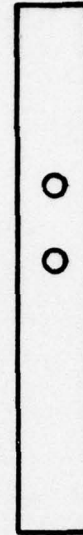


Fig. 4.56 Test #9--Web cross section with two tendon ducts

The isochromatic diagram shown in Fig. 4.57 and the recorded isochromatics shown in Fig. 4.58 show excellent correlation with Test #6. The top duct has almost the exact configuration as found in Test #6. The bottom duct, however, shows an interesting consideration. The isochromatic fringe marking a region of tensile stress in the top duct is missing from the bottom duct. There are small regions around the bottom duct which may be tensile and are indicated by small 1/2 order fringes, but apparently the compressive stress from the top duct has a tendency to remove this tensile stress. The tendons themselves still apparently act as concentrated loads.

The isoclinic diagram for Test #9 (Fig. 4.59) once again depicts an extremely complicated area around the top duct and shows good correlation with Test #6. The bottom duct seems to reflect the influence of the compressive stresses from the top duct and has a much simpler orientation. Both bottom and top ducts still

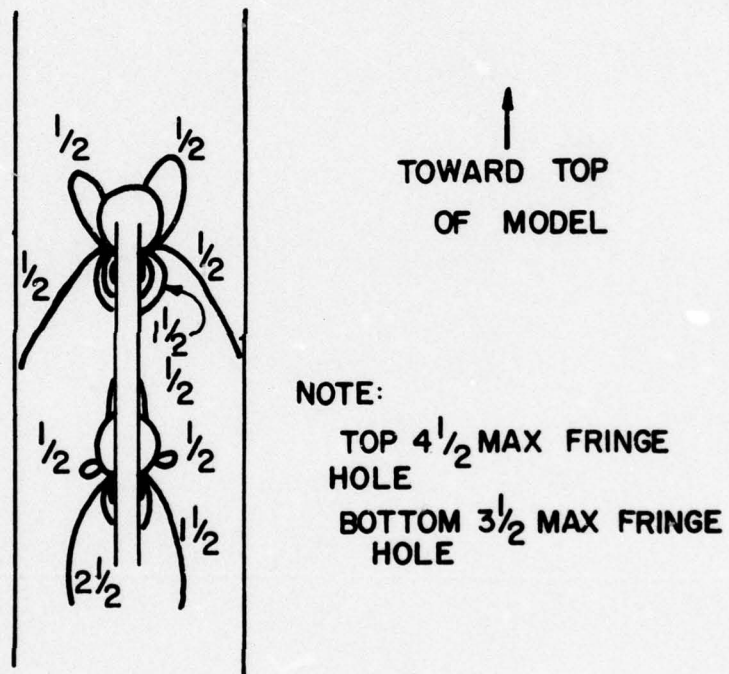


Fig. 4.57 Test #9 isochromatic diagram, light field

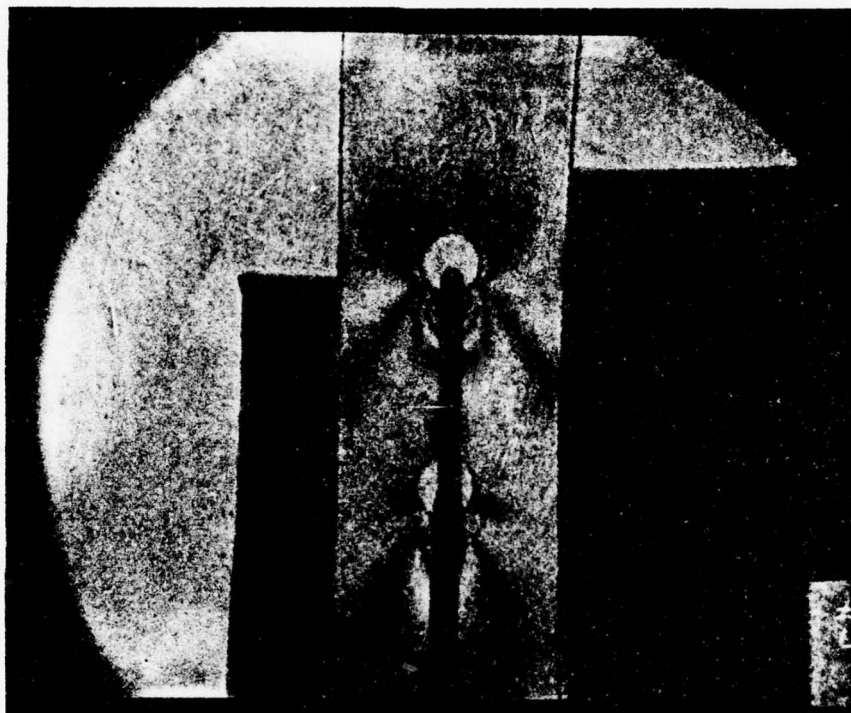


Fig. 4.58 Test #9 recorded isochromatics, light field

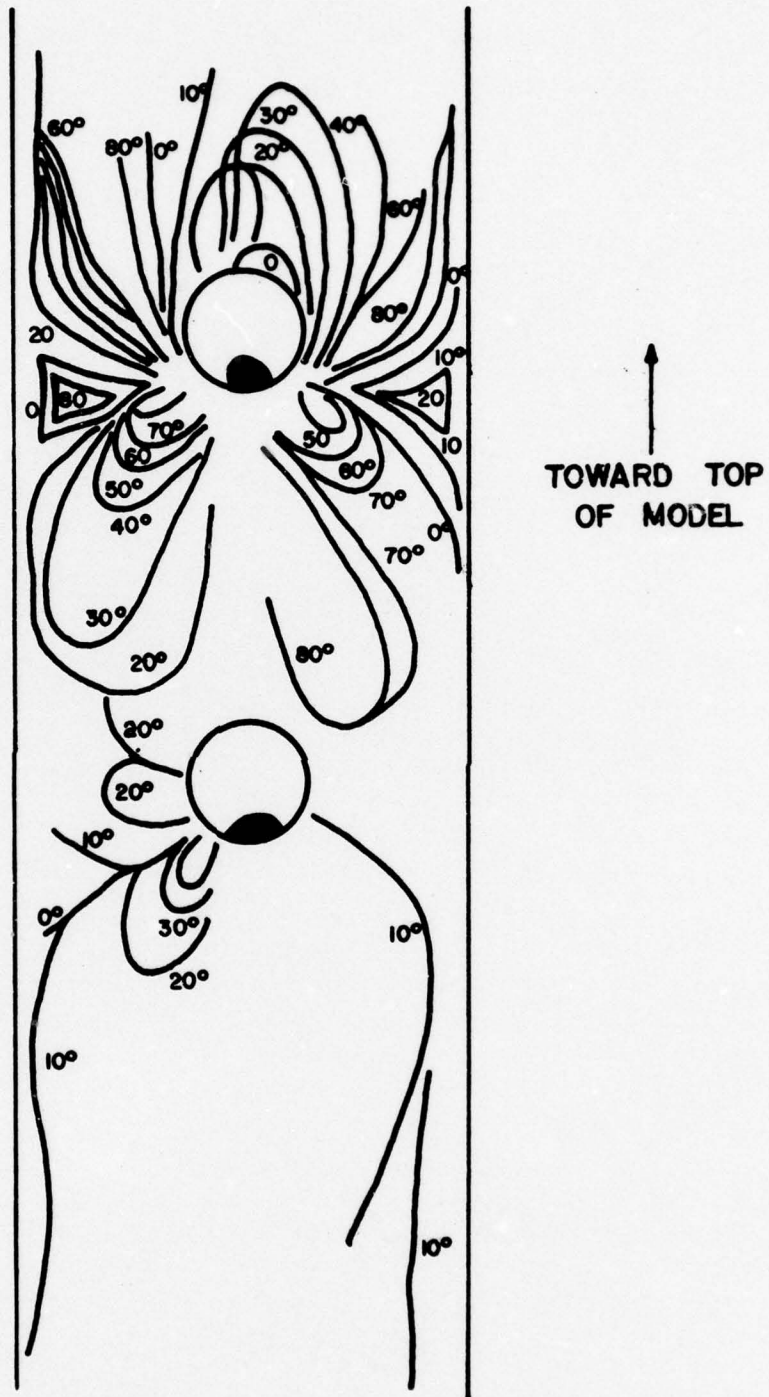


Fig. 4.59 Test #9 isoclinic diagram

reflect loading biases created by the loading system. The stress trajectories shown in Fig. 4.60 show best perhaps the influence of the top duct in apparently orienting the flow of the stress in the model and influencing the stresses created in the lower duct.

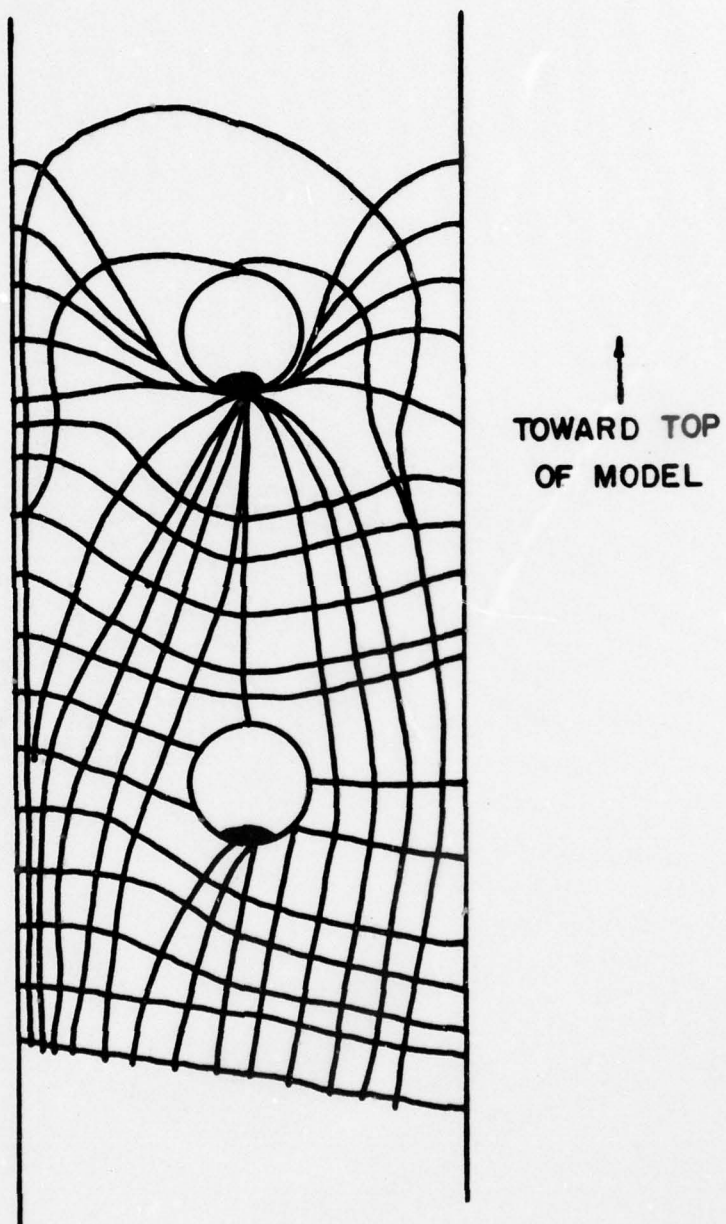


Fig. 4.60 Test #9 stress trajectory

CHAPTER 5

DISCUSSION OF TESTING PROCEDURES AND RESULTS

5.1 Testing Procedures

The first two objectives of this investigation were to (1) develop a two-dimensional photoelastic model of the anchorage zone of a thin-web post-tensioned concrete member, and (2) to develop a photoelastic testing procedure for the model. Chapters 3 and 4 have discussed the model design, the testing procedures, and the results of the tests conducted. A great deal of information was also generated by the investigations, stemming from the problems encountered during the conduct of the tests, which would be useful to investigators conducting subsequent photoelastic studies. The following section will address itself to a discussion of the lessons learned concerning the design of the testing model and the conduct of the photoelastic investigation.

5.1.1 The Anchorage System Models. The selection of lead as the material for the anchorage models was based on several positive considerations, including ease of manufacture, cost of manufacture, and the fact that models cast from the same mold should be similar for comparisons between different tests. What was not initially realized was that lead would also create several problems. The lead anchorage models varied geometrically from casting to casting. These differences were not large, but the required tolerances between the machined surface of the photoelastic sheet and the anchorage model to ensure a uniform transfer were very close. The small discrepancies in the dimensions of the anchorage models caused by the casting process created noticeable bias in what

should have been uniform load transfer. Also, the surface of the lead anchorage model had a rough texture which could not be effectively smoothed. The rough texture tended to create points of concentrated load between the anchorage model and the photoelastic sheet. These concentrated loads disrupted the transfer of load and changed the loading conditions slightly from test to test. The contact surface conditions did not affect stress distribution at greater depths in the models, but they did create slightly different testing conditions for each test. The consideration to use lead should not be ultimately governed by the desire to create similitude between prototype and model by having the same modular ratios between the anchorage system and the end block in both prototype and model. While a corresponding modular ratio for both model and prototype is certainly desirable, the differences in internal geometry between the models and their prototypes really affects the corresponding stiffnesses to such an extent that similitude is unobtainable. The decision to use lead, therefore, to provide the proper modular ratio should not be an overriding criterion. For future photoelastic studies of this nature, in light of the problems created by the use of lead for the anchors, it would be better to take the initial time and expense to machine more exact anchorage models using a material such as brass. These more durable and precise models could then be used for the entire set of experiments to provide more uniform loading conditions for each test. They would make it much easier to make comparisons between tests.

5.1.2 Anchorage Zone Model. The use of PSM-5 photoelastic sheet as the basic component of the anchorage zone model precluded the use of the more time-consuming, complicated photoelastic casting procedures to produce the model. The manufactured photoelastic sheets also provided known material constants which aided greatly in the reduction of data and calibration of equipment. The machining of these sheets, however, to construct the different models created

residual stresses which were serious enough to cause rejection of the initial models constructed. Eventually, as the machinists gained more experience with the material which is extremely hard to machine, the creation of residual stresses was reduced until the test models were usable and the level of residual stresses present would not affect the test results. Also, a reduction in the thickness of the photoelastic sheets purchased from 0.375 in. to 0.25 in. reduced the machining effort and, hence, the creation of residual stresses. Initial attempts were made to anneal the first test models with the large levels of residual stress to remove the residuals. The annealing process is extremely delicate and complicated and the attempts to remove the residual stresses were unsuccessful. It is far better to take the time to machine the plastic sheets slowly and carefully and thus not produce residual stress rather than to machine carelessly and then attempt to anneal the stresses out of the model. The machining of the photoelastic sheets presented another problem in that it was extremely difficult to match the machined sheet surface to the anchorage system model and get a smooth transfer of load. While most of this problem may be attributed to the lead anchor models, certainly the difficulty in producing the exact tolerances required in the anchorage zone model contributed to the problem. If the casting process had been used, then the model would have been cast with the anchor already in place and this might have solved the seating problem. Another consideration is that the photoelastic sheet used should be very sensitive photoelastically. The analysis requires as much data as possible and the presence of a large number of isochromatic fringes would have been extremely useful. The more insensitive the data, the more difficult the analysis, especially employing the "Shear Difference Method". The use of the photoelastic sheet for the model was initially chosen to reflect the effects of the tendon duct on the anchorage zone. As was shown in Fig. 3.15, the model constructed from the sheet did not accurately reflect the boundary conditions of

the tendon duct in the prototype and totally neglected the effects of restraint along the duct due to side cover and the stiffness of the concrete. The creation of the free edge along the duct boundary actually introduced stresses, as discussed in Sec. 4.1.1, into the model which did not exist in the prototype. The assumed "symmetrically loaded model" was actually two eccentrically loaded sections, since each section was independent of the other in the model. This prevented the formation of uniform compression equal to the loaded divided by the cross-sectional area in the model, as would be produced in the symmetrical prototype. The disadvantages of the use of photoelastic sheets greatly outweighed the projected disadvantages considered in the casting of photoelastic material, and for future photoelastic analyses of this type element, it is recommended that the models be cast, even though the process is far more time-consuming.

5.1.3 Testing Procedures. The conduct of the tests brought several important considerations to light concerning the procedures and methods employed. The first and, perhaps, the single most important consideration would be to take extreme care in the recording of data. In the investigation, isoclinic parameters were recorded by casting their image on a large screen and then tracing the images on the screen. This method proved to be too inexact, as small tracing errors created much greater errors when the data were used to calculate interior stresses. While the isoclinics traced gave good general results (stress trajectories, etc.), they were not sufficient for detailed results. A solution could be to photograph the isoclinics similarly to the isochromatics and, also, to use smaller increments, such as 2° to 5° as opposed to 10° . This makes the testing procedure much more complicated, however, as a photograph would be required for each isoclinic. Another consideration would be to provide an adjusting loading platform, so that the load could be more evenly transferred to the anchor. The loading system was

inflexible and any adjustments in the system were long and involved. There also was a need to provide higher loads to the model as an increased loading capacity coupled with a more sensitive photoelastic material would have generated far more sensitive data and make analysis much easier and certainly more exact. Strain gages should have been employed at various predetermined points on the models to provide additional data for analysis and verification of calculated results. The use of strain gages would have provided exact data to work with and would have eliminated the need for assumptions concerning the state of stress at certain points from which to initiate the "Shear Difference Method" of analysis. Some sort of compensator, such as the "Coker" or "Soleil-Babinet" should have been used to interpret between isochromatic fringe orders and determine intermediate values of the fringe order for points located there.^{6,13} This would have eliminated a large source of error in solving for the stress at internal points. Finally, the "Shear Difference Method" for determining the value of interior stresses should not be used over a large area unless the data are exact enough to use very small increments of integration and provide accurate results. The smaller these increments of integration, the more exact are the calculated results, as long as the data are exact enough to justify these small increments.

5.2 Test Results

The series of photoelastic tests conducted generated large values of data in the form of isoclinic diagrams, isochromatic diagrams, stress trajectories, trends in stress distribution, and values at selected internal points. The value of photoelasticity is, however, that it gives insight into what is taking place in a complicated stress distribution. While photoelasticity can generate fairly accurate values for stress, it is not an exact method. It should be used to determine possible problem areas, provide information

concerning the effects on stress of a change in some external parameter, and give a starting place for more exact methods of analysis and correlation for numerical methods of analysis. The following section discusses the results of the tests conducted with these goals in mind.

5.2.1 Influence of Anchorage Systems. The tests provided a good comparison between the conical anchorage system and the flat bearing system. It is unfortunate that the inset bearing anchor could not also be evaluated, but it simply did not work satisfactorily with the testing models designed. What was determined, however, was that the conical anchor system appears to have a marked effect upon the stress distribution in the anchorage zone. The conical anchor appears to create much higher stresses than does the flat bearing anchor. While there are probably large errors associated with the internal stress calculations for both Tests #1 and #3, the trends give much higher stresses being created by the conical anchorage. The isochromatic diagram alone shows a much higher shear stress being created by the conical anchor as opposed to the flat bearing anchor. Since the order of the isochromatic fringes relates to the difference in the principal stresses, this would also indicate larger principal stresses being created. Any further investigation should definitely look deeply into the stresses created by the conical anchorage system and its effects upon the stress distribution in the anchorage zone.

The maximum shear stresses produced in the two tests reflect the effect of the conical anchor to produce higher stresses. The shear stress is directly measured from the isochromatic diagram and is independent of error introduced by the use of the "Shear Difference Method".

Maximum shear stress--flat bearing anchor = 200 psi
(load = 84 lbs.)

$$\text{Ratio} = \frac{\text{Maximum shear stress}}{\text{Uniform compression}} = \frac{200 \text{ psi}}{28.5 \text{ psi}} = 7$$

Maximum shear stress--conical bearing anchor = 520 psi
(load = 85 lbs.)

$$\text{Ratio} = \frac{\text{Maximum shear stress}}{\text{Uniform compression}} = \frac{520 \text{ psi}}{28.8 \text{ psi}} = 18$$

The conical anchor produced two and one-half times as much maximum shear stress as did the flat bearing anchor approximately the same load and geometric conditions. When comparing the maximum compressive stresses produced in the two tests, the conical anchor maximum principal compressive stress ratio to the uniform compression was one and one-half times larger than the same ratio for the flat bearing anchor for similar loading conditions. The maximum transverse tensile stress at the free edge just beyond the end of the anchor for both tests was approximately the same. The interior transverse tensile stresses, however, were much higher for the conical anchor, with the conical anchor maximum stress approximately one and one-half times as large as the flat bearing anchor.

5.2.2 Influence of Eccentricity of Anchorage. Eccentricity of the anchorage system appears to markedly effect the stress distribution within the anchorage zone. First of all, it tends to create an extremely complicated region of stress between the free edge of the member and itself. The eccentricity appears to create a region of longitudinal tensile stress in the vicinity of the corner of the prestressed member close to the edge. The photoelastic tests indicate the formation of a zero value isotropic point, and earlier photoelastic investigations also confirm this point, and in so doing indicate a region of longitudinal tensile stress.^{2,4} The importance of these tensile stresses is that they would be spalling stresses in the post-tensioned member and would create a problem area in this spalling zone. The indication of a half-order isochromatic in this spalling region in Test #4 also indicates that these tensile stresses along the free edge can be of considerable magnitude and of approximately the same value as the uniform compressive stresses created in the model.

Comparing Test #4 which had an eccentric tendon to Test #1 which had a concentric tendon produced some interesting results. The load applied to the eccentric case (Test #4) was slightly lower than the load applied to Test #1 (76 lbs. vs. 84 lbs.), but the maximum magnitudes for compressive and transverse tensile stress were approximately the same. The eccentric case produced longitudinal tensile stresses in the near corner of the model which were of the same magnitude as the transverse tensile stresses produced along the free edge of the model just beyond the anchor. The concentric case produced no measurable longitudinal tensile stresses. Comparisons using the uniform compression ratios were avoided as the two models are not geometrically similar and interpretation of the comparisons could be misleading (see Sec. 4.1.1).

5.2.3 Influence of Multiple Anchorages. Test #7 provided an insight into the effects of multiple anchors on the anchorage zone. The geometry of the tendon ducts tend to create a zone between the two anchors where a large load must be carried over a small area at least initially. This is indicated by the high uniform compression value produced in the photoelastic model in this region between the two anchors bounded by the free edges of the tendon ducts. While the action in the third dimension, which is neglected in a two-dimensional study, would overcome this reduced area effect, it is still a consideration for a plane taken through the tendon ducts. The multiple anchors tend to create a region of high transverse tensile stresses between the anchors near the free edge. This transverse tensile stress region would become a region of spalling in a post-tensioned concrete member. The stresses created appear to be of approximately the same magnitude as the uniform compression created in the model. There is also an apparent tendency for the stress distribution to rapidly go to the uniform compression state due to the influence of the two anchors within a relatively small distance of each other. It should also be noted

that the multiple anchors produced a symmetrical loading situation when equal post-tensioning loads were applied. These test results compared most favorably with previous existing work.^{2,4}

5.2.4 Influence of Tendon Inclination. Tests #5 and #8 were designed to look into the influence of tendon inclination on the creation of stress in the anchorage zone. Neither of the tests really produced data on the stresses which would be caused by the tendon's pressure against the wall of the tendon duct. The tendons were straight within the duct and created no downward component of force against the duct.

What was shown, however, was that the inclined tendon duct markedly affected the geometry of the anchorage zone and in this manner had considerable impact on the stresses created. The areas over which the stress had to be distributed were constantly changing and this affected the distribution of stress with depth. Also, the geometry of the inclined tendon duct influenced the orientation of the principal stresses. The stress trajectories in Tests #5 and #8 show how the tendon duct acted as a free edge to orient stress flow. The notches created in the end blocks for the inclined anchors to rest on may produce longitudinal tensile stresses in regions of the end block above the loaded surface of the notch.

5.2.5 Influence of Tendon on the Tendon Duct along Cross Section of Web. Test #6 examined the cross section of the web of a post-tensioned member. The test was designed to examine the immediate effects around the tendon duct of the pressure of an inclined or draped tendon against the tendon duct wall. The testing method introduced the load to the model while it was sitting in a loading frame and so the loading frame introduced reactions in the base of the model which would not actually occur in a post-tensioned member between its supports. If the analysis is limited, however, to the region strictly around the tendon duct, then these base reactions

would not have a great effect and the model should fairly represent what takes place around the tendon duct of the member. In the test the applied downward load from the tendon acted much like a concentrated load and produced compressive stresses below the point of application of the load and the duct. There were also tensile circumferential stresses produced around the duct above the point of application of the load. This one point is important, because it indicates the possible creation of tensile forces around the duct due to tendon pressure against the walls of the duct. If the pressure between duct and tendon is substantial, then large tensile stresses could be produced which could lead to cracking along the duct from the inside of the member and possibly lead to cracks developing through the web to the exterior of the member. While it is difficult to gauge the intensity of these circumferential tensile stresses, this situation would certainly warrant further study to determine their actual effects on post-tensioned members. Test #9 showed that when two ducts run fairly close to each other, they influence one another with the compressive stresses created in one duct appearing to reduce the tensile stresses created around the other duct below it. Also, both Tests #6 and #9 seemed to indicate sizable shear stresses created under the point of application of the tendon pressure in comparison to the load applied. This would also indicate a region of high principal stresses where this maximum shear stress was also high.

CHAPTER 6

RECOMMENDATIONS AND CONCLUSIONS

In order to examine the nature of stresses created in the anchorage zone of post-tensioned concrete members using two-dimensional photoelastic techniques, a total of nine photoelastic tests was conducted. The loading system, specimen models, and testing procedures were designed to reflect an actual existing post-tensioned concrete member. The basic variables in the test program were anchorage system types, eccentricity of load, multiplicity of anchors, tendon duct inclination, and effects of tendon pressure on tendon duct walls. The investigation was exploratory in nature, so a major portion of the study was devoted to the creation of a usable two-dimensional photoelastic procedure which would examine the anchorage zone of a post-tensioned member and provide insight into the stress distributions created there.

6.1 Recommendations for Further Photoelastic Testing

Based on the results presented in Chapters 4 and 5, the following recommendations are made with regard to the conduct of future two-dimensional photoelastic investigations. It is hoped these recommendations will assist future investigators in conducting their investigations and provide a source of experience from which to build on.

(1) Consideration should be given to casting models as opposed to using photoelastic sheet. While casting models requires a great deal more time and expertise, it may provide a specimen which is easier to test and which certainly eliminates the need for exact

machining and more exactly represents the boundary conditions of the prototype.

(2) The anchorage systems should not be cast from lead, but rather should be machined from brass and reused throughout the testing sequence. The brass anchorages would eliminate the problems in surface transfer of load between anchor and end block model and also could be machined to very exact tolerances.

(3) A very sensitive photoelastic material should be used which will generate a large number of isochromatic fringes for a given load. This will create more sensitive data from which analysis may be more exact.

(4) A compensator to interpret values of fringe order for points located between isochromatic integral fringe orders should be employed in any future analysis.

(5) The models should be broken up into key areas for analysis and enlarged photography employed to produce blown-up photographs of these areas to aid analysis and provide more exact data for interior stress calculations.

(6) Isoclinics should be recorded using small differences in relative angle (2° to 5°) and the method of recording should be permanent so that constant reference can be made to the data. Tracing, unless very carefully performed, is not exact enough for recording isoclinics.

(7) Extensive use of strain gages should be employed at key points on the model to provide exact values for stress at interior points. This could be extremely valuable as a check of the analysis using the "Shear Difference Method".

(8) Extreme care must be taken to ensure the proper orientation of the testing model normal and perfectly vertical to the incident light rays.

5.2 Recommendations for Further Anchorage Zone Stress Investigations

Based on the results of the two-dimensional photoelastic investigation into the anchorage zone bursting stresses created in post-tensioned concrete members, the following recommendations are provided for future study. Since the study was exploratory in nature, and the number of test specimens was few, these recommendations are qualitative.

(1) The effects of conical end anchors should be studied in detail as they tentatively appear to create large stresses and may have an adverse effect on the anchorage zones of post-tensioned concrete members.

(2) The effects of eccentricity of load should be analyzed to gain insight into its effect on spalling stresses created in the corners of post-tensioned concrete members.

(3) The region between multiple anchors should be investigated as this appears to be a region with high spalling stresses.

(4) A detailed study of the effects of tendon duct inclination or drape should be conducted as the inclined or draped tendon geometry appears to greatly affect the distribution of stresses within the anchorage zone.

(5) The effects of tendon pressure on the tendon duct wall should be investigated as tentative photoelastic analysis indicates the formation of tensile stresses surrounding the duct.

6.3 Conclusions

The two-dimensional photoelastic analysis conducted provided valuable insight into the anchorage zone bursting stresses created in post-tensioned concrete. One disappointing portion of the investigation was the failure to initially generate and record data sensitive

AD-A053 516

TEXAS UNIV AT AUSTIN

F/G 13/13

AN EXPLORATORY PHOTOELASTIC INVESTIGATION OF POST-TENSIONED CON--ETC(U)

AUG 77 S D VAUGHN

. NL

UNCLASSIFIED

3 OF 3
AD
A053516



END
DATE
FILMED
6-78
DDC



enough to provide accurate results for the calculation of stress at interior points in the model by the "Shear Difference Method". This method can provide accurate results but is prone to error if the data are insensitive and if internal stress values are not provided by external means to provide checks and initial starting points for calculations. The required accuracy in the data is surprisingly high to provide accurate results using the "Shear Difference Method". A great deal of knowledge, however, was provided by the analysis and while it is qualitative in nature, it certainly is useful and accomplishes the goal of photoelasticity, which is to provide understanding of complicated regions of stress. A summary of observed results of the photoelastic tests includes:

- (1) Conical anchors appear to create substantially higher shear and normal stresses than flat bearing anchors.
- (2) Eccentricity of tendons develops spalling stresses at the free edges near corners in post-tensioned concrete members.
- (3) Multiple anchors create high transverse spalling stresses between the anchorages if the anchors are close together.
- (4) Inclined tendons greatly affect geometric considerations and the manner of distribution of stresses when compared to straight tendons.
- (5) The pressure of the post-tensioning tendon on the duct in a curved or inclined tendon creates circumferential tensile stresses around the duct and acts like a concentrated load to produce compressive stresses below the duct.

The main objectives of the study were accomplished. A two-dimensional model was developed which partially reflected the actual geometric and loading conditions found in post-tensioned concrete. Recommendations for improvement of the model to better represent the prototype were developed. A photoelastic testing procedure was

developed which was consistent with the model and the procedure was refined as the testing was conducted. A series of models was tested and considerable insight into the stress distribution in anchorage zones of post-tensioned concrete was generated with respect to the effects of various post-tensioning parameters. A limited source of directly measured values for stress in the models was provided to be used in conjunction with analytical and numerical methods of analysis. The use of the "Shear Difference Method" proved to have large errors (especially in the calculation of transverse stresses), but did provide a source of measurement and did show general trends in distribution of stress over depth. Certain values for internal stress were accurately calculated directly from the isochromatics. Finally, extensive insight was provided into the conduct of future photo-elastic tests to eliminate problems and possible pitfalls, and insight was provided concerning the distribution of bursting stresses in anchorage zones of post-tensioned concrete for use in future investigations.

A P P E N D I X A

SAMPLE CALCULATIONS FOR "SHEAR DIFFERENCE METHOD"

TABLE A4.1 TEST #1--SHEAR STRESS

$$\tau_{xy} = \frac{(Q - P)}{2} \sin 2\theta = \frac{n(160)}{2} \sin 2\theta = 80 n \sin 2\theta$$

Level	0-1	1-2	2-3	3-4
0-A	$n = 1\frac{1}{2}$ $\theta = 0^\circ$ 0	$n = 2$ $\theta = 80^\circ$ 54.7	$n = \frac{1}{2}$ $\theta = 60^\circ$ 34.64	$n = \frac{1}{2}$ $\theta = 5^\circ$ 6.9
A-B	$n = 1$ $\theta = 0^\circ$ 0	$n = 1$ $\theta = 80^\circ$ 27.4	$n = 1$ $\theta = 62^\circ$ 66.3	$n = \frac{1}{2}$ $\theta = 60^\circ$ 33.2
B-C	$n = 1$ $\theta = 0^\circ$ 0	$n = 1$ $\theta = 78^\circ$ 32.5	$n = \frac{1}{2}$ $\theta = 71^\circ$ 24.6	$n = \frac{1}{2}$ $\theta = 56^\circ$ 37.1
C-D	$n = 1$ $\theta = 87.5$ 6.97	$n = 1$ $\theta = 79^\circ$ 30	$n = \frac{1}{2}$ $\theta = 73.5$ 21.8	$n = \frac{1}{2}$ $\theta = 68^\circ$ 27.8
D-E	$n = 1$ $\theta = 86.5$ 9.75	$n = 1$ $\theta = 79^\circ$ 30	$n = \frac{1}{2}$ $\theta = 76^\circ$ 18.8	$n = \frac{1}{2}$ $\theta = 74^\circ$ 21.2
E-F	$n = 1$ $\theta = 87^\circ$ 8.36	$n = \frac{1}{2}$ $\theta = 81.5$ 11.7	$n = \frac{1}{2}$ $\theta = 78.5$ 15.6	$n = \frac{1}{2}$ $\theta = 77^\circ$ 17.6
F-G	$n = \frac{1}{2}$ $\theta = 87^\circ$ 4.18	$n = \frac{1}{2}$ $\theta = 84^\circ$ 8.3	$n = \frac{1}{2}$ $\theta = 82^\circ$ 11.0	$n = .5$ $\theta = 80^\circ$ 13.7
G-H	$n = .4$ $\theta = 89^\circ$ 1.1	$n = .4$ $\theta = 86^\circ$ 4.4	$n = .4$ $\theta = 84^\circ$ 6.65	$n = .4$ $\theta = 83^\circ$ 7.74
H-I	$n = .3$ $\theta = 0^\circ$ 0	$n = .3$ $\theta = 88^\circ$ 3.3	$n = .3$ $\theta = 87^\circ$ 2.5	$n = .3$ $\theta = 86^\circ$ 3.3
I-J	$n = .2$ $\theta = 0^\circ$ 0	$n = .2$ $\theta = 0^\circ$ 0	$n = .2$ $\theta = 89^\circ$.6	$n = .2$ $\theta = 88.5$.84

TABLE A4.2 CALCULATION OF NORMAL STRESSES--TEST #1, LINE 1

$$\sigma_x = \sigma_y + (\sigma_1 - \sigma_2) \cos 2\theta$$

Level	τ_{0-1}	τ_{1-2}	$\Delta\tau$	σ_y	$\sigma_1 - \sigma_2$	θ	σ_x
0				-200.4	$1\frac{1}{2}(160)$ +240	90°	+39.6
0-A	-0	-54.7	54.7				
A				-145.7	$1\frac{1}{2}(160)$ 240	80°	+79.8
A-B	-0	-27.4	27.4				
B				-118.29	$1(160)$ 160	86°	+40.15
B-C	-0	-32.5	32.5				
C				-85.8	$1(160)$ 160	83°	+69.4
C-D	-6.97	-30	23.03				
D				-62.76	$1(160)$ 160	82°	+91.04
D-E	-9.75	-30	20.25				
E				-42.51	$.8(160)$ 128	83°	+81.7
E-F	-8.36	-11.7	3.34				
F				-39.17	$\frac{1}{2}(160)$ 80	84.5°	+39.4
F-G	-4.18	-8.3	4.12				
G				-35.05	$\frac{1}{2}(160)$ 80	86°	+44.17
G-H	-1.1	-4.4	3.3				
H				-31.75	$.35(160)$ 56	88°	+24.1
H-I	-0	-3.3	3.3				
I				-28.45	$.2(160)$ 32	90°	+ 3.55
I-J	-0	-0	0				
J				-28.45	$.178(160)$ 28.48	90°	0

TABLE A4.3 CALCULATION OF NORMAL STRESSES--TEST #1, LINE 2

$$\sigma_x = \sigma_y + (Q - P) \cos 2\theta$$

Level	τ_{1-2}	τ_{2-3}	$\Delta\tau$	σ_y	Q-P	θ	σ_x
0				-28.64	$\frac{1}{2}$ 80	90°	+51.4
0-A	-54.7	-34.64	-20.06				
A				-48.7	$1\frac{1}{2}$ 240	72°	+145.5
A-B	-27.4	-66.3	+38.9				
B				-9.8	1 160	74°	+125.9
B-C	-32.5	-24.6	-7.9				
C				-17.7	1 160	75°	+120.9
C-D	-30	-21.8	-8.2				
D				-25.9	.8 128	76.5°	+88.1
D-E	-30	-18.8	-11.2				
E				-37.1	$\frac{1}{2}$ 80	78°	+35.98
E-F	-11.7	-15.6	+3.9				
F				-33.2	$\frac{1}{2}$ 80	81°	+42.9
F-G	-8.3	-11.0	+2.7				
G				-30.5	$\frac{1}{2}$ 80	84°	+47.7
G-H	-4.4	-6.65	+2.25				
H				-28.25	.35 56	86°	+27.2
H-I	-3.3	-2.5	-0.8				
I				-29.05	.2 32	88°	+2.87
I-J	0	-0.6	-0.6				
J				-28.45	.178 28.48	90°	0

TABLE A4.4 CALCULATION OF NORMAL STRESSES--TEST #1, LINE 3

Level	τ_{2-3}	τ_{3-4}	$\Delta\tau$	σ_y	$\sigma_1 - \sigma_2$	θ	σ_x
0				-2.1	$\frac{1}{2}$ 80	90°	+77.9
0-A	-34.64	-13.7	-20.94				
A				-23.1	$\frac{1}{2}$ 80	60°	+16.9
A-B	-66.3	-33.2	-33.1				
B				-56.2	$\frac{1}{2}$ 80	58°	-21.13
B-C	-24.6	-37.1	+12.5				
C				-43.7	$\frac{1}{2}$ 80	70°	+17.6
C-D	-21.8	-27.8	+6				
D				-37.7	$\frac{1}{2}$ 80	73°	+28.6
D-E	-18.8	-21.2	+2.4				
E				-35.28	$\frac{1}{2}$ 80	76°	+35.3
E-F	-15.6	-17.6	+2				
F				-33.28	$\frac{1}{2}$ 80	79°	+40.9
F-G	-11.0	-13.7	+2.7				
G				-30.6	.4 64	82°	+30.9
G-H	-6.65	-7.74	+1.09				
H				-29.49	.3 48	85°	+17.78
H-I	-2.5	-3.3	+0.8				
I				-28.69	.2 32	87°	+3.13
I-J	-0.6	-0.84	+0.24				
J				-28.45	.178 28.48	90°	0

TABLE A4.5 CALCULATION OF PRINCIPAL STRESSES
TEST #1, LINE 1

σ_1 = Larger principal stress

σ_2 = Smaller principal stress

Level	σ_y	σ_x	$\sigma_1 = \frac{(\sigma_x + \sigma_y)}{2} + \frac{(\sigma_1 - \sigma_2)}{2}$	$\sigma_2 = \frac{(\sigma_x + \sigma_y)}{2} - \frac{(\sigma_1 - \sigma_2)}{2}$
O	-200.4	+39.6	$-80.4 + \frac{-240}{2}$ -200.4	+39.6
A	-145.7	+79.8	$-32.95 + \frac{-240}{2}$ -152.9	+87.0
B	-118.29	+40.15	$-39.07 + \frac{-160}{2}$ -119.07	+40.93
C	-85.8	+69.4	$-8.2 + \frac{-160}{2}$ -88.2	+71.8
D	-62.76	+91.04	$+14.14 + \frac{160}{2}$ +94.14	-65.86
E	-42.51	+81.7	$+19.6 + \frac{128}{2}$ +83.6	-44.4
F	-39.17	+39.4	$+0.115 + \frac{80}{2}$ +40.115	-39.88
G	-35.05	+44.17	$+4.56 + \frac{80}{2}$ +44.56	-35.44
H	-31.75	+24.1	$-3.82 + \frac{-56}{2}$ -31.82	+24.18
I	-28.45	+3.55	$-12.45 + \frac{-32}{2}$ -28.45	+3.55
J	-28.45	0	$-14.22 + \frac{-28.48}{2}$ -28.48	0

TABLE A4.6 CALCULATION OF PRINCIPAL STRESSES
TEST #1, LINE 2

σ_1 = Larger principal stress

σ_2 = Smaller principal stress

Level	σ_y	σ_x	$\sigma_1 = \frac{(\sigma_x + \sigma_y)}{2} + \frac{(\sigma_1 - \sigma_2)}{2}$	$\sigma_2 = \frac{(\sigma_x + \sigma_y)}{2} - \frac{(\sigma_1 - \sigma_2)}{2}$
O	-28.64	+51.4	11.38 + 80/2 +51.4	-28.64
A	-48.7	+145.5	48.4 + 240/2 +168.4	-71.6
B	-9.8	+125.9	58.05 + 160/2 +138.05	-21.45
C	-17.7	+120.9	51.6 + 160/2 +131.6	-28.4
D	-25.9	+88.1	31.1 + 128/2 +95.1	-32.9
E	-37.1	+35.98	-0.56 + -80/2 -40.56	+39.44
F	-33.2	+42.9	+4.85 + 80/2 +44.85	-35.15
G	-30.5	+47.7	+8.6 + 80/2 +48.6	-31.4
H	-28.25	+27.2	-0.525 + -56/2 -28.525	+27.47
I	-29.05	+2.81	-13.09 + -32/2 -29.09	+2.91
J	-28.45	0	-28.45/2 + -24.48/2 -28.45	0

TABLE A4.7 CALCULATION OF PRINCIPAL STRESSES
TEST #1, LINE 3

σ_1 = Larger principal stress

σ_2 = Smaller principal stress

Level	σ_y	σ_x	$\sigma_1 = \frac{(\sigma_x + \sigma_y)}{2} + \frac{(\sigma_1 - \sigma_2)}{2}$	$\sigma_2 = \frac{(\sigma_x + \sigma_y)}{2} - \frac{(\sigma_1 - \sigma_2)}{2}$
O	-2.1	+77.9	$37.9 + 80/2$ 87.4	-2.1
A	-23.1	+16.9	$-3.1 + -80/2$ -43.1	+36.9
B	-56.2	-21.13	$-38.66 + -80/2$ -78.66	+1.33
C	-43.7	+17.6	$-13.05 + -80/2$ -53.7	+26.95
D	-37.7	+28.6	$-4.55 + -80/2$ -44.55	+35.45
E	-35.28	+35.3	$0.01 + -80/2$ +40.01	-39.99
F	-33.28	+40.9	$-3.81 + -80/2$ -43.81	+36.19
G	-30.6	+30.9	$0.15 + 64/2$ 33.14	-31.85
H	-29.49	+17.78	$-5.85 + -48/2$ -29.85	+18.15
I	-28.69	+3.13	$-12.78 + 32/2$ -28.78	+3.22
J	-28.45	0	-28.45	0

R E F E R E N C E S

1. American Concrete Institute, Building Code Requirements for Reinforced Concrete (ACI 318-71), Detroit, 1971.
2. Christodoulides, S. P., "A Two-Dimensional Investigation of the End Anchorages of Post-Tensioned Concrete Beams," The Structural Engineer, V. 33, No. 4, April 1955.
3. Christodoulides, S. P., "Three-Dimensional Investigation of the Stresses in the End Anchorage Blocks of a Prestressed Concrete Gantry Beam," The Structural Engineer, V. 35, No. 9, September 1957.
4. Christodoulides, S. P., "The Distribution of Stresses Around the End Anchorages of Prestressed Concrete Beams. Comparison of Results Obtained Photoelastically with Strain Gauge Measurements and Theoretical Solutions," Publ. Int. Assoc. Bridge and Structural Engineering, V. 16, 1956.
5. Cooper, R. L., "An Exploratory Investigation of Anchorage Performance in a Post-tensioned Thin-web Box Girder Bridge Model," unpublished Master's thesis, The University of Texas at Austin, 1975.
6. Dally, J., and Riley, W., Experimental Stress Analysis, McGraw-Hill Book Company, New York, 1965.
7. Dilger, W. H., and Ghali, A., "Remedial Measures for Cracked Webs of Prestressed Concrete Bridges," Journal of the Prestressed Concrete Institute, V. 19, No. 4, July-August 1974.
8. Douglas, D. J., and Trahair, N. S., "An Examination of the Stresses in the Anchorage Zone of a Post-Tensioned Prestressed Concrete Beam," Magazine of Concrete Research, V. 12, No. 34, March 1960.
9. Frocht, M. M., Photoelasticity, Volume II, John Wiley & Sons, Inc., New York, 1948.
10. Gerstner, R. W., and Zienkiewicz, O. C., "A Note on Anchorage Zone Stresses," Journal of the American Concrete Institute, V. 59, No. 7, July 1962.

11. Hawkins, N., "The Behavior and Design of End Blocks for Prestressed Concrete Beams," Civil Engineering Transactions, Institution of Engineers of Australia, October 1966.
12. Hendry, A. W., Photo-Elastic Analysis, Pergamon Press, Oxford, 1966.
13. Hetényi, M., Handbook of Experimental Stress Analysis, John Wiley & Sons, Inc., New York, 1950.
14. Jessop, H. T., and Harris, F. C., Photoelasticity, Principles & Methods, Dover Publications, Inc., New York, 1950.
15. "Materials for Photoelastic Coatings, Photoelastic Models," Bulletin P-1120-2, Photoelastic Inc., 67 Lincoln Highway, Malvern, Pennsylvania 19355.
16. Middendorf, Karl H., "Anchorage Bearing Stresses in Post-Tensioned Concrete," Journal of the American Concrete Institute, V. 32, No. 5, November 1960.
17. Norris, C. H., and Wilbur, J. B., Elementary Structural Analysis, McGraw-Hill Book Company, New York, 1960.
18. Ross, A. D., "Some Problems in Concrete Construction. Part 1. Stresses in the End Block of a Post-Tensioned Beam," Magazine of Concrete Research, V. 12, No. 34, March 1960.
19. Rowe, R. E., "End Block Stresses in Post-Tensioned Concrete Beams," Structural Engineer, V. 41, No. 2, February 1963.
20. Rydzewski, J. R., and Whitbread, F. J., "Short End Blocks for Prestressed Beams," Structural Engineer, V. 41, No. 2, February 1963.
21. State of Illinois Department of Transportation Plans for Proposed Federal Aid Highway, F. A. Route 408, Section (75,86)-7(B,B-1), Project EBRF-408-1(26), Pike & Scott Counties, prepared and recommended by Howard, Needles, Tammen, and Bergendoff, Consulting Engineers, Chicago.
22. Sundara Raja Iyengar, K. T., "Two-Dimensional Theories of Anchorage Zone Stresses in Post-Tensioned Prestressed Beams," Journal of the American Concrete Institute, Proc. V. 59, No. 10, 1962.
23. Sundara Raja Iyengar, K. T., and Prabhakara, M. K., "Anchor Zone Stresses in Prestressed Concrete Beams," Journal of the Structural Division, ASCE, V. 97, ST3, March 1971.

24. Zielinski, J., and Rowe, R. E., "An Investigation of the Stress Distribution in the Anchorage Zones of Post-Tensioned Concrete Members," Research Report No. 9, Cement and Concrete Association, London, September 1960.
25. Zielinski, J., and Rowe, R. E., "The Stress Distribution Associated with Groups of Anchorages in Post-Tensioned Concrete Members," Research Report No. 13, Cement and Concrete Association, London, October 1962.

V I T A

Captain Stephen Donald Vaughn was born in Denver, Colorado, on October 31, 1949, the son of Jean Burch Vaughn and Donald Edward Vaughn. After completing his work at Irvin High School, El Paso, Texas, in 1967, he entered the United States Military Academy at West Point, New York, and received the degree of Bachelor of Science (General) in June 1971. He was commissioned a 2nd Lieutenant in the Army Corps of Engineers in June 1971. He is a graduate of the U. S. Army Airborne School, U. S. Army Ranger School at Fort Benning, Georgia, and an honor graduate of the Engineer Officer Basic Course at Fort Belvoir, Virginia. He subsequently served as platoon leader and executive officer in both airmobile and armored combat engineer companies at Fort Hood, Texas. In April 1974 he was assigned Company Commander of B Co, 8th Engineer Battalion, Fort Hood, Texas. In April 1975 he was assigned to the Engineer Officer Advanced Course at Fort Belvoir, Virginia, and in November of the same year was promoted to Captain. He was an honor graduate of the Engineer Officer Advanced Course in December 1975. In November 1975, Cpt. Vaughn received his Professional Engineering Registration from the Commonwealth of Virginia. In December 1975 he entered the Graduate School of The University of Texas at Austin.

Permanent address: 5305 Gulfport Drive
El Paso, Texas 79924

This thesis was typed by Maxine R. DeButts.